Advances in River Bedload Tracking Technology: Self-righting Radio Frequency Identification Tracers and an In-stream Automated Station

by

Christopher Muirhead

A thesis
presented to the University of Waterloo
in fulfillment of the
thesis requirement for the degree of
Master of Applied Science
in
Civil Engineering

Waterloo, Ontario, Canada, 2018

Author's Declaration

I hereby declare that I am the sole author of this thesis. This is a true copy of the thesis, including any required final revisions, as accepted by my examiners.

I understand that my thesis may be made electronically available to the public.

Abstract

Understanding of bedload transport rates in natural streams has been an area of focus for researchers for decades. Recently, researchers have begun to use Radio Frequency Identification (RFID) technology to track individual particles. The application of RFID technology allows for the classification of movement of individual clasts while increasing recovery rate of tracers particles. Small glass cylinders hold a copper coil around a ferrite rod which allows the tag to communicate a unique identification code to an antenna. The unique identification code allows researchers to analyze individual particle movement in a manner which was not possible prior to RFID technology. Despite the popularity, there are still improvements to be made to the technology and methodology of tracking RFID-tagged tracers. Existing tracking methods include manually walking the streambed between flood events with an antenna, while flagging and marking tracers which have been detected. This method only provides inter-flood data while also being extremely time consuming. Additionally, the detection range of RFID tags can be highly variable depending on the orientation of the tag. Vertical tags produce a circular detection range while horizontal tags have a much smaller detection range, shaped like a peanut with two lobes. Inconsistency in detection range limits the ability to accurately locate a tracer's position while decreasing recovery rates.

The goal of this research is to advance RFID technology in two manners: develop a customized system of tracking RFID tracers during a flood event and develop a method for ensuring consistent detection range in RFID tags. The first goal is accomplished by designing a stationary antenna array system to be installed into the bed of the stream to detect tracers as they move over-top during a flood event. The system automatically records the tracer movement allowing for in-depth analysis of the timing of particle movement during a flood event. The second goal is accomplished through the design of the "Wobblestone", a unique and innovative product to ensure a consistent detection range while increasing the viability of smaller RFID tags for field studies.

A case study was performed at Schneider Creek in Kitchener, Ontario. Schneider Creek was previously a concrete channel which was recently restored to a natural channel. This case study includes seeding and inter-flood tracking of RFID-tagged particles and field testing of the customized stationary antenna array.

Acknowledgements

I would like to thank my supervisor, Dr. Bruce MacVicar, for his continued guidance and support as I sought to complete this degree. Thank you to Stantec Ltd. for the financial support and collaboration which made this research project possible.

Thank you to everyone at the University of Waterloo who have helped me complete this thesis in a wide variety of ways. Thank you to Elli Papangelakis, Terry Ridgeway, Aryn Cain and Alastair Yu for all your help in the field and in the lab to get this research project where it is today.

Finally, thank you to my friends and family who I continually relied on for support as I navigated the rollercoaster that is a Master's Degree. I could not have gotten this far without you and I am ever grateful for all your support.

Table of Contents

List of Figures

List of Tables

Chapter 1.0 – Introduction

Anthropogenic activities have impacted hydraulic and hydrologic processes for centuries, beginning with irrigations canals in Mesopotamia (2300 BC) and continuing to modern day stormwater management and conveyance controls (Viollet, 2014). Recent trends such as urbanization have led to shifts in hydrologic behavior, resulting in wide-spread changes to the urban ecosystem, including streams and rivers.

The degradation of natural steams due to urbanization has been termed the "Urban Stream Syndrome (USS)" by Paul and Meyer (2001). USS encompasses all changes caused by the transition from a natural environment to an urban environment. These changes include hydrologic, geomorphic, ecologic changes, along with disturbance of the natural water chemistry. While a stream will often experience natural fluctuations, an unnatural change to each of these components can cumulatively result in the disturbance of urban streams. Disturbance will often transition the stream from a state of quasi-stability to instability. Hydrologic changes affect the volume of water entering the river while geomorphic changes often result in an engineered narrowing of the channel. Changes in floodplain composition can lead to reduced ecological diversity while land use and runoff changes can greatly affect the natural water chemistry (Paul & Meyer, 2001). An unstable stream will seek equilibrium and will go through several stages of evolution (Schumm et al. 1984). As shown in Figure 1, a channel which seeks equilibrium will change morphology rapidly with severe erosion and deposition occurring concurrently. Erosion and deposition can lead to significant changes to both the affected reach as well as downstream sections of the river.

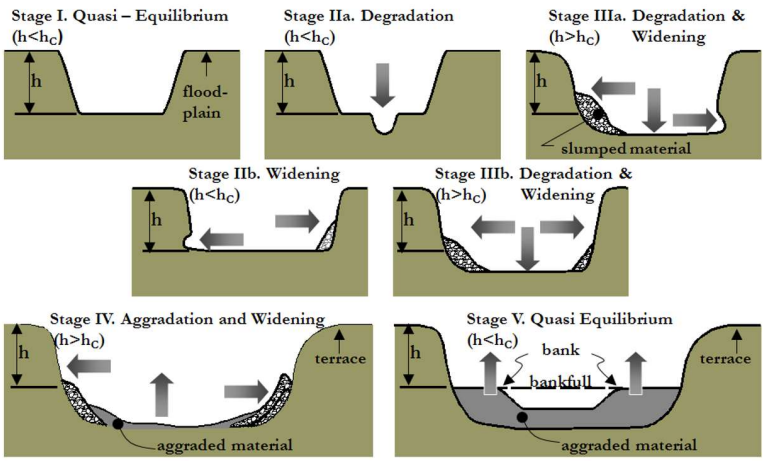

Figure 1: Stages of Channel Evolution (Schumm et al. 1984)

To combat urban stream degradation, the field of restoration has been developing rapidly, addressing issues as they occur. In the United States alone there were 37,099 projects in the National River Restoration Science Syntheses (NRRSS) database as of July 2004 and at the time it was estimated the United States spends upwards of $1 billion yearly on river restoration projects (Bernhardt, et al., 2005). Despite the amount of restoration projects currently completed or in the process of completion, proper restoration techniques for ensuring hydraulic stability, while providing sediment continuity, are not fully understood. A common method of restoration includes instituting a stable riffle-pool sequence within a meandering stream. This method incorporates natural geomorphic characteristics to reduce flow velocity and provide a stable channel. These channels are often designed in urban areas around and through infrastructure and thus are meant to be immobile. Riffle-pool morphology is a common design strategy to successfully create a quasi-equilibrium stream, however, the mechanisms which form and maintain the riffle-pool design are not yet known (Milan et al., 2002). As is depicted with the riffle-pool design, restoration efforts tend to focus on recreating the past physical features without understanding the processes behind these features and how they might have changed due to anthropogenic activities (Hobbs & Harris, 2001). These hydraulic processes and mechanisms are what manifest in the physical properties we see on the surface and as such, understanding these processes is integral to creating a successful restoration.

One such process which governs the formation of physical features in a river is bedload transport. While suspended sediment transport is often visible to an untrained eye (turbidity in the water column or fine depositional bars), bedload transport is harder to quantify both visually and through instrumentation. Defined as the movement of particles in a stream which experience intermittent contact with the bed of the stream, bedload transport occurs through the processes of saltation, sliding or rolling (McGee, 1908). Often these larger particles form the fabric of the stream bed. Therefore, disturbing the natural bedload transport rate can lead to fundamental changes in morphology.

Measurement of bedload transport is an issue that has confused researchers since the early 1900's. Bedload transport was defined by Einstein (1937) as a stochastic process with each particle experiencing individual periods of rest and mobility. As such bedload transport estimates have often relied upon significant experimental data to establish empirical relationships. Collection of data for these empirical relationships has been done using many different methods as there has yet

to be an ideal solution. Collection methods for field data have ranged from samplers placed along or within the bed of the stream (Helley & Smith, 1971, Reid & Frostick, 1986) to individual particle tracking (e.g. Carre et al., 2007). Flume studies often attempt to replicate natural features and processes in a simulated environment. While significant strides in terms of understanding the fundamental processes behind bedload transport have been made, these laboratory studies can suffer from an oversimplification of natural processes.

To understand the processes behind particle movement, Radio Frequency Identification (RFID) technology is being used to track individual particle movement paths (e.g. MacVicar et al., 2015). RFID technology consists of a transponder and an antenna. In an active RFID system, the transponder is in constant communication with the antenna, requiring the transponder to have an internal battery to operate. Comparatively, a passive system occurs when the antenna transmits an energy pulse to the transponder, charging the magnetic coil within the passive RFID tag. Once charged, the tag then transmits a signal back to the antenna including an identification number (Violino, 2005). Each tag comes with a unique identification number to easily identify which tag is being detected. Passive Integrated Transponder (PIT) tags are more common than active tags in bedload tracking as they are generally smaller, do not require an internal battery and allow for long-term studies of the movement of individual clasts. By recording the know locations of the tags and returning to the study site periodically or after a rainfall event, one can determine the length of travel of each individual tag.

A shortcoming of inter-flood particle tracking is the limited information regarding in-flood movement of the individual clasts. Questions such as, “which particles move when during a flood?” and “what is the flow at incipient motion?” still need to be answered. Researchers have attempted to quantify these questions by incorporating automated bedload tracking systems. While these in-flood tracking systems are less developed than inter-flood tracking methods, significant strides have been made with regards to several different monitoring types. Historically, researchers have attempted to use acoustics sources, seismic activity and impact plates to attempt to categorize the bedload transport of a stream (e.g. Habersack, et al., 2016, Belleudy, et al., 2014). While each of these methods have provided the ability to collect data during flood events, the ability to discern between different particle sizes and points of incipient motion has been unsuccessful. The studies which have collected in-flood bedload data using RFID technology are limited to flume studies (Hufnagel & MacVicar, 2018) or small-scale field studies (Mao et al., 2017).

Inter-flood tracking of tracers also allows for the possibility of "losing" the tagged stone if the stone goes undetected during tracking. Researchers have sought to quantify the exact detection range of PIT tags to improved recovery rates (Chapuis et al., 2014). One issue with detecting PIT tags is the change in detection range from a vertical tag to a horizontal tag. A horizontal tag results in a smaller detection range than a vertical tag. A reduced detection range can be problematic with smaller PIT tags (smaller detection range in general) or when the PIT tag is buried. As such, there is a need to improve the detectability in order to further develop PIT tags as a reliable method of tracking bedload in all hydraulic situations.

The goal of this thesis to improve the methods for measuring bedload transport in-situ in order to develop a greater understanding of the mechanisms behind bedload transport. This goal is accomplished in the following chapter through several objectives. The objectives include; 1) improving the detection range of PIT tags in the field; 2) development an automated system for tracking PIT-tagged tracer particles; and 3) investigate sediment transport at a local restored stream, Schneider Creek in Waterloo. Chapter 2 of this thesis will focus on a literature review of articles surrounding bedload monitoring methods. Chapter 3 will discuss the development of a self-righting RFID tag for consisted detection range. The methodology of the creation of the automated system will be described in Chapter 4. Chapter 5 will include a summary of the case study performed at Schneider Creek including installation of the automated system. Finally, the thesis will conclude in Chapter 6 with the current state of the research and future steps.

Chapter 2.0 – Background

This chapter will provide background information on the research which has been previously performed with regards to measuring sediment transport. Focusing on the objectives of creating a bedload tracking system for an urban restored stream, the literature review will review the early research studies performed on sediment transport analysis. It will then delve into methods of bedload transport data collection. These methods can be grouped into direct sampling methods, indirect monitoring methods and bedload tracking methods. These methods will include both inter-flood tracking methods and in-flood recording methods. An in-depth review of RFID technology will also be included, focusing on how it relates to bedload tracking.

2.1 – Bedload Transport

2.1.1 – Sediment Movement Research

The movement of sediment in water has been studied since at least the early 20th century when McGee (1908) stated the mechanisms of a stream bed forming are 1) erosion, 2) transportation, and 3) deposition. Since then, researchers have been attempting to quantify sediment transport through a series of empirical equations and experiments, beginning in 1914 when Gilbert and Murphy set up the first flume experiment. The experiment set out to determine the effects of discharge, slope, depth of flow, width of flow among other variables on transport of fine sediment. The experimental apparatus (shown in Figure 2) consisted of a head tank flowing into a wooden trough with a constant sediment feed being applied near the start of the trough (Gilbert & Murphy, 1914). The sediment was collected in a "sediment trap", labeled (B) in Figure 2. Gilbert and Murphy tested many different variables including different grain sizes, changes of slope, change in discharge as well as depth and width of the flow.

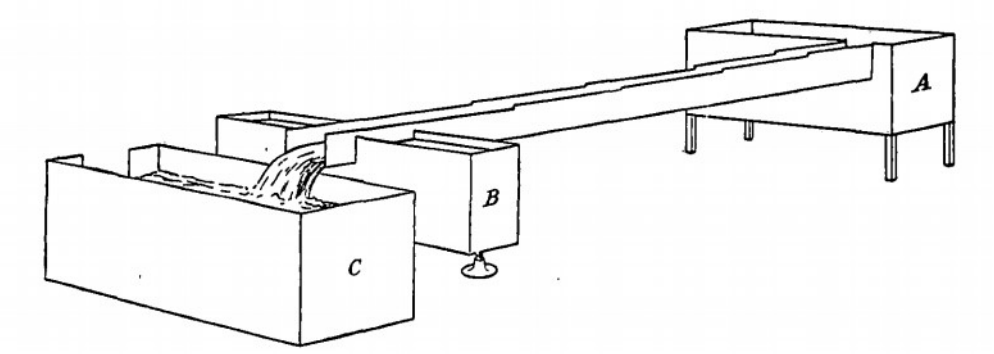

Figure 2: Flume used to determine transport of sand by Gilbert & Murphy (1914)

Shields conducted independent experiments in the 1930's, continuing to develop the relationships between physical variables and sediment transport. Shields was the first to develop the connection between the boundary Reynolds number and the critical shear stress for incipient motion leading to Equation 1 (1939). Reynolds number is the ratio of a given fluid's inertial forces to its viscous forces and is commonly used to determine whether a flow is turbulent or laminar in nature.

Equation 1: Shields original equation for bedload transport

$$\frac{283}{\sqrt{\lambda}} - 5.75 \log \frac{R}{k} + 3.75 = a + b \log \frac{v_* k}{\nu} = A$$

Shields stated the above equation does not define bedload transport but is a starting point for continued research. The work also led to the development of a diagram, now commonly referred to as the Shields diagram, defining the relationship between the boundary Reynolds number and the dimensionless shear stress, establishing the critical shields parameter in the process (Julien 1995). The critical shields parameter is a dimensionless variable used to define the moment when the shear stress applied to a given particle is large enough to result in motion.

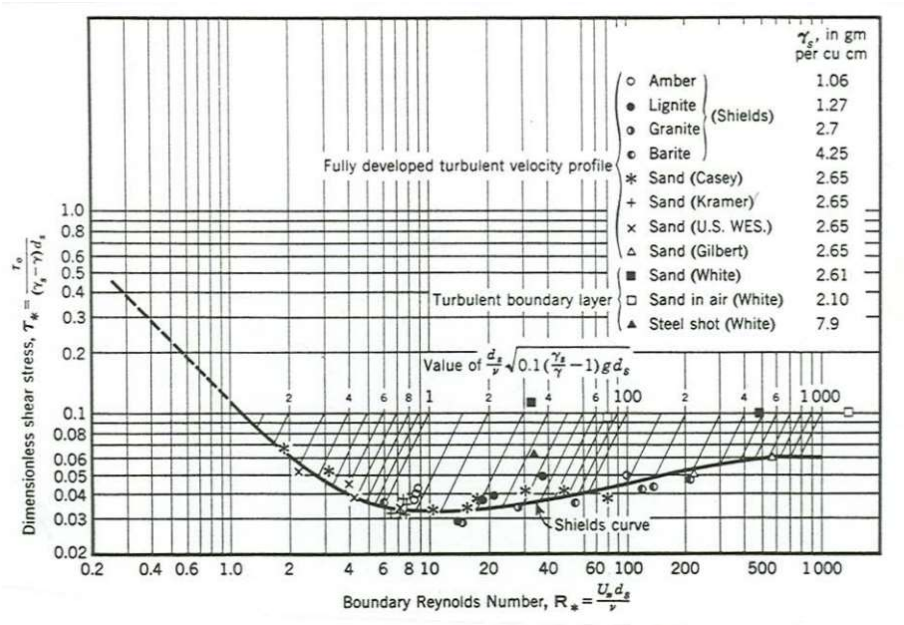

Figure 3: Particle motion diagram after Vanoniv (1975)

As the Reynolds number was a well-defined parameter at the time, the critical shields parameter became a fundamental building block of sediment transport equations moving forward. Using flume date, several researchers were able to recreate Shields' work and develop further empirical formulae. For example, Meyer-Peter and Muller (1948) developed an equation for dimensionless bedload transport rate (q*) based on new flume results and those of Gilbert and Murphy (1914).

Equation 2: Meyer-Peter Muller formula (Meyer-Peter & Muller, 1948)

$$q^* = 8(\tau_* - \tau_C^*)^{3/2} \quad \tau_C^* = 0.047$$

Einstein (1950) established a different manner for characterizing sediment transport based on stochastic methods. Einstein developed Equation 3 based on a less empirically-driven approach. This equation diverged from the need for a critical shear stress, instead focusing on the rest time of the particle as well as the moment when the lift forces were greater than the weight of an individual particle (Parker, 2009). This stochastic approach has led to the development of particle tracking methods as an effective form of determining bedload transport.

Equation 3: Einstein transport equation originally derived in Einstein (1950), taken from Parker (2009)

$$1 - \frac{1}{\sqrt{\pi}} \int_{-(0.143/\tau^*)-2}^{+(0.143/\tau^*)-2} \exp(-t^2)\mathrm{d}t = \frac{43.5 q_b^*}{1 + 43.5 q_b^*}$$

Note q^*_b in Equation 3 is the same variable (bedload transport rate) previously defined as q^* in Equation 2. While Einstein's equation was less empirically driven than previous attempts to categorize sediment transport, it still relied heavily on experimental data for calibration. As such, these equations may fit some data sets while improperly characterizing sediment transport of other systems. The non-universal nature of these equations demonstrate there is a need for continued sediment transport monitoring and analysis to determine the mechanisms behind a stream's sediment transport.

Measurement methods used to determine bedload movement have developed significantly in the last 100 years. Gilbert and Murphy incorporated the first method of bedload transport tracking in their flume design by incorporating a "sand arrester" (Gilbert & Murphy, 1914). However, developing methods for tracking bedload in natural streams is far more difficult than in a flume. The difficult nature of bedload tracking has resulted in two distinct methods of bedload

monitoring: direct sampling methods and indirect monitoring methods. Direct sampling methods can be defined as methods which physically sample bedload from the stream without the need for a surrogate or proxy. These methods often include placement of invasive measuring devices in the stream to collect a sample or directly monitor the sediment movement. Inversely, indirect monitoring methods are often less invasive to the river processes but require a surrogate to characterize bedload transport. Both direct and indirect methods of bedload transport monitoring will be summarized in the sections to follow.

2.1.2 – Direct Sampling Methods

Direct bedload transport sampling methods have been historically more prevalent than indirect methods. They often include the placement of a sampler in or along the stream bed either permanently or temporarily to secure a sample of sediment as it passes the sampler.

2.1.2.1 – Helley-Smith Sampler

One of the initial methods to attempt to characterize sediment transport in natural streams directly, which is still in use today, was created by Helley and Smith in 1971. As it has become known today, the Helley-Smith sampler was designed to sample from the previously "unmeasured zone" while providing minimal disturbance to the flow regime and remaining hydraulically stable in velocities up to 10 ft/s (Helley & Smith, 1971). Shown in Figure 4, the Helley-Smith sampler consists of a nozzle leading to a large mesh bag for collecting the sample.

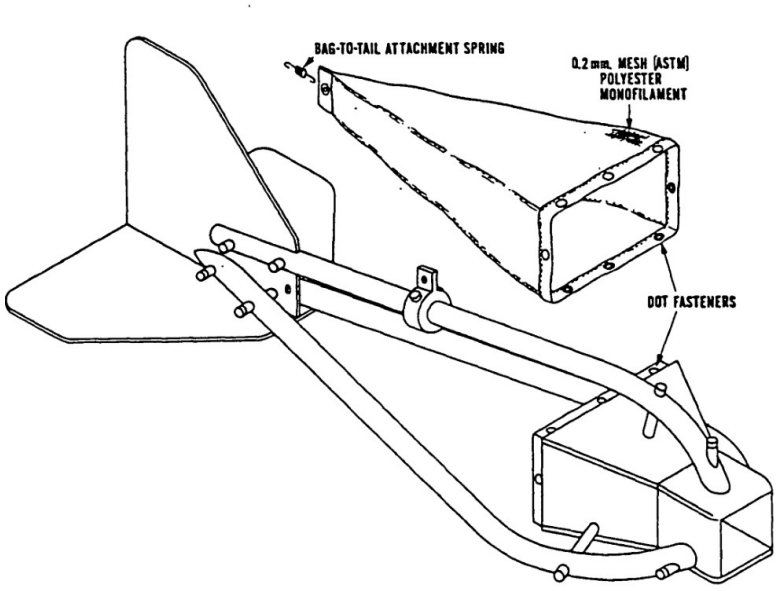

Figure 4: Helley-Smith Sampler (Helley & Smith, 1971)

The nozzle is designed to sit directly on the stream bed to ensure complete bedload sampling. The mesh bag is made of a polyester monofilament mesh to allow water to pass through while collecting both coarse and fine sediment. The sample is then removed by turning the sampler on its head. The mesh bag is designed to be removed, however, the material of the mesh allows the sediment to be removed easily by inverting the sampler. Due to the need to remain stable in high flows, the original Helley-Smith sampler was rather heavy with a mass of approximately 30 kg. Currently, different sizes of samplers are available, however, they have the same approximate weight to ensure stability in the stream. As such, these samplers often require the use of a bridge or over-hanging structure to deploy properly.

Limitations of the Helley-Smith sampler include the limited sampling area compared to a stream's cross-section area. Due to the small entrance nozzle, a sample is only being taken in a very small portion of the stream cross-section. Additionally, the requirement of having either a small crane or a bridge to deploy the Helley-Smith sampler limits its usability. Finally, the sampler can only be used for a limited amount of time before the bag fills. As such, monitoring an entire flood event is exceedingly difficult. Despite these drawbacks, the Helley-Smith sampler is still used today as, in certain cases, it is a viable form of tracking bedload transport.

2.1.2.2 – Slot Sampler

A secondary method of direct bedload sampling includes the installation of a box with a small entrance hole into the bed of the stream. As shown in Figure 5, small slots would be dug into the bed of the stream for the sediment to fall into, leaving the rest of the stream bed undisturbed (Hubbell, 1964). These are referred to as slot samplers. A slot of 100-200mm in width was found to capture nearly 100% of the bedload passing overtop (Hubbell, 1964).

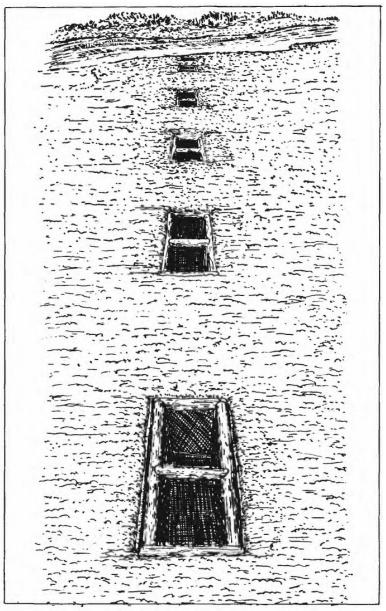

Figure 5: Slot sampler as depicted in Hubbell (1964)

Issues with early slot samplers included the need to dig these slot samplers into the bed of the stream resulting in significant disturbance to the streambed. In addition to the significant disturbance, once a slot sampler was full the sample needed to either be dug out or pumped out during low flow. Finally, it is difficult to discern when the sample was collected as the sampler is permanently in place and could not be removed or closed. Since the original design several researchers have attempted to rectify these issues.

To combat the issue of unknown timing of the sample, Reid and Frostick established a bedload sampler with a pressure-pillow at the base (1986). The pressure-pillow was filled with water and would continuously record the internal pressure with a pressure transducer. When compressed by deposition of the sampler, a signal would be sent to a manual logger to record the magnitude of compression and the time the deposition was occurring. A cross-section view of the slot sampler can be seen in Figure 6.

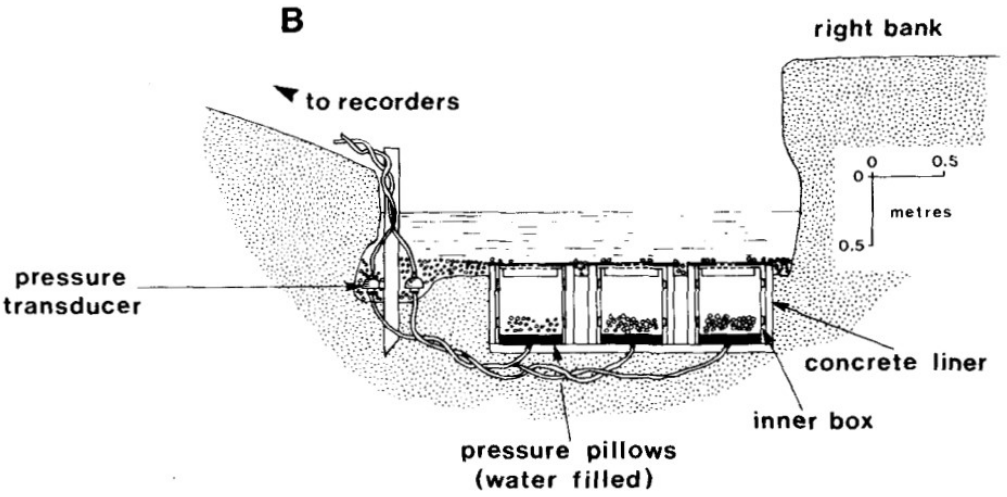

Figure 6: Slot sampler with pressure pillows (Reid & Frostick, 1986)

Harris and Richards expanded on previous work to establish a bedload sampler with an electronic data logger (1995). Instead of requiring wires to travel to a recorder the pressure was recorded on the data logger before being retrieved for analysis. The slot sampler also included a removable box with rollers to ensure ease of removal of the sample.

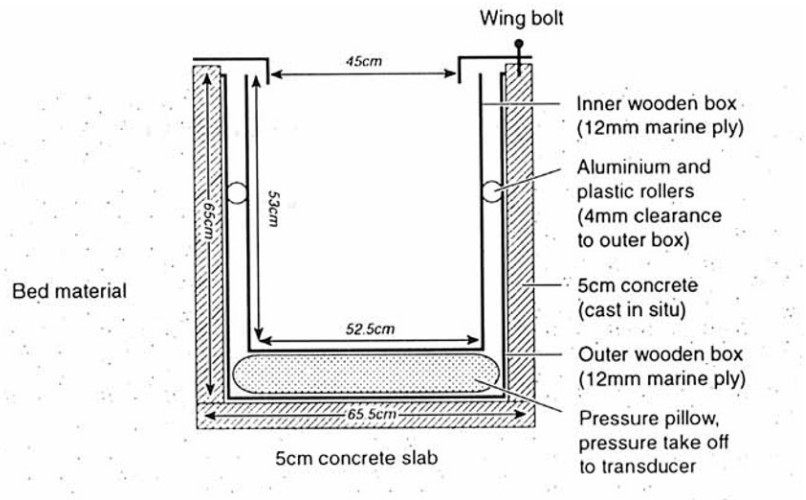

Figure 7: Automated recording slot sampler (Harris & Richards, 1995)

While an improvement from the previous design, the water-filled pressure pillow had significant sensitivity to changes in temperature as well as the potential to be damaged during sampling. As such, Lewis designed a system which included a load cell instead of a pressure-pillow which was compressed as the sample was deposited. This load cell was "essentially an

electronic strain gauge" connected to a data logger allowing for continuous monitoring with regards to the timing of deposition (Lewis, 1991). A cross-section view of the new design is shown in Figure 8. The load cell was successful in reducing the amount of noise produced by fluctuations in temperature or other unexpected stream mechanics.

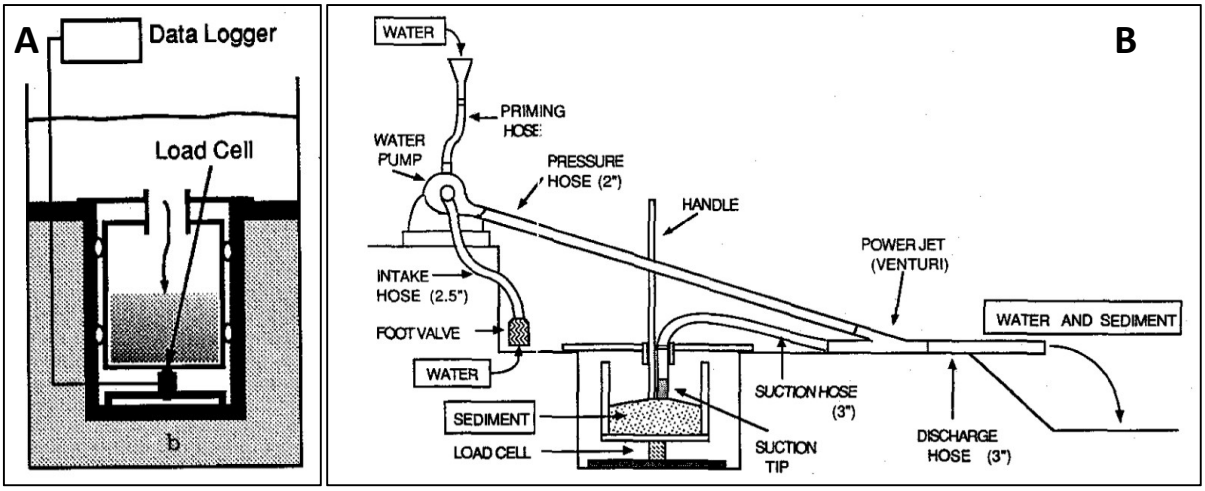

Figure 8: (A) Slot sampler with a pressure pillow to record the deposition of material. (B) Sediment removal mechanism (Lewis, 1991)

In addition to monitoring when the slot sampler was being filled, Lewis also designed a system of removing the sediment during a storm event. Due to the low flows of the field site, workers were able to be suspended above the river during the flood to operate a suction hose. The sample could be pumped to a discharge location for analysis later. By removing sediment from the sampler Lewis ensured the ability to capture the entire flood.

In an attempt to track bedload in real-time using slot sampler technology, Leopold and Emmett created a fully automated slot sampler which included a stream-wide slot in the channel with a moving conveyor belt below. The sediment would fall into the slot, as is typical of slot samplers, before being carried out of the channel area to a weigh station. Figure 9 depicted simplified engineering drawings of the entire design with Figure 10 showing the eventual installation of the mechanical slot sampler.

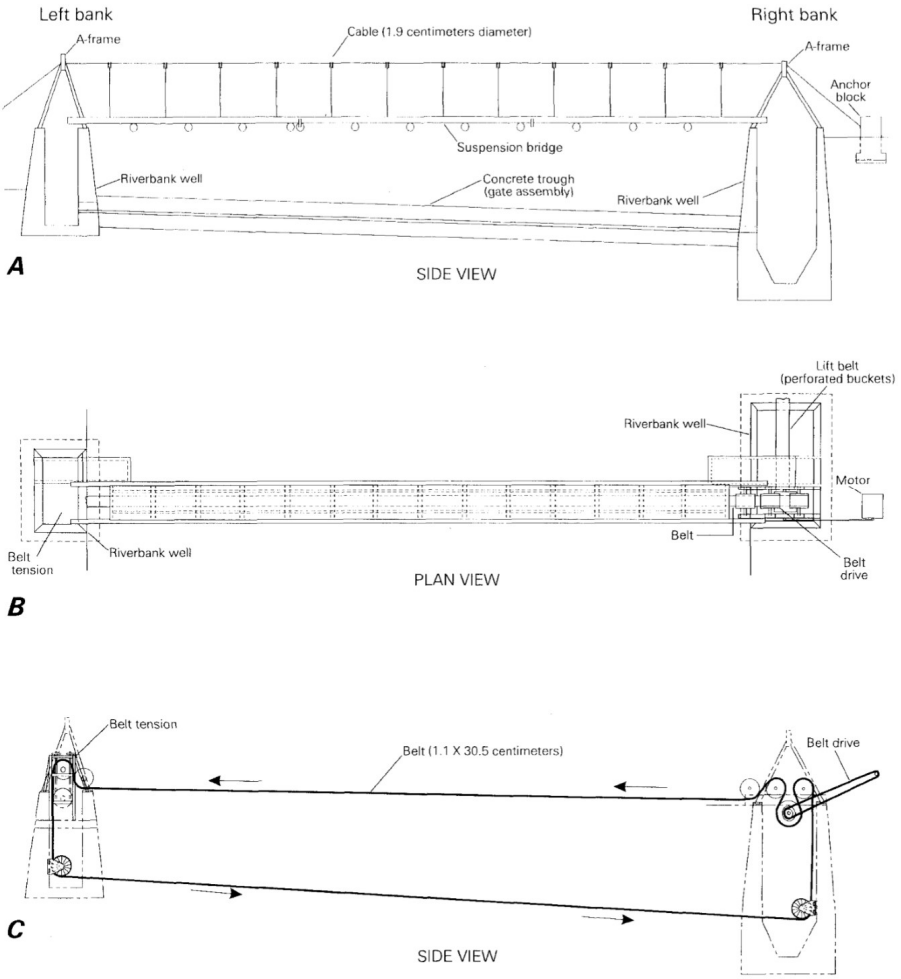

Figure 9: Simplified engineering drawings of bedload slot sampler designed by Leopold and Emmitt (1997)

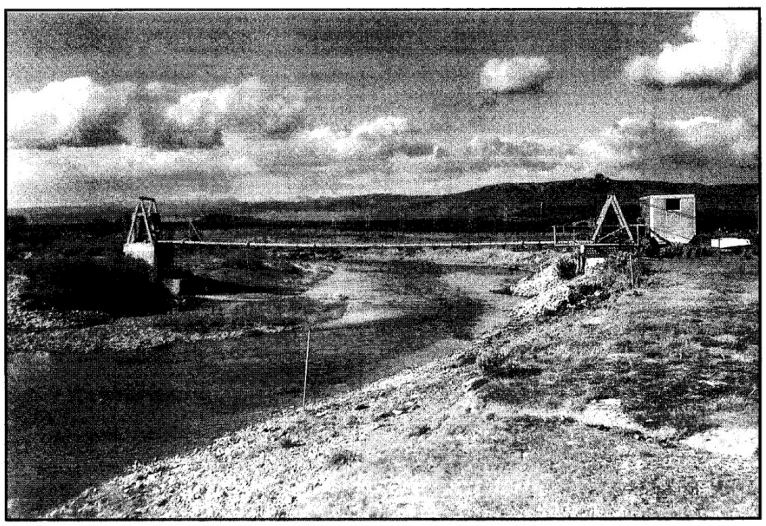

Figure 10: Installed Leopold & Emmett mechanical slot sampler

While the sampler functioned for 114 days and collected usable data for quantifying bedload transport in the East Fork River, the design was not implemented again due to the large construction costs and limited reuse value. As such, the issue of slot samplers completely filling with bedload before a flood event has finished has yet to be resolved.

While certain issues have been unable to be solved, such as filling during a flood event and the general invasiveness to the stream bed, slot samplers are still currently being used to quantify bedload transport. Studies such as Laronne and Reid (1992) and Cohen and Laronne (2005) have used slot samplers to track bedload transport in ephemeral streams. Additionally, Lucia et al. (2013) and Garcia et al. (2000) have used slot samplers to quantify bedload transport in steep streams with both sand and gravel beds.

2.1.3 – Indirect Monitoring Methods

As mentioned previously, indirect methods of bedload monitoring include the use of a surrogate to estimate the bedload transport of the river. While the assumption of a surrogate representing the bedload transport of a stream has the potential to be inaccurate, if the surrogate is chosen correctly, indirect tracking methods can be just as effective as direct methods. Additionally, by using a surrogate, indirect methods can remain non-invasive to the stream bed. Examples of surrogates to be discussed in this thesis include geophones, hydrophones, seismic sensors and acoustic doppler for measuring virtual velocities.

2.1.3.1 – Geophones & Impact Plates

The term geophone simply refers to a device which measures the amount of vibrations present in the ground or on the surface due to a disturbance (Ion Products, 2018). Geophones are common in many different applications around the globe including mining safety and seismic activity monitoring. Consisting of a magnet and a coil of wire, the magnet reacts to vibration around it while the coil remains stable. The movement of the magnet results in an impulse which can be used to measure the magnitude of the vibration (Rickenmann et al., 2012). For bedload monitoring, geophones are connected to steel plates which are inserted into the bed of the stream. As the bedload travels over the plate (also know as an impact plate) the impact of particles with the plate creates vibrations in the geophone, allowing for calculation of bedload transport. Figure 11 is an example of a geophone implemented in a stream study.

Figure 11: Geophone placed in the Erlenbach stream (Rickenmann et al., 2012)

While experiments to determine the sound generated by bedload particle movement have been occurring since the early 1930's (Mulhofer, 1933 from Bogen & Moen, 2003), it wasn't until the early 2000s when a geophone was used to measure bedload transport in a natural stream. Bogen & Moen first explored the topic, creating a sensor with an acoustic sensing device, a signal amplifier, a high/low pass filter and a digital signal processor (2003). As a similar time, Richardson et al. were creating a self-described "impact sensor and impact plate" for implementation in a natural stream (2003). Using an acceleration sensor, this technology also measured the impact of bedload on the plate above to determine the amount of bedload transport in a stream. The sensors can then be placed side-be-side across a cross-section of the river as shown in Figure 12.

Figure 12: Geophone installation across a channel (Habersack, et al., 2016)

The example in Figure 12 includes flat impact plates, however, there has been a separate type of geophone developed by a group out of Japan called the Japanese Pipe Geophone (Mizuyama et al., 2010a, Mizuyama et al., 2010b). Instead of relying upon impact sensors to record vibrations, a hollow pipe is placed along the bed of the stream. A microphone is placed within the pipe allowing for recording of the acoustic sounds of bedload passing over the pipe. Field studies showed promising results for calibration, however, a long-term study is yet to be published.

The technology of geophones is robust and has the potential to collect data for >10 years (Hilldale et al., 2015). While the installation and removal of the system does require disturbance of the stream bed, the depth of a geophone in the stream bed is significantly less than that of a slot sampler. In addition, a geophone can collect measurements across the entire cross-section, unlike a slot sampler. The main issue associated with geophones as a technology is the correlation of impact signals to bedload transport. Figure 13 shows 2 graphs depicting the attempted calibration of data in 2 separate studies using geophones.

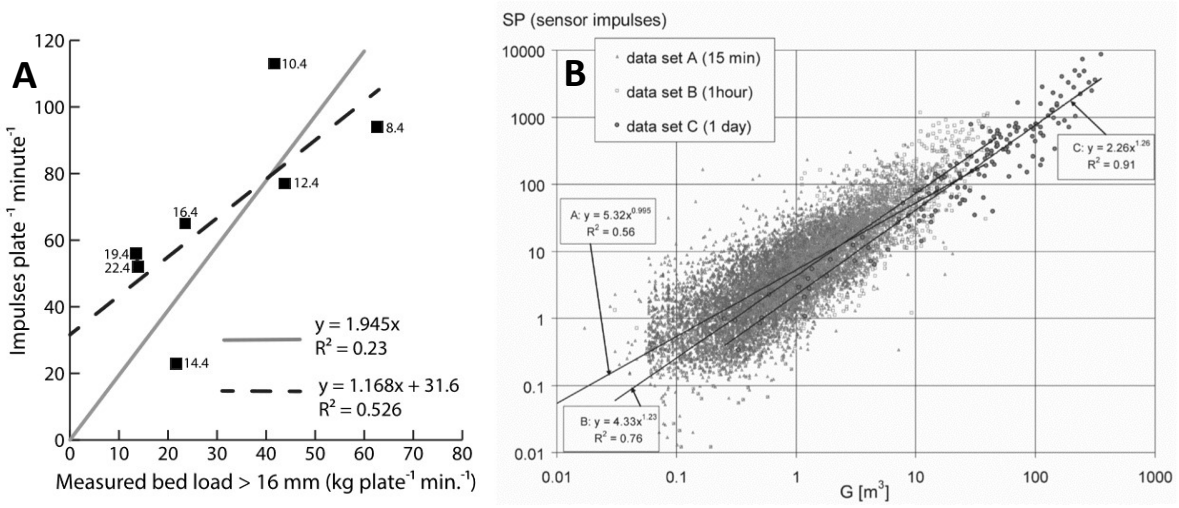

Figure 13: (A) Calibration chart for impact plates in the Elwha River, Washington, USA, (Hilldale et al., 2015). Dashed line denotes the best-fit linear regresion while the solid line depicts a linear regression from the origin. (B) Calibration data from Rickenmann & McArdell (2008). G is total sediment load.

As can be seen above, the correlation of bedload impulses to total bedload is an inexact science and requires significant calibration data to do so. Hilldale et al. (2015) performed calibration in-stream which resulted in significantly less points to calibrate from while Rickenmann & McArdell (2008) calibrated their sensor in a flume. Additionally, since there is limited standardization of the sensors being used, each geophone installed would likely have a unique calibration curve associated with it. Each river also has a set of unique characteristics, different from other streams as well as flume environments adding an additional complexity to calibrating a geophone. Geophones calibrated in the field would likely rely upon one of the direct sampling methods mentioned previously to calibrate. Once the geophone is calibrated, there will also be significant post-data collection processing which must occur to determine the bedload of the stream. Finally, geophones do not have the ability to differentiate between different particle sizes, only the total bedload of the stream.

2.1.3.2 – Hydrophones

A different method of indirectly continuously monitoring bedload in a stream is using a hydrophone. A hydrophone uses acoustics to passively record self-generated noise. Unlike the Japanese geophone, where the microphone is encapsulated with a pipe, the hydrophone is simply held in the stream by a fixed frame attached to the side of the river. Figure 14 demonstrates a hydrophone in use in the Isere River.

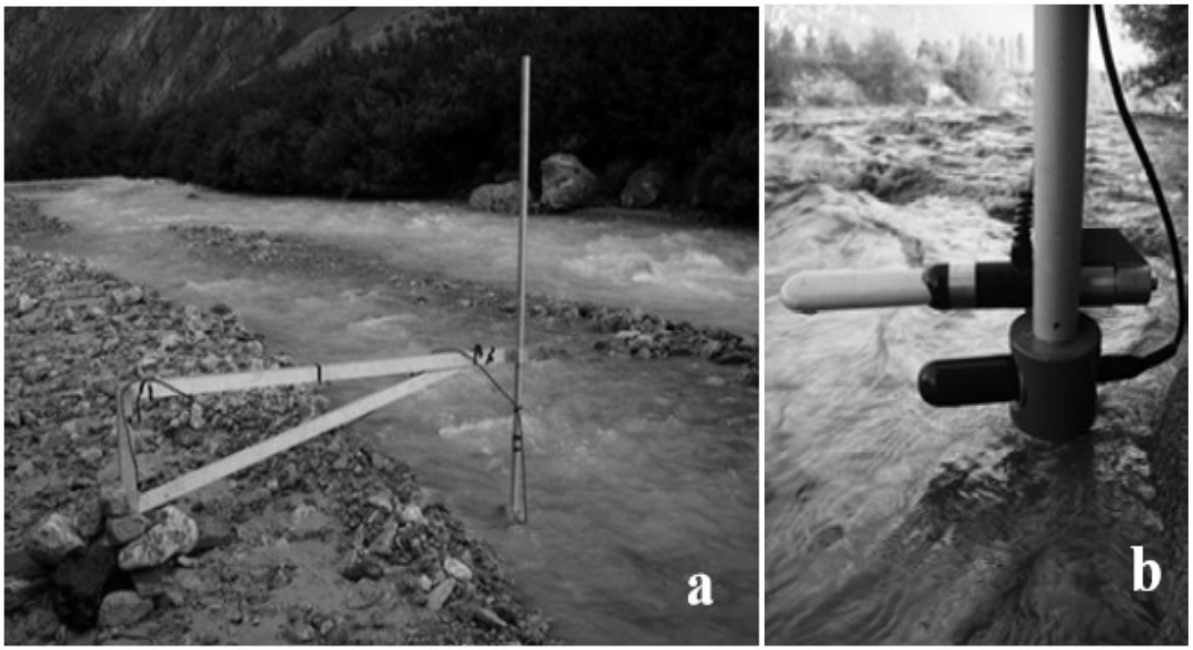

Figure 14: Hydrophone put in place by Belludy et al. (2010)

Limited research has been performed using hydrophones to measure bedload transport however, the research performed has found similar limitations as geophones. These issues include a significant amount of calibration required to track bedload, no tracking of individual particles as well as significant post-data collection processing. While a promising concept, there needs to be significant research to continue the development of the technology.

2.1.3.3 – Seismic sensors

One of the more radical idea for measuring bedload in a natural stream includes the use of seismic sensors placed around the stream bed to measure the subtle vibrations caused on the stream bed by moving bedload particles. Two main studies have been performed to test this technology; Burtin et al., 2011 and Schmandt et al., 2013. In these articles, seismic sensors were dug into the ground in an area surrounding the stream. While the seismic sensors were able to record differences in seismic activity during periods of high flow, Burtin et al. (2011) found there were too many variables to accurately predict the bedload transport from the data. Issues noted included the impact rain had on the seismic activity as well as the impacts of a nearby road, and rising water levels. Both studies were performed in remote areas as an urban environment would likely have far too much disturbance for a sensitive measurement method such as seismic sensors.

2.1.3.4 – Other Methods

Another method for bedload transport monitoring is the use of acoustic Doppler current profilers (aDcp) to measure velocities at the bed of the channel. Comparing aDcp with conventional bedload transport methods has resulted in high correlation values suggesting aDcp could be an effective indicator of bedload transport (Rennie et al., 2002). However, this study required significant calibration to produce effective correlation when compared with direct sampling methods. Gaeuman and Jacobson (2007) also found aDcp correlated well when compared to bedload transport rates determined through the assessment of dune migration.

2.2 – Bedload Tracking Technology

As different from sampling and monitoring methods, tracking bedload incorporates the use of tracer particles. These tracer particles are used to determine the movement of individual particles without removal of these particles from the streambed. Bedload tracking technology can take the form of painted clasts, magnetic tracers and RFID transponders as examples. Each of these methods of tracking will be discussed in the following sections.

2.2.1 – Painted Stones

One of the original methods for tracking individual clasts in a natural channel included painting the stones prior to placing them in the river. As a relatively simple method of identifying stones for tracking, painted stone tracking has been taking place for at least 50 years (Leopold et al., 1966). The methodology behind tracking painted stones includes identifying a grain size distribution to track. Which grains to use as tracers is often based on a pebble count of the reach in question. The method of matching grain size distribution of the study reach is a common practice for each method of tracking individual particles.

Once the particles have been identified they are marked with a bright, non-natural colour paint. Brightly coloured paint allows for easy retrieval at later dates. While this particle tracking method was effective when there were limited other options, the drawbacks of painted tracer studies are numerous. Limitations include; disturbance by human activity (the tracer particles stand out to anyone walking by the river); the inability to identify with certainty which specific particle each painted stone is; abrasion over time leading to mis-identification and; the inability to find the stone once it is buried under even a thin layer of gravel. Despite these limitations, painted stones are the simplest form of tracking individual stones and if used properly can be effective. Recently, Milan (2013) placed 288 painted stones in the River Rede to characterize virtual velocity of tracers.

Recovery rates of the painted stones began at 70-80% over the first several surveys but dropped below 40% by the fourth survey.

2.2.2 – Magnetic Tracers

One of the first methods to replace painted stones for tracking bedload transport in natural streams was through the use of magnetic tracers. Magnetic tracers provided three key advantages over painted tracers; (1) the ability to detect stones beneath a surficial layer of sediment; (2) remain unaffected by abrasion over time allowing for longer studies and; (3) limited human intervention since the stones look similar to other natural stones in the river. In one of the first field tests of magnet-embedded cobble, Ergenzinger and Conrady (1982) placed a stationary coil in the bed of the stream as shown in Figure 15. Additionally, this field test was one of the first tests which allowed for tracking in-flood movement of individual particles.

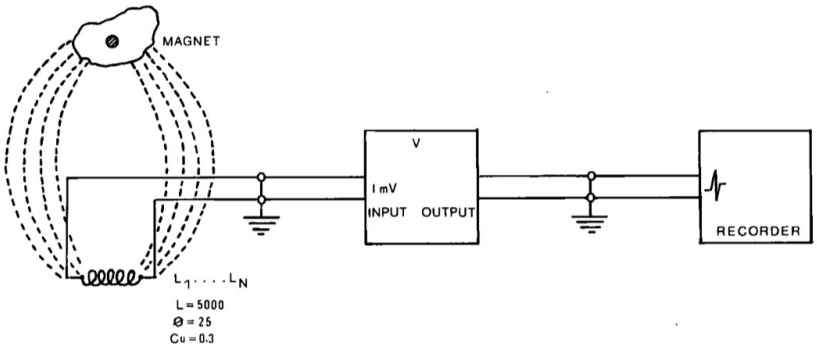

Figure 15: Schematic of communication between magnet-embedded particle and recording device

Magnetic tracers are easier to find after a flood event than magnetic stones, allowing for longer, more comprehensive studies. Gintz et al. (1996) was able to continually track magnetic tracers for 3 years including 13 tracking events with the final tracking event having an 88% recovery rate of the particles seeded. In another study stating the durability of magnetic tracers Papangelakis et al. (2016) tracked magnetic tracers once a year for 10 years with recovery rates ranging between 77-88% each year.

While magnetic tracers were an improvement upon painted stones, several key issues still exist. The main issue is the inability to differentiate between individual stones. Each stone is detected without a unique marker or identification. Papangelakis et al. (2016) dealt with the lack of a unique identifier during detection by picking up (or digging out) each stone before identifying

it. Removing the stone results in minor disturbances to the bed material which could affect the mobility results.

2.2.3 – Other Methods

Another method of tracking individual clasts was done so by Schmidt and Ergenzinger (1992). In combination with the use of iron and magnetic tagged particles, radio-transmitting tracers were used to gain more information surrounding rest periods and travel lengths of particles. Figure 16 displays the equipment used to track the radio-transmitting tracer. As a method of inserting the tag into the stone, a hole was drilled into a natural stone. A tag with a magnetic coil was then inserted, and the hole was filled with a resin mixture to seal the hole. The tag inserted into the stone was 30mm by 16mm and included a battery for transmission purposes. The tags would remain in constant communication with the receiver in order to track movement. The stones were active for two summer field seasons before removal of the system.

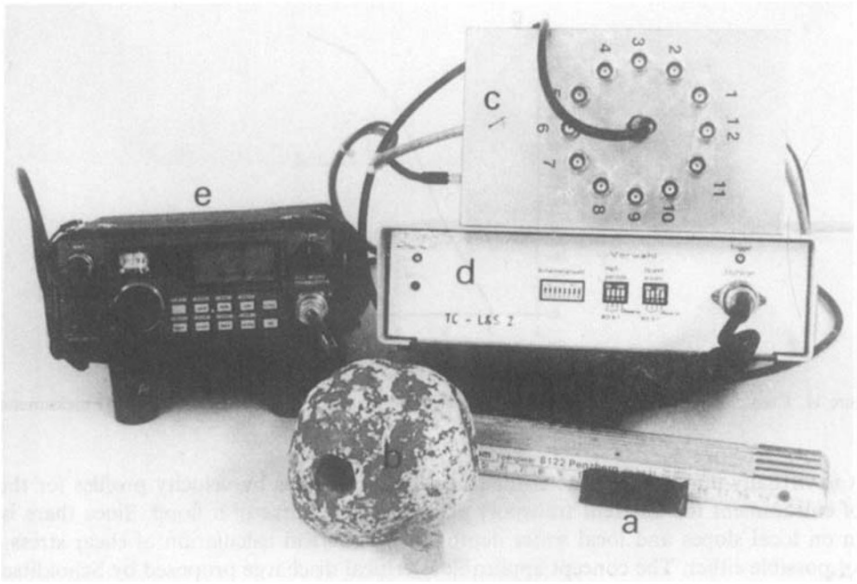

Figure 16: Radio transmitting tracer particle set-up from Schmidt and Ergenzinger (1992)

Another unique example of tracer particle tracking is Houbrechts et al. (2011) where the researchers tracked iron slag particles previously dumped in the river by industry up until the 19th century. Based on the historical locations of the ironworks sites, the iron slag was traced back to its origin point, allowing for an indirect calculation of movement in the stream bed since ironworks stopped.

2.2.4 – RFID Technology

RFID technology is an expanding form of tracking the movement of a wide variety of objects from cars and trucks to wildlife. It has become increasingly popular as a method of tracking bedload sediment as well. The history of RFID technology and relevance to bedload tracking will be discussed in the following sections.

2.2.4.1 – History of RFID Technology

The core of RFID technology is the ability to send a radio wave from an antenna to a device and receive a response which will identify the device. RFID technology has been around for many years, in many different applications. The first example of RFID technology being implemented was during World War 2 when the British government developed a system to identify if a plane was friendly or not (Violino, 2005). An antenna on the ground would send a signal to the plane. A device on the plane would then activate and send a signal back with a unique identification code, thus allowing the operator to determine if it was friendly or not. Development of the technology continued through the 1950s and 60s as researchers began experimenting with RFID technology as an anti-theft system and a method of unlocking doors (Violino, 2005). The technology continued to develop and is common today in many different areas including tracking shipping containers, identifying trailers as they enter as well as exit a facility and animal tracking (Violino, 2005).

2.2.4.2 – Passive & Active RFID Technology

There are two main types of RFID technology; active and passive (Violino, 2005). In a passive system, the RFID device will receive a signal from an antenna, charging the magnetic coil within the tag. Once charged, the transponder will then send a signal back to the antenna reader including the identification. In order to send and receive a signal, the reader must send a pulse to charge the coil. It will then switch to a "listening phase" waiting for a response. These phases will continue to oscillate as the reader searches for tags. Figure 17 displays a passive 12mm PIT tag sold by Oregon RFID. While detection distances depend on the antenna being used, a 0.5m loop antenna results in a detection range of approximately 0.7m for 23mm tags (Chapuis et al., 2014). This detection range can increase or decrease depending on the size of the tag, orientation of the tag and the size of the antenna.

Figure 17: 12mm Passive Integrated Transponder Tag. Taken from Oregon RFID (June 3rd, 2018)

In an active system, once the device receives the signal from the antenna, it will send its own signal back to the antenna with no charging required. As such, active systems will require a battery to run while passive systems rely on a magnetic coil to become charged and retransmit the identification code. Figure 18 displays an active COIN-HC tag sold by ELA Innovations. The COIN-HC tag is stated to have a detection range of 40-80m. This detection range will vary significantly depending on the equipment used to detect the tag. Previously, batteries of active tags were expected to last 1-2 years however recent studies place the lifespan of the COIN-HC tag at 8 years (Cassel et al., 2017).

Figure 18: COIN-HC active transponder tag. Taken from ELA Innovations (2012)

2.2.4.3 – RFID Applications

Animal tracking is one area which RFID tags have become increasingly more prominent, mostly using a passive technology instead of active transmission. Household pets can be RFID-tagged in case they are lost. Livestock can be tagged to see where they travel during the day and which feed trough they tend to eat from. The use of RFID tags has extended to many different species of wild animals from fish to mammals, birds and reptiles (Gibbons & Andrews, 2004). The first study to use RFID technology in wild animals was a fish study in 1983 by Prentice and Park. This study looked at the optimal location for implementation of a RFID tag as well as the

long-term effects of implementation on the animal and the tag. Animals are often caught and checked for a tag to determine their movement. In recent fish movement studies, stationary antennas placed in the bed of the stream have been used to determine the movement of Atlantic Salmon and other fish species through a natural river (Armstrong, et al., 1996 and Johnston et al., 2009). Johnston et al. were among the first to place a dense array of antennae in a natural stream to monitor movement patterns in and around a gravel bar.

2.2.4.4 – RFID Tags in Bedload Tracking

RFID technology was first introduced to bedload tracking as method of tracking individual particles in a streambed. RFID tracking of bedload began in the early 2000s as an alternative to magnetic tracing. RFID-tagged particles allowed for the unique identification of each individual stone without the need to remove it from the stream bed. The incorporation of a unique identifier greatly increased the data which could be collected as researchers could now determine which particles moved and where it moved to in precise terms. Most RFID tracking studies perform inter-flood tracking of the tracers after flood events. Inter-flood tracking helps determine the path lengths of particles during transport as well as the mobilization flows. However, inter-flood tracking also resulting in limited data during high flows. Some studies have begun to develop automated tracking systems. These studies will be discussed in greater detail in Section 2.2.5.

2.2.4.4.1 – RFID Advantages and Disadvantages

RFID technology has advanced individual clast tracking of bedload sediment from painted and magnetic tracers and is still in use today. Advantages of RFID can be summarized by the following points:

- Ability to track buried stones until the depth exceeds the detection range;
- Tracking of individual particles to determine path lengths;
- Easy to manufacture tracer particles; and
- Passive tags have no battery resulting in the ability to conduct lengthy studies.

While these advantages make RFID tracking a better option than painted or magnetic stones, there is still uncertainty which needs to be explored. One such uncertainty is the detection range of the tags. The detection range of passive tags was explored in depth by Chapuis et al. (2014). Experiments were performed to fully define the detection distance of vertical and horizontal tags while also quantifying the effect of burial depth, submergence and clustering. The

detection distance can vary greatly depending on whether the tag is vertical or horizontal. Figure 19 demonstrates the different theoretical detection zones for horizontal and vertical tags.

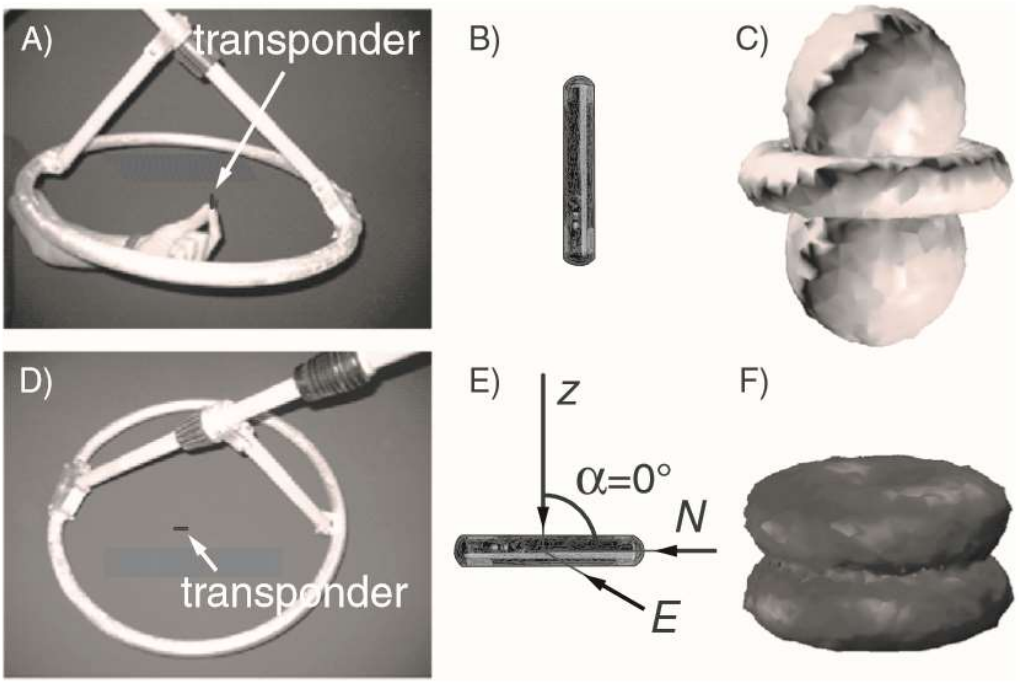

Figure 19: Detection zones for vertical and horizontal tags (Chapuis et al., 2014)

Chapuis et al. (2014) found burial depth resulted in no significant effect on detection range, matching previous work performed by Liebault et al. (2012). It was found that submergence and saturation can influence the detection distance, however, this reduced detection range can largely depend on the orientation of the RFID tag. If the tag is vertical, then submergence and saturation have an insignificant effect. However, a submerged horizontal tag can have up to 20% decrease in detection range when compared to a dry horizontal tag. Decreased detection when submerged is a clear disadvantage as most tracking of PIT-tagged stones takes place below the water surface.

Another significant issue raised by Chapuis et al. (2014) is collision. If multiple tags are within readable range the antenna will only detect the closest tag. In addition, if the tags are of similar range then their signal may cancel each other out, with neither tag being detected. Based on laboratory tests, Chapuis et al. (2014) demonstrated tags 0.8m apart experience a detection distance reduction of 50%. Considering the potential for clustering upon stone movement in a natural channel, signal collision can present a significant source of error with PIT tag studies.

2.2.4.5 – RFID Studies Performed

The use of PIT tags for tracking particles became increasingly common in the mid-2000s, starting with Nichols (2004). Nichols molded concrete particles around 32mm PIT tags to be placed in ephemeral streams in Arizona. All particles to be tracked were synthetically made to have a diameter of 57.2mm with the transponder placed in the wet concrete prior to the concrete solidifying. These particles were then tracked using an antenna and portable computer pairing as seen in Figure 20, producing a recovery rate between 94-98%. An example of the particles tracked, and the PIT tag used can also be seen in Figure 20B

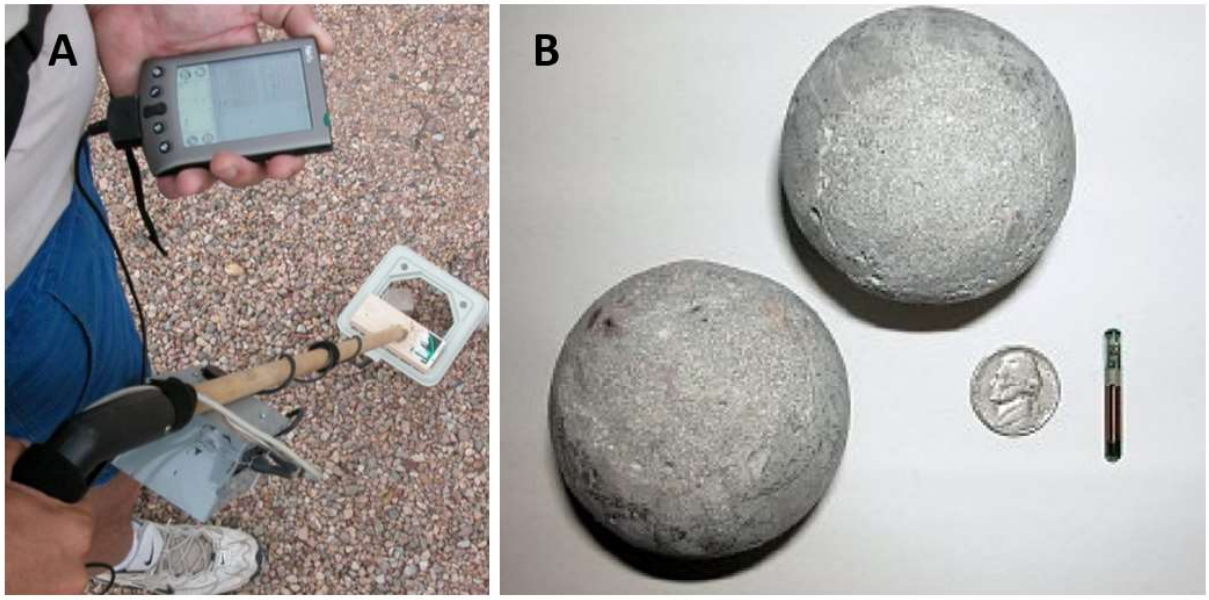

Figure 20: (A) PIT tag tracking system (Nichols, 2004); (B) Synthetic particles and RFID PIT tag (Nichols, 2004)

There are two main methods for creating PIT-tagged particles; creation of synthetic particles (as done by Nichols (2004)); and drilling of natural particles (Lamarre et al., 2005). Drilling of natural particles, likely taken directly from the stream bed, allows for complete replication of the natural bed characteristics in terms of size, shape and density. The stone is secured, and a hole is drilled with a hammer drill or a drill press along either the A or B axis depending on the size and shape of the stone. However, due to the force required for the machinery to create a hole for the RFID tag, the stones may break. It has been reported the rate of catastrophic failure of a drilled stone can be as high as 66% of stones drilled and breakage of stones increases the smaller the stone to be tagged (Slaven et al., 2014). Research has been performed to improve drilling methods in order to decrease the failure rate and allow for smaller stones to be tagged. The

smallest stone able to be tagged with an RFID transponder has been 23mm by Slaven et al. (2014). The tagging of this stone was achieved by incorporating a specific method for gripping the stones prior to drilling called the GABI method with a failure rate of 13% for stone smaller than 30mm. After the hole is drilled, the tag is sealed in place through an epoxy glue.

Figure 21: Example of the insertion method for RFID tags. (Leibault et al., 2012)

Creation of synthetic particles is a more complex procedure, requiring the correct mold and mixture to properly recreate a natural stone. When done correctly, synthetic particles allow the researcher flexibility to determine the precise grain size distribution of their sample size while inserting large or oddly-shaped transponders. However, issues in representativeness can arise if synthetic particles do not match the density and irregular size characteristics of natural stones. While drilling stones can be time consuming, synthetic stone creation can be significantly more labour intensive depending on the process and quantity of stones. One of the most successful studies to manufacture synthetic stones was performed by Cassel et al. (2016). In this study, the authors used a mixture of aluminum oxide powder and resin to create a stone with the density of 2.15-2.22 g/cm3 which is slightly below the natural pebble measured in the study (2.65 g/cm3) while matching sphericity of the natural pebbles.

Significant studies have been performed since Nichols (2004) proving the viability of PIT-tagged particles for determining bedload transport. These articles have been summarized in Table 1.

Table 1: Summary of recent RFID tracer studies

YEAR OF PUBLICATION	AUTHORS	# OF TRACERS SEEDED	ACTIVE OR PASSIVE	SYNTHETIC OR DRILLED
2004	Nichols	124	Passive	Synthetic
2005	Lamarre et al.	204	Passive	Drilled
2006	Allan et al.	400	Passive	Drilled
2007	Carre et al.	110	Passive	Drilled
2008	Lamarre & Roy	204	Passive	Drilled
2008	Lauth & Papanicolaou[+]	-	Both	Synthetic
2009	Curtiss et al.	48	Passive	Drilled
2009	Lauth & Papanicolaou[+]	-	Passive	Synthetic
2010	Camenen et al.	300	Passive	Drilled
2011	MacVicar & Roy	299	Passive	Drilled
2011	Miller et al.	515	Passive	Drilled
2012	Bradley & Tucker	893	Passive	Drilled
2012	Liebault et al.	451	Passive	Drilled
2012	Liedermann et al.	40	Active	Synthetic
2012	Miller & Warrick	209	Passive	Drilled
2013	Phillips et al.	300	Passive	Drilled
2013	Slaven	42	Passive	Drilled
2014	Bright	800	Passive	Drilled
2015	Arnaud et al.[+]	-	Passive	-
2015	Chapuis et al.	232	Passive	Drilled
2015	MacVicar et al.	443	Passive	Drilled
2015	Olinde & Johnson	1566	Both	Both
2018	Tritthart et al.	40	Active	Synthetic
2018	Hufnagel & MacVicar[+]	-	Passive	Drilled

Note [+] **- Flume experiment**

PIT tags have presented a significant advance from other particle tracking technology in most respects. The ability to determine exactly which particle moved from which position allows for the potential to analyze individual particle path length, travel distances and virtual velocity of

movement. The technology is continually advancing with active research on detection range and collision issues.

2.2.5 – In-Flood Bedload Tracking Methods

One way forward in the evolution of tracking tracer particles is using an array of stationary RFID-tracking antennae. The benefits of this system include many of the benefits from inter-flood tracking RFID stones including the ability to track individual clasts as they move down stream. However, a stationary antennae array would have the added benefit of recording in-flood data of the movement of bedload particles. Limited research has been performed on this technique, however, the studies which have been performed have been promising. The University of Iowa has done research on the use of stationary antenna with both active and passive tags to monitor bridge scour (Lauth & Papanicolaou, 2008, Papincolaou & Elhakeem, 2010, Moustakidis, 2012). While different from the placement of an antenna in a natural stream to track bedload, these studies performed proof-of-concept lab studies as well as a brief field study.

Schneider et al. (2010) performed laboratory studies to determine the detection range of tagged-particles and the proper orientation of the antenna for tracking bedload; pass-over or pass-through. The pass-over antenna was found to be the most effective antenna orientation.

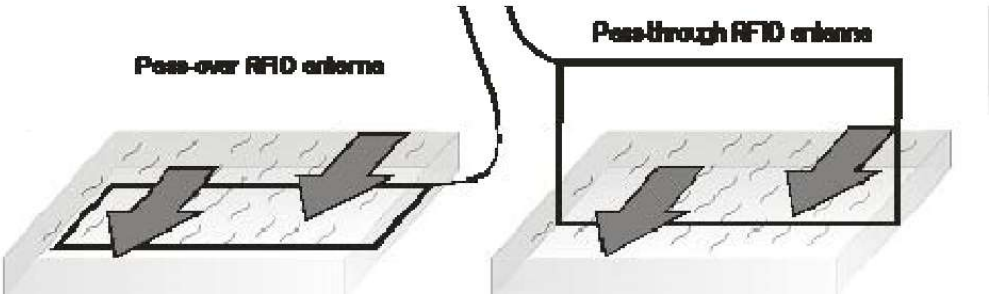

Figure 22: Stationary RFID antenna orientations (Schneider, et al., 2010)

In combination with the development of the antennae array, a stationary RFID tracking system must include a reader capable of communicating with multiple antenna and synthesizing the data. Hufnagel (2016) focused on developing an automated RFID tracking system with multiple antennae in a flume. The automated RFID tracking system included a cartridge which could move underneath the flume and detect RFID-tagged stones as they passed through the flume. After a review of multiple different options, Hufnagel (2016) determined the most efficient and

cost-effective method of communicating between multiple antennae is using the Oregon RFID Multiple Antenna Reader (MAR).

Hufnagel and MacVicar (2018) summarizes the research from Hufnagel (2016), specifically providing additional detection test data from the automated RFID flume carriage. The carriage was equipped with 12 RFID antennae connected to a 3 MAR in total. During a flume experiment, the carriage will move below the flume, detecting tracer particles in real-time during an experiment. The high density of antennae allowed for determination of the location of a RFID tracer to within ±1cm streamwise and ±3cm laterally.

Mao et al. (2017) took a further step in this research direction, implementing a stationary antenna system into the field. The field set-up included 4 pass-over style antennae in series. Initially, the antennae (composed of a simple loop of wire) were hammered into the bed of the stream and held in place using U-shaped rebar. However, 3 of the antennae were dislodged from the stream, leading the researchers to suspending the antenna over the top of the stream instead. To test the system, 636 passive RFID tags were seeded upstream of the antenna with the hopes of detecting the particles as they moved through the antenna array. From 2011-2013 there were 297 stones detected by at least one antenna from the array. Using backpack antenna readers in the summer of 2013, the researchers found another 103 particles which remained in the seeding reach and thus did not pass through the antenna array. There were 236 clasts left undetected. The authors hypothesize the tracers either became buried upstream of the antenna or passed through the study reach without a detection from any of the 4 antennae.

The creation of a stationary RFID antenna array has several key advantages over other bedload monitoring technology as well as inter-flood RFID tracking. When compared to other bedload monitoring technology with in-flood monitoring capabilities, a stationary antenna array requires minimal preparatory work before the system is functional. Geophones and hydrophones require significant calibration where as a stationary RFID antenna array will only require pebble counts and stone preparation to be functional. In addition, a stationary RFID antenna array can provide data on the location and velocity of specific stones through the study reach. Other bedload monitoring systems only capture the total bedload without being able to look at individual clast sizes.

In comparison to inter-flood RFID tracking, a stationary antenna array as the ability to provide in-flood data, allowing for greater precision when determining the moment of incipient motion. Additionally, in-flood data can provide more insight into the hysteresis effect which occurs during the rising and falling limb of a hydrograph. Finally, a stationary antenna array can significantly reduce the amount of field work required to monitor a field site.

2.3 – Summary of Research Gaps

Based on the information previously summarized, RFID technology is a viable method for tracking bedload, with limitations including inconsistent detection range and collision issues. Advancements in technology are required to improve the results from RFID tracking studies. Additionally, an RFID-based stream monitoring system would be an effective method to monitor bedload in an urban restored stream. A RFID-based monitoring system would allow for the tracking of individual particles to determine the effectiveness of the restoration. RFID technology is minimally invasive to the stream bed and therefore will not disturb the recent restoration efforts. Additional criteria for the RFID-based monitoring system include; durability to conduct a multi-year study and; the use a stationary antenna array to record in-flood tracking data and determine particle movement during a flood event.

Chapter 3.0 – Wobblestone Technology

Several issues associated with RFID stone tracking technology were outlined in Section 2.2.4.4.1 including detection range uncertainty. The following chapter will describe a new and innovative tracer design for ensuring consistency in the detection range of an RFID tag. While there are many different sizes of passive RFID tags, most common sizes for tagging bedload are either 23mm or 12mm long tags. Both size tags have been presented as have a 60cm read range, however, in a field test, the furthest detection possible with the 12mm tag was 52cm (Chapuis et al., 2014). Due to the ability to make smaller tracers, this section will focus on 12mm passive integrated transponder (PIT) tags.

Chapuis et al. (2014) demonstrated the detection range of RFID tags can be highly variable depending on the orientation of the tag and the antenna. In a separate study, the detection range of a horizontal tag compared to a vertical tag was shown to be reduced by 26-78% (Tsakiris et al., 2015). The reduced detection range can lead to difficulty determining the precise location of the tag while generally reducing recovery rates. The detection range of a 12mm tag in a laboratory setting when placed vertical versus horizontal is shown in Figure 23. As can be seen, the shape of the detection range transitions from a circular shape when vertical to a peanut shape when horizontal.

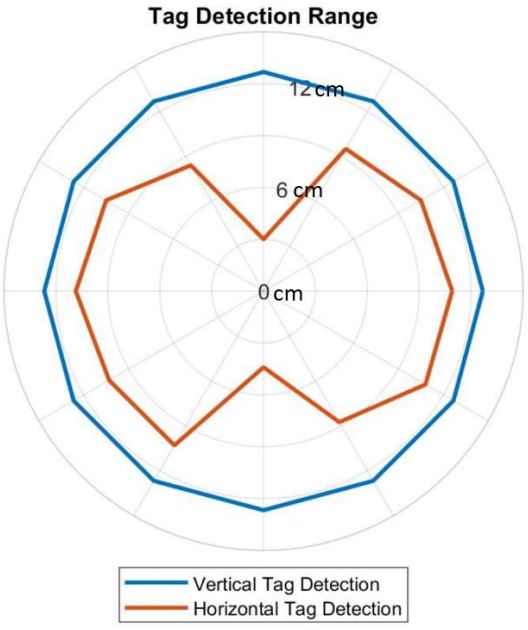

Figure 23: Vertical and Horizontal tag detection

While the reduced horizontal tag detection range is often not an issue when it comes to fish tracking (as they generally will be swimming roughly parallel to flow), tracer stones will come to rest in many different orientations. Due to the stochastic nature of rest position of the stones, a tag could end up vertical, horizontal or any angle in between.

An underutilized aspect of RFID detection is the relationship between the detection distance and the voltage of the detection. It has been found the voltage of the detection is inversely proportional to the distance between the antenna and the tag at the time of the detection (Tsakiris et al., 2015). Therefore, with a known orientation of the tag and the voltage return from the detection, the user would theoretically be able to calculate the distance from the reader to the tag with much greater accuracy. A consistent detection field would allow for significant advances in PIT tracking technology including determining the burial depth of the tracer while determining the location of the tracer with increased accuracy. The following sections will discuss the development of a new technology for ensuring a known orientation of a RFID tag inside a tracer particle referred to as the Wobblestone. Included in the design process was the construction of a SolidWorks model, prototype testing including the design as well as different lubricating processes, and the creation of a plastic injection mold for final production.

3.1 – Prototypes

To maximize the distance of detection and ensure a uniform detection range, the design must ensure the RFID tag remains vertical at all times. To achieve a consistently vertical tag, the design consists of a ball-within-a-ball. A conceptual model of the design can be seen in Figure 24.

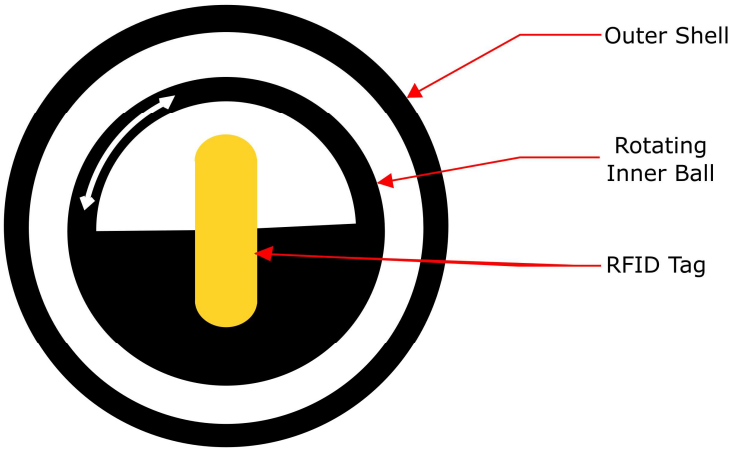

Figure 24: Conceptual model of ball-within-a-ball design. The white arrow demonstrates the rotating mechanism of the inner ball

The inner ball is weighted and a lubricant is applied between the two balls. This ensures that when the ball lands in a non-vertical orientation, the inner ball will rotate within the outer sphere so the RFID tag remains vertical. As stated previously, the 12mm tag will be used to construct a design which is as small as possible. The concept of a ball-within-a-ball design was first explored by Papangelakis et al. (in review). In this publication, a commercially available plastic ball was weighted using a resin-corundum powder mixture. A RFID tag was then inserted into the ball, creating a sphere which will always result in a vertical tag if allowed to rotate. A synthetic stone was cast around the ball by creating two halves, each with a cavity slightly larger than the ball in the center. Glycerin was placed in the cavity along with the ball and the two halves were sealed together, creating a tracer with a self-righting tag embedded. Issues with this design included the size of the commercially available ball (20 mm), variability of the size of the cavity within the synthetic stone and potential leakage of glycerin through the seams of the synthetic stone. The paper presented a potential solution to these issues through the creation of a customized 3D printed prototype. The design presented hereafter will build on this prototype.

Prototype designs were initially drawn in SolidWorks and constructed for testing using a 3D printer. The design specifications included the creation of a weighted inner sphere which includes the RFID tag and an outer sphere to allow for rotation. To do so, the outer sphere was first broken into two halves to allow both the inner sphere and lubricant to be placed inside. The entire design was built to be as small as possible to reduce the final size of the RFID tracer particle. The design of the outer shell is 18mm in diameter. A 3D printer printed several prototypes for testing at a relatively cheap cost. Prototypes were printed in ABS, Polycarbonate and a mixture of Polycarbonate-ABS plastic. The mixture of Polycarbonate-ABS produced the cheapest and most precise prototype and was used for all remaining 3D-printed prototyping since the initial printing. The 3D printer used was a Fortus 360mc printer made by Statasys, housed at the University of Waterloo. The cost per prototype came out to $5.14. This low cost allowed for the production of multiple prototypes including design changes. However, due to the small-scale nature of the design, the 3D printer used to print the prototypes could not create a smooth finish but instead left “levels” in the half-spheres. While these levels were smoothed as much as possible using a combination of fine grained sand paper, a file and a rotary tool, the curves of the spheres were often not entirely smooth, thus limiting the ability for the inner ball to rotate (Figure 25). The first prototype of the inner ball included a full sphere with a diameter of 12mm in order to exactly fit

the RFID tag. The first prototype design can be seen in Figure 25 after filing was performed to limit the effect of the leveling.

Figure 25: Prototype 1 of Wobblestone design.

To insert the RFID tag into the ball, a hole was drilled in both the top and the bottom of the sphere. The inner ball was weighted using a mixture of Aluminum Oxide and resin to ensure smooth rotation. The resin mixture used to weight the inner ball is discussed in greater detail in Section 3.5. To weight the inner ball, the bottom hole was plugged, and Aluminum Oxide mixture was injected into the sphere. Before the mixture could set, the RFID tag was put in place, sealing both holes. The lubricant was then applied around the inner ball before sealing the outer ball around the inner ball. Further details on the lubricant design are described in Section 3.2. The outer ball was initially sealed around the inner ball and held in place using external clamps. Upon testing the design, it was difficult to place the resin mixture within the inner ball without leakage while also ensuring it hardened in the bottom of the ball. Because of this shortcoming, a second prototype was developed.

The second major prototype split the inner ball into two halves, with one half containing a holder for the RFID tag (Figure 26). The split sphere allowed the resin mixture and the RFID tag to be placed within the inner ball more easily than the earlier prototype.

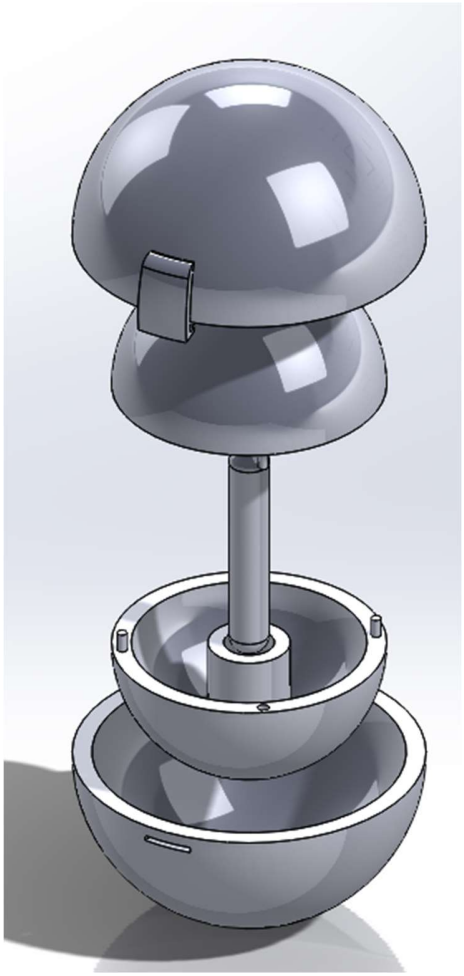

Figure 26: Prototype 2 with dowels on the inner ball

However, glue was necessary to seal the ball together and the user was always careful not to get any glue outside the inner ball or the glue would interfere with rotation of the inner ball. While the design alteration of splitting the inner ball into two halves worked well, the dowels and holes used to keep the two halves together were extremely small (1mm dia.). The small diameter of the dowel and accompanying holes presented a problem for the 3D printer and resulted in significant errors in the printed prototype, preventing the inner ball from being sealed properly.

The final prototype, Figure 27, used a ribbing edge instead of dowels to seal the two halves of the inner and outer balls together. The ribbing edge allowed the resin to be injected in an easy manner, the RFID tag securely placed inside and the inner and outer balls to be sealed efficiently.

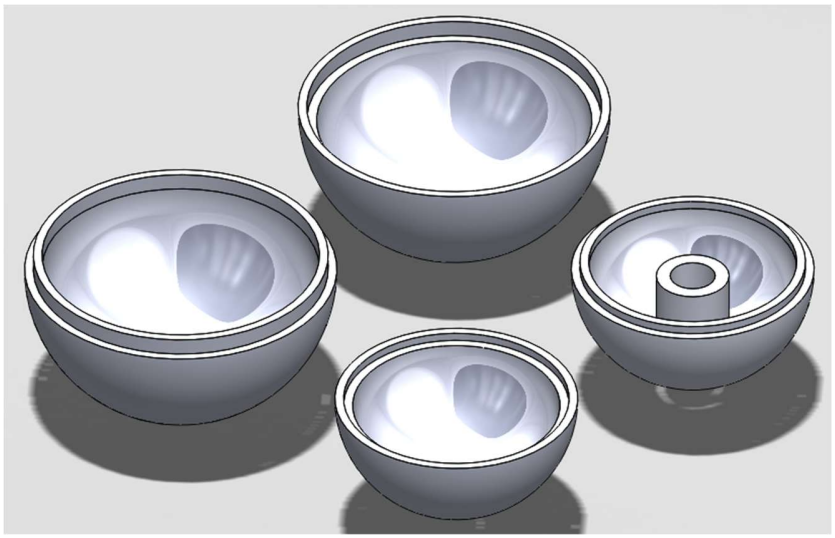

Figure 27: Final prototype of Wobblestone design

3.2 – Lubricant Design

Once the conceptual prototype design was finalized, several lubrication methods were tested. The criteria for the lubricant included the ability to be contained between the inner and outer shell, durability to withstand several years in the field through the winter and summer weather cycles and provide no interference to the transmission of the radio wave from the tag to the reader. As such, there were two main types of lubricants explored for this design; a glycol solution (wet lubricant) and a graphite mixture (dry lubricant).

3.2.1 – Glycerin Solution

Glycerin is a viscous substance which can be effective in lubricating a surface and allowing for easy rotation of the inner sphere. A 70% solution of glycerin and 30% water produces a solution with a freezing temperature of -38°C, allowing the solution to remain in liquid form in the field in all four seasons. Glycerin has no properties which would prevent transmission of radio waves. If the spheres are sealed properly the glycerin would not be able to leak or evaporate out of the design. To test this lubricant, the glycerin was added to the base of the outer shell after the inner sphere was sealed with glue. The inner ball was placed within the base and the top was then glued in place to seal the ball. Once the ball was sealed shut, the detection range of the ball could be tested. The advantages of using a wet lubricant include ease of lubrication and ease of procurement of the lubricating material. The potential disadvantage anticipated prior to testing included the potential for leaks if the ball was not entirely sealed, reducing the effectiveness of the lubrication.

3.2.2 – Graphite Mixture

As an alternative to a wet lubricant, a dry graphite lubricant was tested. Several dry lubricants were examined including graphite powder and several aerosol sprays. After examining the ingredients list and testing several prototypes, SLIP Plate No. 4 was decided as the best option as a dry lubricant. Criteria for selecting a dry lubricant included easy of application, environmentally friendly and durability. SLIP Plate No. 4 is an environmentally friendly, water-based dry film graphite lubricant and as such is safe for creating tracers for the field. Additionally, SLIP Plate No. 4 was applied as a liquid solution before it dried as a lubricating coating allowing for easy application.

Figure 28: Graphite lubricant used to assist in rotation of the inner ball (SLIP Plate, 2018)

This graphite lubricant contained no components which would reduce transmission of radio waves and, as a dry lubricant, it would be durable enough to survive outdoor weather cycles. The advantages of the dry lubricant included no potential for freezing, evaporating or leaking thus increasing the durability. The disadvantage included the tedious procedure to apply the dry lubricant and wait for it to dry before continuing.

3.3 – Prototype Testing

The lubricants were first tested using the final prototype design. Prototypes of each lubricant were created. The first test which was performed was a visual test. The lubricated inner ball was placed in the lubricated bottom of the outer ball and the inner ball was rotated to a non-vertical angle. Visually, the author was able to see the glycerin prototype rotate naturally while the graphite prototype did not rotate as smoothly and required shaking of the ball to fully rotate. With

this anecdotal evidence, the next step was to seal both prototypes for blind testing. Unfortunately, due to the 3D printing capabilities and the inability to make one solid structure, the glycerin mixture leaked through the prototype, rendering the glycerin prototype unmeasurable. The tests continued with the graphite prototype to determine the viability of the design. The sealed ball was placed in the center of a sheet of paper with the tag in an unknown orientation. A reader then approached the ball from 12 different angles to determine the detection limit. Once a test was preformed; the ball was picked up and rotated gently into another random orientation. 20 detection limit tests were performed on the graphite prototype and the results have been synthesized into Figure 29. The vertical and horizontal tag detection limits were performed with a bare RFID tag held in place using a paper placeholder.

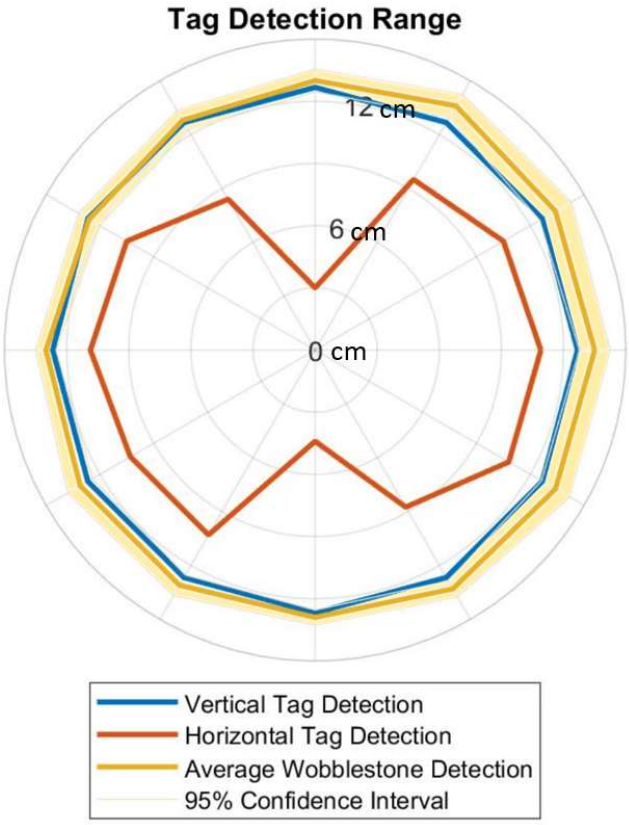

Figure 29: 3D printed Wobblestone detection limits

As can be seen, the average detection distance of the Wobblestone as well as the 95% confidence interval produced by the tests are very similar to vertical tag detection zone. This test, while inconclusive for the glycerin mixture, proved the viability of the design for a graphite lubricant.

3.4 – Mold Design and Injection Molding Procedure

Due to the cost of mass producing Wobblestones, the time to 3D print each stone and the inaccuracies created by the "leveling" of the plastic as it is put into place, a plastic injection mold was designed for full-scale production. Commercial injection molding firms were approached to produce the Wobblestone, however, due to the limited quantity required and the small volume of each part, the price to create a die for production significantly exceeded the project budget. Instead, the mold was designed for a desktop injection molding machine available through WATiMake at the University of Waterloo. In consultation with the licensed mold makers at the Machine Shop at the University of Waterloo, and using the specific mold making tools in SolidWorks such as Draft Analysis, Parting Lines, Parting Surface and Tooling Split, the SolidWorks model of the final prototype was used to create a mold. The design was mirrored, creating individual molds including a core (inner part of the design) and a cavity (outer part). Several key factors were considered in the creation of the mold including; draft angle of the sides, shrinkage of the plastic post-injection and ease of removal of the piece from the mold. Figure 30 is the bottom of the outer shell showing the results of the molding functions from SolidWorks.

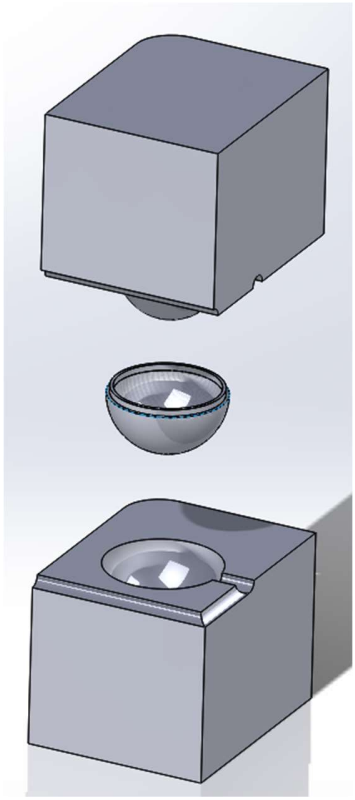

Figure 30: Mold created around the bottom of the outer shell

As can be seen, based on the dimensions of the original part, a mold is cast around with the inverse dimensions. After completion of the SolidWorks model, the Machine Shop provided several key modifications to be made manually to the final mold before manufacturing. First, all 4 components of the final design were combined into one mold for ease of injection. The combination of the 4 components can be seen in Figure 31.

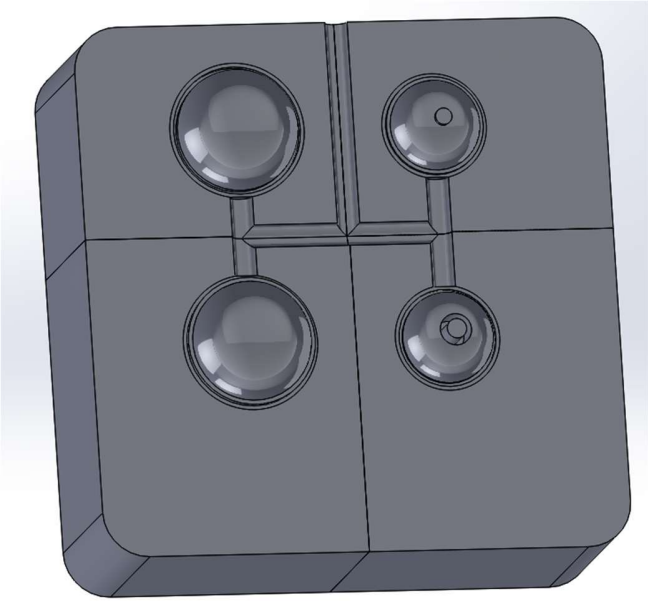

Figure 31: Core of the mold including runners for plastic injection

Second, the runners, the pipes for the liquid plastic to flow through to the piece, were designed with a diameter of 1/8" with a narrowing to 1/16" at the connection to the part. The narrowing is not shown in Figure 31 as this was done manually. The narrowing of the runner allows for easy removal of the part from the plastic "tree". The parts were also all located as close to the entrance as possible so that the runner lengths were minimized. Smaller distances of plastic travel helps to form a consistent and uniform part. In addition to these changes, several pins were put in place to ease the construction of the mold. In total, 5 pins were added to the core of the mold. These pins replaced each of the dome-shaped part of the core for the 4 hemi-spheres. The final pin was used in the base of the outer shell to aid in the creation of the RFID tag holder. A cross-section view of the inner shell base pins can be seen in Figure 32.

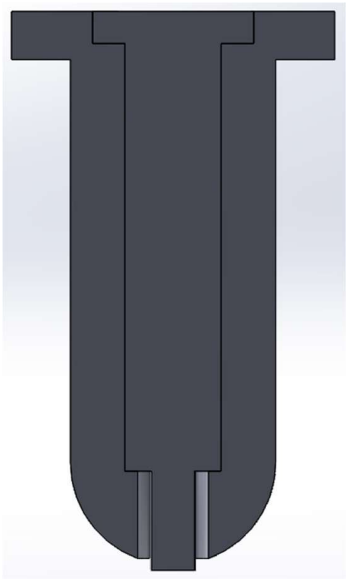

Figure 32: Double pin cross-section view

The final alterations were done manually by the Machine shop. These alterations included the addition of gas-release vents situated around each of the 4 parts. The gas vents allow for the release of any trapped gas as the liquid plastic is injected into the mold. A picture of the final mold including the gas-release vents can be seen in Figure 33.

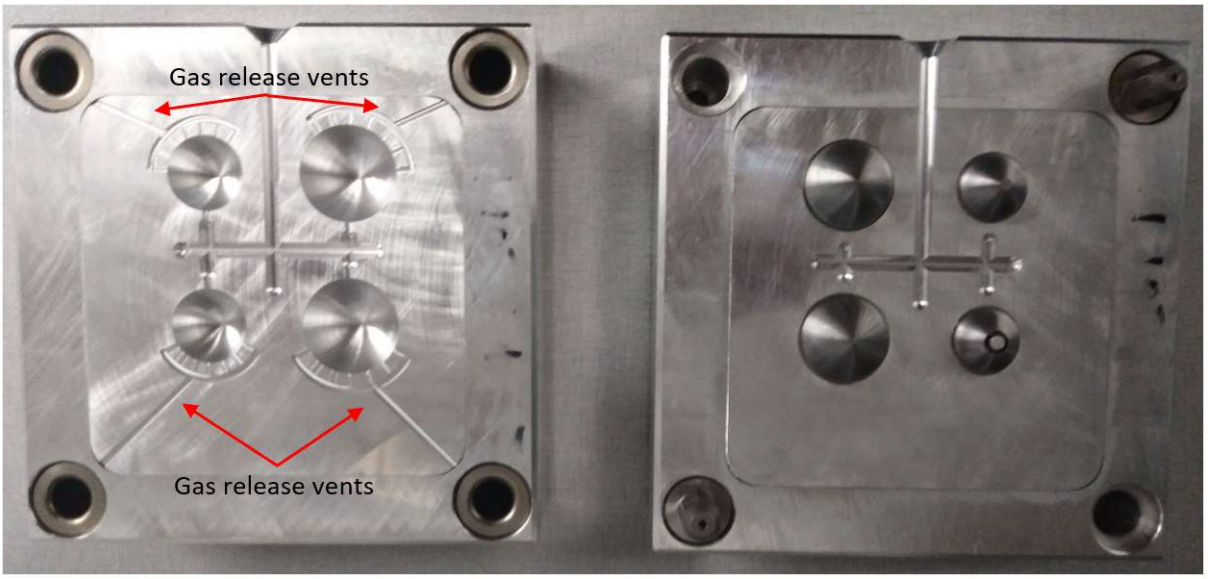

Figure 33: Wobblestone mold for injection molding of parts

The desktop injection molding machine (manufactured by MCP Equipment) is located in WATiMake at the University of Waterloo. The molding machine incorporated a heated cylinder

filled with beads of the desired plastic, two pressurized clamps to secure the mold in place and a hydraulic press to push the “shot” of liquid plastic into the mold. The heated cylinder could be heated to well over 400°F however, since the temperature was only being applied around the edges of the plastic, there was potential for non-homogenous heating of the plastic. As a result, the types of plastics to be used in this machine were limited to polystyrenes and polyethylenes. After an analysis of the plastics available for molding, both Low Density Polyethylene (LDPE) and High-Density Polyethylene (HDPE) were tested. The machine also allows the user to customize the pressure forcing the shot into the mold, the temperature of the cylinder as well as the time duration for the shot to be pushed into the mold. The longer the duration, the more plastic was pushed into the mold. Through trial and error, it was determined the optimal settings for LDPE were 60 kPa of pressure, heated to 440°F with a shot duration of 4s. The optimal settings for HDPE were similar with 60 kPa of pressure and a shot duration of 4s however a temperature of 400°F ensures the plastic will not burn. After comparison of the LDPE and the HDPE, it was concluded the HDPE is better material for this design as it is stiffer than the LDPE. To remove the part from the mold, a mold release spray was added to the mold prior to injection and a plastic tool was used to pry the plastic away from the mold. The injection molding machine used can be seen in Figure 34 along with a picture of an injection molded tree and completed Wobblestone.

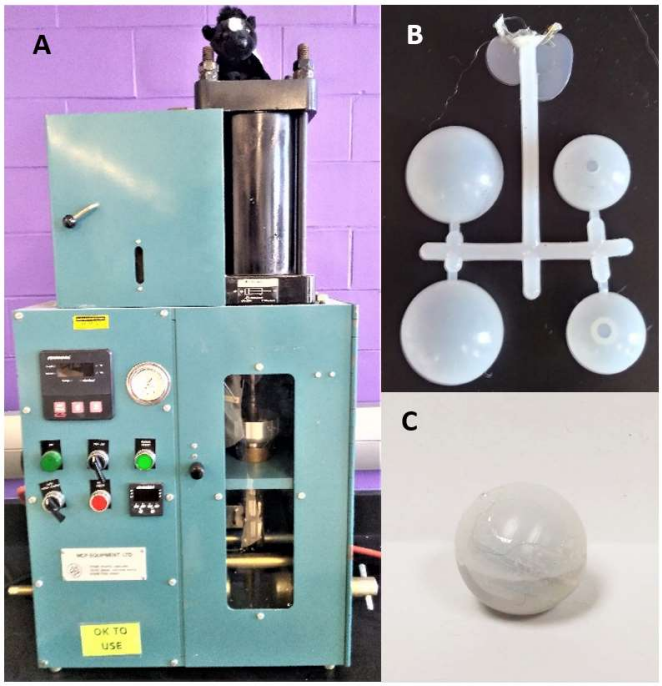

Figure 34: (A) Injection Molding Machine at WATiMake (B) Injection molded tree (C) Completed Wobblestone

The injection molded parts were significantly superior to the 3D printed parts. Advantages included one complete piece with no leveling, translucent plastic to see the ball rotate on the inside and more precise dimensions with no minor flaws as were found in the 3D printed versions. Once several parts were printed, the lubrication testing began once again. Due to the smooth sides of the injection molded part, the dry lubricant did not stick to the spheres and would instead pool and dry in the bottom of the spheres. Pooling of the lubricant was counter to the ideal of coating all surfaces evenly. Several prototypes were made including different locations of the dry lubricant. The detection ranges of each test including the location the lubricant was applied are shown in Figure 35.

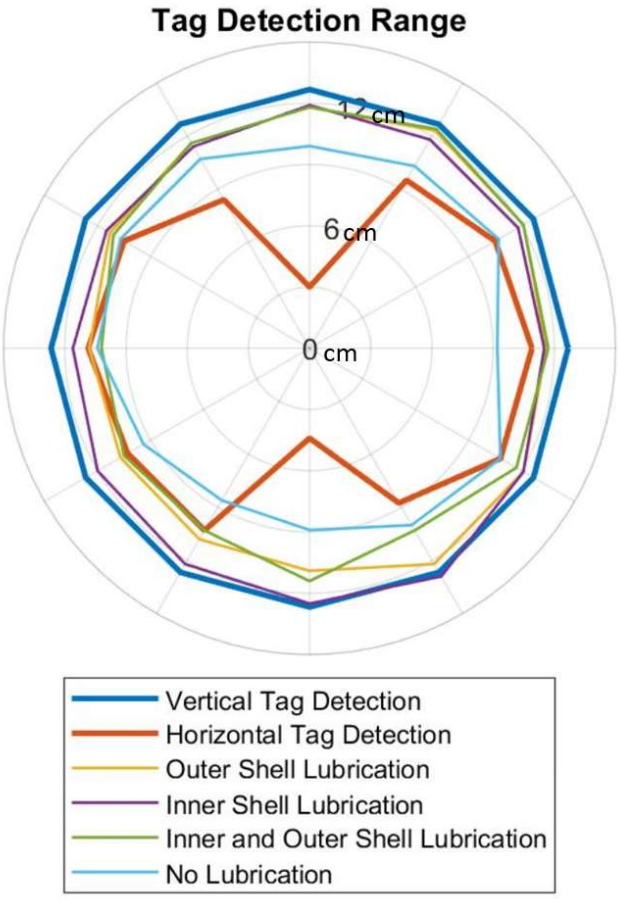

Figure 35: Detection limit test for lubrication testing

The tests were performed in the same manner as the previous detection limit tests with one change. Between tests, instead of gently picking up, rotating and replacing the ball, the ball was rolled briefly on the ground to simulate a rock moving down a stream. It was then picked up and

placed in the appropriate location for the test. The rock was left to rest for 1-2 minutes, allowing for the RFID tag to rotate fully on the inside of the shell. As can be seen, the average detection distance at each location was smaller than that of a vertical tag, indicating the inner ball would rotate fully only some of the time. The average standard deviation of the tests performed with the injection mold and the dry lubricant was 2.9cm compared to the average standard deviation from the 3D prototype test of 1.5cm. The high standard deviation of the detection range tests demonstrates the failure of the dry lubricant to produce a prototype with a consistent detection range.

Due to the issues with the dry lubricant, another prototype was made using the glycerin solution. Since the only known issue with the glycerin prototype was associated with the holes in the 3D printed prototype, the glycerin was reintroduced as a potential solution. 3 prototypes with glycerin as the lubricant were produced. The glycerin was added to the base of the outer ball prior to sealing the outer ball. Great care was taken to ensure even distribution of the glue around the outside of the outer ball to ensure no leaks could occur. This completed prototype was then tested in the same manner as the dry lubricant prototypes. All tests resulted in a circular detection range demonstrating the inner ball is rotating fully within the outer ball with an average standard deviation of 0.6cm. Due to the clear plastic, the rotation of the inner ball can also be confirmed visually during the testing procedure. As a final test to ensure viability of the prototype, it was placed in a freezer at a temperature of approximately -15°C. After 4 hours, the prototype was removed, and the detection test was performed again. The frozen tracer resulted in circular detection limits with a standard deviation of 0.8cm. Results from both the initial glycerin test and the frozen test can be seen in Figure 36.

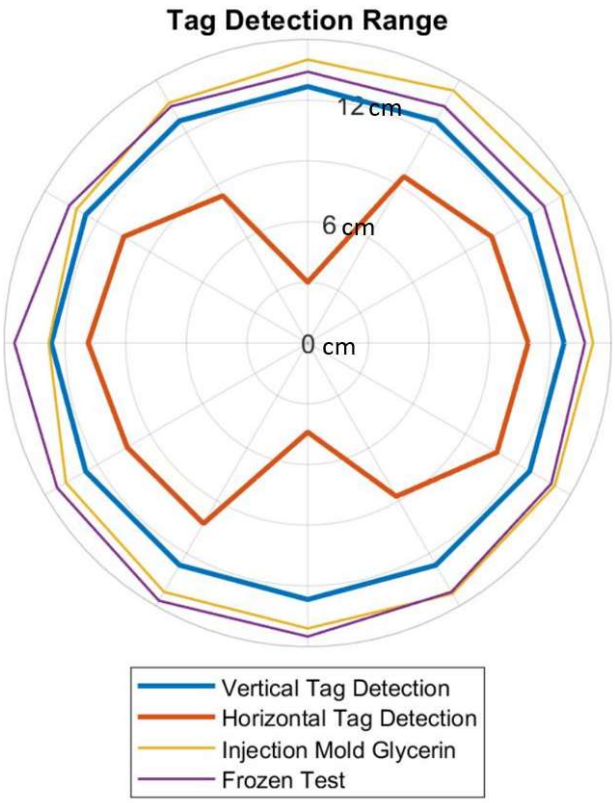

Figure 36: Injection Molded part Detection Range with Glycerin as lubricant

3.5 – Synthetic Stone Design

To create a fully functioning tracer, the injection molded ball must be inserted into a tracer particle. Due to the circular shape, a significant hole would have to be drilled into a rock to place this ball into a natural stone. The large hole required would drastically increase the required size of the stone to put a tracer in while potentially altering the density of the stone. As such, the Wobblestone technology is best used in the creation of synthetic stones around the outer ball. The method for creating these synthetic stones is outlined below.

The method used to create synthetic particles is largely adapted from Cassel et al. (2016). In this paper, Aluminum Oxide (also known as corundum powder) was mixed with a resin to create a synthetic stone. Corundum powder has several key properties which make it a viable option for creating a synthetic stone around a RFID tag. Corundum powder is non-magnetic, allowing the radio waves from the reader and the tag to pass through without impedance. Additionally, corundum powder has a high density (3.9-4.1) allowing the mixture with resin to create a synthetic stone with a similar density to natural stone. With a 4:1 ratio of corundum powder to resin Cassel

et al. (2016) produced a stone with a density of 2.15-2.22 g/cm3. Since the density of the synthetic stones produced by Cassel et al. was less than that of a natural stone particle (2.65 g/cm3), in a laboratory test the synthetic stones tended to travel farther than natural stones. However, the synthetic stones were able to survive abrasion with natural stones without failure, suggesting corundum powder is a durable substance for synthetic stone production.

To cast a synthetic stone around the injection molded particle, a stone was first taken from a local natural stream. A silicon mold was then created around the stone particle using Mold Star 15 Slow Platinum Silicon Rubber. Once the silicon had solidified around the stone, it was cut in half and the stone was removed, creating a pliable mold for casting synthetic stones in the shape of natural stones. The silicon and resulting mold are shown in Figure 38.

Figure 37: Part A and B of the solution used to create the silicon mold

Figure 38: Silicon mold used to create the synthetic stone

The methodology of casting a synthetic stone with the injection molded particle goes as follows. The resin used to hold the particle together was Smooth Cast 380. 1 part of the A mixture was mixed with 1 part of the B mixture to initiate a chemical reaction, solidifying the resin. As stated previously, the proper ratio of corundum powder to resin is 4:1. Once the correct quantity of corundum powder was added the mixture was stirred until homogenous. A sandy-clay like mixture was created. The mixture was then pressed into either half of the mold. Once each half mold was full, a small area in the center of either half was removed for the placement of the injection molded particle. The injection molded particle was then place inside the mold and the top half of the corundum powder mixture was placed on top, sealing the synthetic stone. To ensure proper cohesion between the two halves of the corundum powder mixture, a mass was placed on top of the silicon mold for 1 hour while the resin dried. Once the resin was dry the silicon mold was easily removed, and the final synthetic stone was complete.

Figure 39: Synthetic stone beside original stone. The synthetic stone is on the left and the natural stone is on the right.

Upon creation of the final stone, detection limit, durability and density tests were performed. Durability testing consisted of a fall from approximately 3 ft onto a concrete floor. While this test is more rigorous than any fall the stones would experience in the field, there was minimal to no damage to the stone after the drop. The density of the final stone with injection molded piece inside came to 2.30 ± 0.6 g/cm3. This density is greater than the densities achieved by Cassel et al. (2016) and falls within the density range of natural limestone (1.76-2.56 g/cm3) while remaining slightly below the density of natural granite (2.63-2.75 g/cm3) as well as the stone that served as the template for the mold (2.52 g/cm3). The detection limit test replicated the circular detection shape of a vertical tag indicating rotation. The average standard deviation

produced during this test was 0.7cm when unfrozen and 0.8cm when frozen. The results from the detection limit test can be seen in Figure 40.

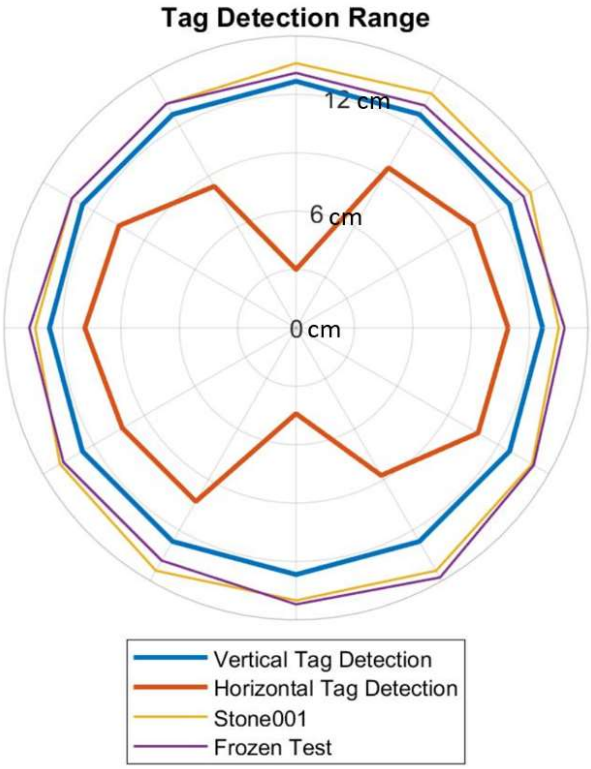

Figure 40: Synthetic stone detection range

The final test to be performed was a burial test to ensure sand or other soil would not disrupt the detection range. The stone was placed in a wooden sand box at increasing depths and the height at which detection occurred above the stone was measured. The results of the burial test can be seen in Table 2.

Table 2: Detection test results when Wobblestone was buried in sand

Burial Depth (cm)	Average Detection Height (cm)	Detection Distance (cm)
0.0	11.0	11.0
3.0	9.0	12.0
6.0	6.7	12.7
9.0	3.0	12.0
12.0	0.0	12.0

The Wobblestone design is a promising advancement in RFID stone tracking technology allowing for a uniform detection range and the potential for determination of burial depth and

precise location of tracers. Next steps for the technology include a field test and comprehensive analysis to determine the optimal methodology for determining burial depth of stones while in the field.

Chapter 4.0 – Design of RFID Bedload Tracking Station

This chapter outlines the development of a RFID bedload tracking system for measuring bedload mobility in an urban restored stream. RFID technology was used due to the benefits of being able to track movement of individual particles while presenting low frequency of lost particles. The ability to track individual particles provides valuable insight into mobility of clast sizes at different flow events. A stationary antenna array was incorporated to track particles during a flood event. Using a stationary antenna array provides insight into the moment of incipient motion as well as the mobility across the rising and falling limbs of the hydrograph.

This study uses Half-Duplex (HDX) RFID tags instead of Full-Duplex RFID tags (FDX). The difference between an HDX tag and an FDX tag lies in their communication with the antenna. An FDX antenna continuously sends a signal to the tag with the tag responding simultaneously (Oregon RFID, 2018). An HDX antenna instead sends a signal before waiting for a reply, resulting in asynchronous communication. While FDX tags can be manufactured smaller than HDX tags (8mm vs 12mm length), FDX tags also have a smaller detection range. Due to the difficulty of recovering stones once they are seeded in the river, HDX tags are preferred for RFID stone tracking due to their greater detection range. This chapter describes the components of a customized stationary RFID monitoring system for HDX tags.

4.1. – Overall System Component

With the goal of creating a customized bedload monitoring system for a restored stream the follow criteria were established:

- Use RFID technology to track individual clasts;
- Limit the manual labour required to track tracer particles;
- Record in-flood data of tracer stone movement.

These criteria were met through the creation of an array of stationary antennae placed into the bed of the stream, connected to a centralized box. The centralized box communicates with each antenna and records the data collected. The components of the system include; a commercially available multi-antenna reader; a Raspberry Pi controller; a float switch; a power source; and an antenna for installation into the bed of the stream. Figure 41 is a conceptual model of each of the components of the system. Each component will be discussed in greater detail in the following sections. This work builds on the research presented by Hufnagel (2016). Significant progress has

been made in creating the automated stationary RFID tracking system for field use, however, the system is not fully functional at this time. There are still several outstanding issues with the communication, specifically saving the detection data in the correct location. A summary of the current state of the technology will be presented in Section 4.6.

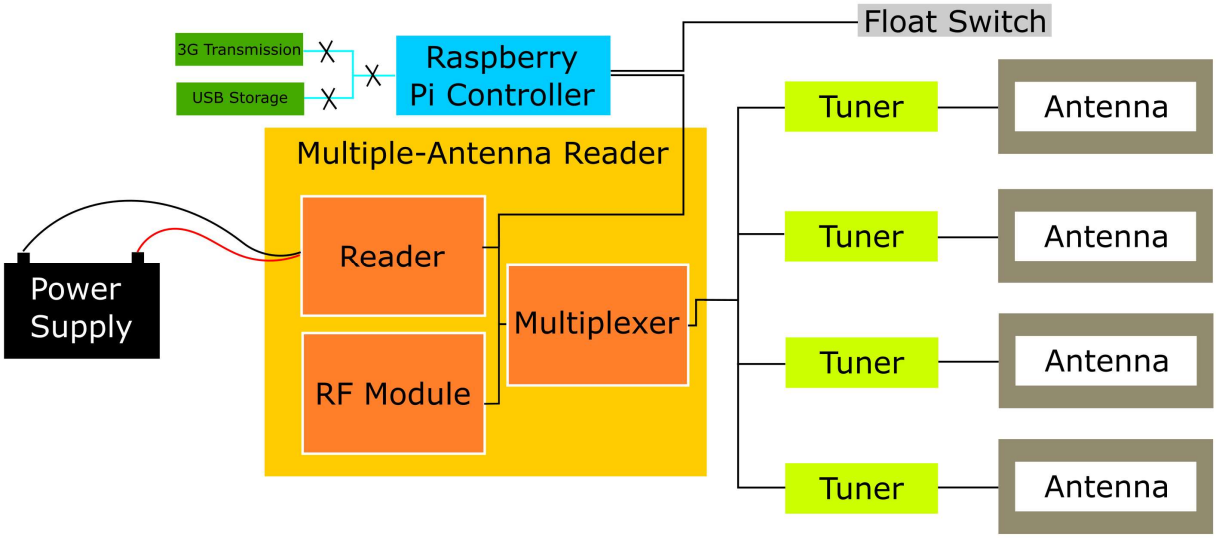

Figure 41: RFID Bedload Tracking System design. The connections which are not functioning at this time are marked in blue with an X

4.2 – Commercial Multi-antenna Reader

The centralized box used in this study to combine the signals from the antenna array must be able to power the antenna, receive signals from each antenna individually and record the data in a readable format. The Oregon RFID Multi-antenna Reader (MAR) is the most cost-efficient example of a commercial reader which can accomplish those criteria. The MAR, which can communicate with up to 4 antennae, consists of a multiplexer, Remote Antenna RF-module, and reader. The multiplexer and Remote Antenna RF-Module were previously produced by Texas Instruments as products RI-MOD-TX8A and RI-RFM-008B respectively. Texas Instruments has since sold the rights to manufacture these products to Oregon RFID. The reader is a customized circuit produced in-house by Oregon RFID. As such, the only method of obtaining these components is by purchasing a MAR through Oregon RFID. The MAR has previously been used in fish tracking studies across North America as method of determining the viability of fish passage effort (e.g. Steffensen, et al., 2013).

Figure 42: Oregon RFID Multi-antenna Reader (Oregon RFID, 2018)

The MAR is set up to communicate with HDX tags and thus emits a signal before waiting for a response from the RFID tag. The default settings for the MAR includes scanning for RFID tags 14 times per second, however, the read rate can be adjusted manually (Oregon RFID, 2018). As a by-product of having multiple antennae connected to one system, the MAR must scan each antenna sequentially. As shown in Figure 43, the default settings are for the MAR to send and receive a signal from antenna 1, followed by antenna 2, antenna 3 and finally antenna 4. It will then check antenna 1 again.

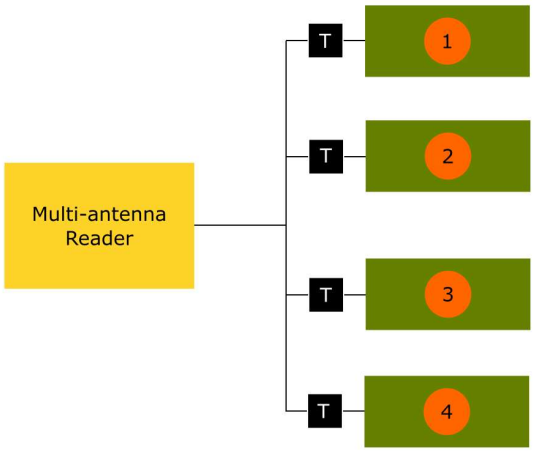

Figure 43: Antenna scan sequence

The result of the sequential scanning is that the overall scan rate of an individual antenna is equal to the MAR's scan rate divided by the number of antennae attached. Thus with 4 antennae

attached, each antenna will scan 3.5 times per second. The antenna can be set to scan up to 28 times per second, however, adjusting the scan rate too high can reduce the detection range to the RFID tag. The reduction is due to insufficient time for the capacitor in the RFID tag to charge fully when the antenna is farther from the tag and scanning for shorter periods of time.

The order of antenna scans can also be customized. If desired, the box sequence can be set to repeat a certain antenna more often than the others (e.g. A1, A2, A1, A3, A1, A4). Altering scan sequence can have a significant effect on the scan rate of individual antennas as you can ensure one antenna is being scanned consistently while scanning the other antennae less frequently. Once the MAR has received a signal, it records the date, the time of detection and the identification number of the tag. Figure 44 demonstrates the text format of a detection of an RFID tag. By default, the data is saved to an SD card in the MAR, however, the location the data is saved can be altered so that it is transmitted through the serial or USB ports in the reader module.

```
2014-04-24 00:51:45.99 00:00:00.00 HA      900_228000236374 A1   9    67 DETECT
```

Figure 44: Text line depicting a detection has occurred

In addition to recording the data automatically, the MAR has 4 lights for user feedback. A red light blinks consistently when the reader is on demonstrating the MAR is scanning for RFID tags. A second red light will come on to communicate there is an error scanning, detecting tags or processing data. A yellow light is associated with noise in the signal transmission. The greater the noise the less likely for a detection to occur. Finally, a green light will flash when a detection occurs.

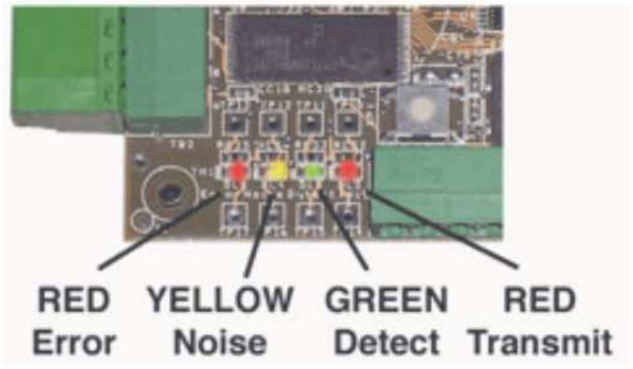

Figure 45: Lights present on the MAR for determining the function of the system (Oregon RFID, 2018)

As can be seen in Figure 41, the MAR requires a power source, an antenna and a tuner to track RFID tags. The power source and antenna are customizable and will be discussed in further detail in sections 4.4 and 4.5 respectively. The tuner can be purchased from Oregon RFID to work in conjunction with the MAR and there must be one tuner per antenna. Specifically, the tuner used for this design is the standard remote tuner board. The tuner board incorporates a series of capacitors which can be connected or disconnected manually to match the inductance of the antenna. Adjusting the active capacitors is done through the movement of a series of "jumpers" connecting different capacitors. Each jumper formation has an equivalent inductance which should be made to match the inductance of the antenna. Once the correct formation has been determined with the help of a Tuning Indicator, the inductance can be fine-tuned by turning the tuning slug with a ceramic tuning tool. Adjustment by the tuning tool helps to optimize the detection range and decrease noise being emitted from the antenna. Each antenna requires its own tuner and if an antenna changes shape for any reason it will need to be retuned.

While the MAR has been successfully implemented in fish tracking studies and flume experiments as previously mentioned, there has yet to be a field study of a stationary monitoring system using the MAR to track RFID stones. The lack of RFID stone tracking in the field using the MAR is due to several key gaps in the MAR's design, preventing it from being a plug-and-play solution. One issue is the power required to run the system. Several options exist for powering the MAR including plugging into an outlet (Steffensen, et al., 2013), running off batteries (Hufnagel, 2016) or using solar or another renewable energy source to power the device. A second issue with the MAR design is the method of collecting the data. The default method of storing data is within a data logger SD card within the box. This data however is difficult to access due to the inconvenient location of the SD card and requires someone to travel to the site location to collect the data. Both issues are addressed in the custom design summarized below.

4.3 – Raspberry Pi Controller

To control the MAR, a Raspberry Pi 3 (running Rasbian Jessie) was incorporated into the design. A Raspberry Pi was chosen over an Arduino UNO due to the ability to communicate data in formats other than HTTP and SMS, allowing for greater flexibility (Yu, 2016). Additionally, Python, the programing language of choice for the Raspberry Pi, is more common with a larger library of resources than C++ which is run on the Arduino UNO (Yu, 2016). The requirements for the Raspberry Pi controller were as follows:

1. Regulate power to and from the MAR, turning the MAR on and off as required; and
2. Receive the detection data from the MAR and transmit it into a more practical location for access by the end user.

As stated previously, currently the MAR receives transmissions from the antenna and stores the collected data on an SD card attached to the circuitry within the box in a very impractical manner. For this design, the Raspberry Pi attempts to collect the data before it reaches the SD card and either send it through the 3G network to a Dropbox account or save it to an easily accessible USB drive. In order to connect, a serial-USB connector was used to link the standard serial port in the reader of the MAR with the Raspberry Pi. The serial-USB connector is a DTEK USB to RS232 DB9 Female Serial Port Adapter Cable with FTDI Chipset and is shown in Figure 46. This cable can connect with a Linux based system without the need for additional driver download or set up.

Figure 46: Serial to USB connector

When the Pi turns on, a python code is set to run automatically in order to record and synthesize RFID tag detections. The code will recognize the MAR as the input and temporarily save all detections recorded while the system is on. When the system is set to turn off, prior to shut down, the Raspberry Pi will self-run a termination program, saving all detection data to the appropriate location. There are two methods for saving the data. If the code is to save the data to a USB drive it will locate the USB drive and create a new folder including the recording time period for safe storage. If the code is to transmit the data to a Dropbox account, the cell modem being used will be identified. The 3G modem will send a text file to a Dropbox account, allowing for near-instantaneous access of detection data.

As mentioned previously, there are several outstanding issues with the communication and saving of detection data. When the system is turned on, the box can detect a RFID tag and transmit

this data to the Pi through the Serial-USB convertor. However, the issue of having the code recognize the signal and implement the proper formatting and transmitting functions is one the author has been unable to solve at this time. The procedure outlined in the previous paragraph surrounding saving of the data to either a USB drive or transmitting through the 3G modem has not been able to be completed due to the communication issues between the MAR and the Pi.

4.4 – Power Supply

Power supply options for the MAR included: batteries, solar power, propane-generated power and an electrical outlet to the power grid. Due to the criteria of installing this system in an urban environment, both solar power and propane-generated power were not considered due to the high likelihood of tampering. The power supply system implemented must be easily concealed to ensure success in an urban environment. Another option would be to connect the box to a transformer and draw power from the municipal grid. While connection to the municipal grid is possible in an urban environment, it would require municipal approval, significant electrical wiring to connect and control of the flow of electricity while also limiting the potential locations for installation of the system. After these considerations, it was determined battery power was the most optimal power source for the system.

The MAR can be powered by a battery supplying power between 7 and 20V (Oregon RFID, 2018). A 12V marine battery was chosen because of its availability, capacity and ability to resist water. One issue with a battery power supply is battery life. A standard 12V marine battery provides 105-amp hours of capacity (Yu, 2016). Based on a wattage requirement of 32.4W drawn by the MAR at 12 volts, one 12V marine battery will power the box for 38.90 hours. It is clearly not feasible to be returning to site each day to replace the battery. Additionally, while connecting multiple batteries in parallel would increase the duration between battery replacement, it would also significantly increase the electrical wiring in the field which could be tampered with or damaged due to weather conditions.

To save power, a float switch was incorporated into the design to turn the system on and off. Sediment transport tends only to occur once the streamflow passes a critical shear stress value. The critical shear stress to generate mobility will vary depending on the stream but will occur during high water events. As such, the system will only need to be turned on when a flood event occurs. Float switches come in a wide variety of designs and sizes from floating arms to floats

around a central pole, rising and falling with water level. When the water level is low the "float" is at the bottom of the device. As the water level rises, the "float" rises as well, either connecting an electrical circuit or pulling up a mechanical lever depending on the float switch type. A float switch was chosen which would fit inside an existing pipe well used for water level monitoring (see Section 5.2.3 for further details). The float switch used is a compact liquid level switch manufactured by Omega model # LVK-150 (Figure 47). The float switch wiring is attached to a latching on/off circuit (Yu, 2016). Once the float switch has connected the circuit, the latching on/off circuit will turn the Pi on. The Raspberry Pi will then turn on the MAR and begins searching for tags.

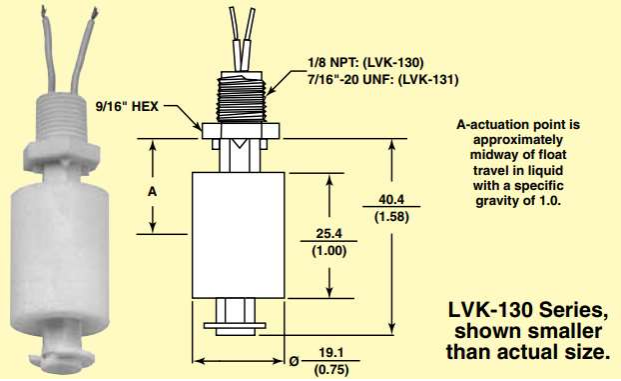

Figure 47: Float switch for turning the MAR on and off (Omega, 2018)

The circuitry required to connect the float switch and the Pi together consists of a Universal Battery Elimination Circuit used to convert the 12V battery power to 5V required to power the Pi. Additionally, a metal-oxide semi-conductor field-effect transistor (MOSFET) is used as a switch to control power to the Raspberry Pi when the float switch is connected versus when it is disconnected (Yu, 2016). When the float switch has been connected for any period of time the MOSFET switches to the ON position. When in the ON position, the MOSFET switches control of the circuitry from the float switch to the Pi. By controlling the circuitry, the MOSFET allows the Pi to determine when the circuit should be shut off while preventing any small decreases in water level from immediately turning off the system. When in the ON position, the Pi also has access to the float switch circuitry. Because of this access, the Pi can determine if the float switch is still connected or not. When it is time for the Pi to shut down, the Pi will cut power to the circuit, resulting in a discharge of capacitors within the MOSFET, switching the circuit to the OFF position.

Embedded within the Python code in the Raspberry Pi is a timer for checking the float switch positioning. Currently set to 30 minutes, once this time has passed the Pi will check if the float switch circuit is still connected. If the float switch is still connected it indicates a flood event is still occurring and the Pi will reset the timer, checking the circuit in another 30 minutes. Once the Pi detects the float switch is disconnected, a shutdown code will be queued resulting in a safe shutdown process. By checking the circuitry every 30 minutes the Pi is prevented from turning off the system due to random short-duration drops in water level during a flood event. Additionally, due to the timer, the antenna will remain on for up to 30 minutes after the water level has receded below the determine elevation of the float switch, ensure any transport occurring on the falling limb of the hydrograph will be monitored. The Pi takes approximately 1 minutes to turn on and 30 second to turn off. As such, if the Pi were to shut down accidently but immediately needs to turn back on due to a fluctuation in the water level, the Pi would take less than 2 minutes before it would be ready to track tracer particles again.

4.5 – Stationary Antenna

The following section will discuss the design of both the antenna wiring and the antenna casing. Based on specifications from Oregon RFID, the MAR can be used to service antennae up to 10m in length and up to 20m away from the MAR. If either of these values are exceeded, the noise generated by the low frequency radio waves becomes too great for reliable detection of RFID tags. Readers from Oregon RFID, including the MAR, have the capability to communicate with antenna with an inductance range between 8-80 μH. Inductance is the measured ability for an electrical component (i.e. coil of looped wire) to store energy. The flow of energy through a coil of looped wire generates electromotive forces, which in turn generate a magnetic field. The size of the magnetic field generated is dependant on the size of the loops, number of loops present and the thickness of the antenna wire. To properly communicate with the reader, the antenna designed uses Twin Axial cable, specifically Beldun Twinax with an impedance of 100Ω. An antenna with a length of 3.5 m, width of 0.4 m and 3 loops produces an inductance of 58μH, well within the range provided by Oregon RFID. Additionally, the wires had a 2.5mm gap between each wire to ensure the antenna remained within the inductance range, thus maximizing the detection range. The size and dimensions of the antenna should be adjusted depending on the size of river the antenna will be placed in; however, the previously stated dimensions were used to test the system.

Once the design of the wiring was complete, the next step was to design a casing for the antenna to ensure the design could be placed in the stream without damage during installation or over time. Mao et al. (2016) installed 3 antennae into the bed of the stream by placing the wires and hammering U-shaped rebar into the streambed around the wires. These 3 antennae all experienced issues remaining stable along the bed of the stream and were ultimately removed and reinstalled above the streambed to reduce the possibility of damage. The 4th antenna installed by Mao et al. (2016) was installed with an excavator in PVC pipes along the bed of the river and successfully remained in the streambed for the duration of the study. In addition to potential failure, loose wires allow for the shape of the antenna to change over time. A change in shape of the antenna can result in de-tuning of the antenna and receiver thus reducing the functionality of the system. The goals for the casing design included;

- A rigid design able to withstand all seasonal weather variations;
- Inconspicuous as to not attract attention in an urban environment;
- Able to conform to the bed of the stream including the entire wetted perimeter; and
- Easy to install without the need for heavy construction equipment.

The base of the casing consists of sheets of PVC with grooves machined in place to secure the wires as can be seen in the SolidWorks rendering in Figure 48.

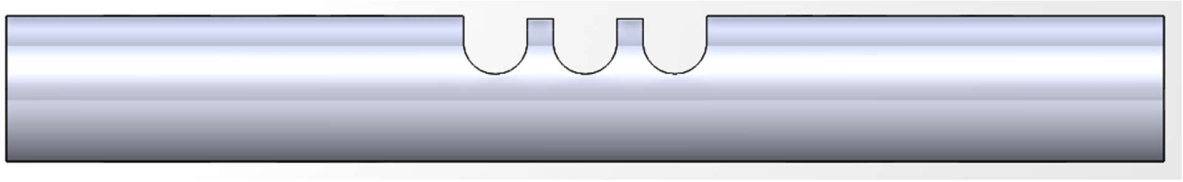

Figure 48: Machined grooves for electrical wiring. Grooves are 5mm in width, spaced 2.5mm apart. Casing is 12.5cm wide in total

Additionally, to ensure the ability to conform to the bed of the river, the casing was not one solid piece of PVC but instead consisted of 2 end pieces with multiple side pieces connecting these end pieces. While the antenna casing requires one of each end piece, the number of side pieces used is customizable depending on the width of the river in question and the size of the antenna design. An example of the antenna casing assembled with 3 pieces on either side is shown in Figure 49.

Figure 49: Assembly of antenna casing. Side pieces and end pieces are 75cm and 100cm long respectively

While the above rendering used 3 side pieces on either side it is possible to increase or decrease the number of components depending on the river width. To allow each piece of PCV to rotate to an appropriate angle, the connection points between each piece was rounded with either a concave or convex curve. As such, two pieces would fit together as a male-female connection, allowing for customized angled connections.

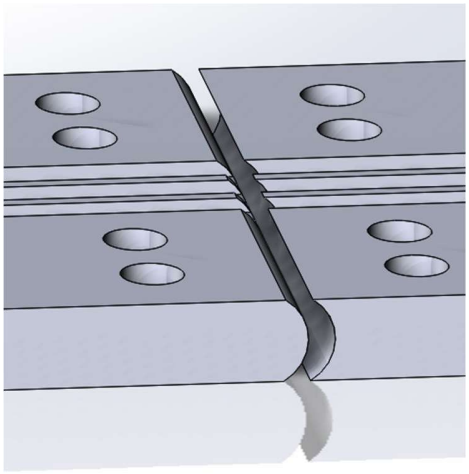

Figure 50: Connection between antenna casing pieces

The joints are then secured together with zip ties while the wires are glued into the machined grooves. Prior to securing the wires, it is necessary for a cross-section survey of the

location of the antenna to be performed to determine the approximate angles necessary for the joints. Further details regarding the installation of the antenna will be given in Section 5.2.2.

4.6 – System Summary

Previous sections detailed the design and construction of an automated RFID bedload tracking station using stationary antennae. As mentioned at the beginning of this section, while significant progress has been made in the creation of this station, there are several issues which remain unsolved. This section will go through the completed sections of the station design as well as the work which remains for a fully functioning system.

Completed work includes;

- Conceptual design of the modification requirements for the MAR;
- Implementation of a float switch and associated circuitry to have the system track RFID tags only during a flood;
- Communication between the antenna, the MAR and the Raspberry Pi using a USB-serial convertor cable and the Linux program “Screen”;
- Python code written to collect the data from the MAR, save it in the proper formatting and either save it on a USB drive attached to the Raspberry Pi or send it to a Dropbox account via a 3G cellular modem depending on the user preference; and
- Design and construction of antenna casing;

The work unable to be completed by the author to ensure a functioning automated tracking system includes;

- Linking the signal detection received by the MAR with the python code on the Raspberry Pi;
- Debugging the Python code to ensure proper data collection; and
- Perform a field test with both the antenna and MAR in place.

Chapter 5.0 – Schneider Creek – Case Study

During development of the automated tracking system discussed in Chapter 4, a field site was chosen to test the components as they were completed. The field site chosen was Schneider Creek in Kitchener, Ontario. Due to issues surrounding tag detection communication, the automated bedload tracking system was not installed in its entirety at the site during this study. Instead, this field study focuses on comparing preliminary bedload tracking results from the restored and natural sections of the river. The following sections will give an overview of the field site description, the installation of the automated tracking station components and bedload tracking results.

5.1 – Site Description

5.1.1 – Site Selection

Schneider Creek is a tributary to Victoria Park Lake in downtown Kitchener. The watershed leading to the reach in question is 3.54 km^2 in total area, consisting mostly urban development (70% urban infrastructure). The remaining 30% is composed of 24% agricultural land and 6% forested area (Ministry of Natural Resources and Forestry, 2018). In addition to the impervious nature of the upstream area, less than half up the upstream area has stormwater management. Upstream tributaries show signs of anthropogenic impacts such as straightening and channelization (Stantec, 2014). The headwaters begin in western Kitchener in agricultural land before entering a more urbanized environment.

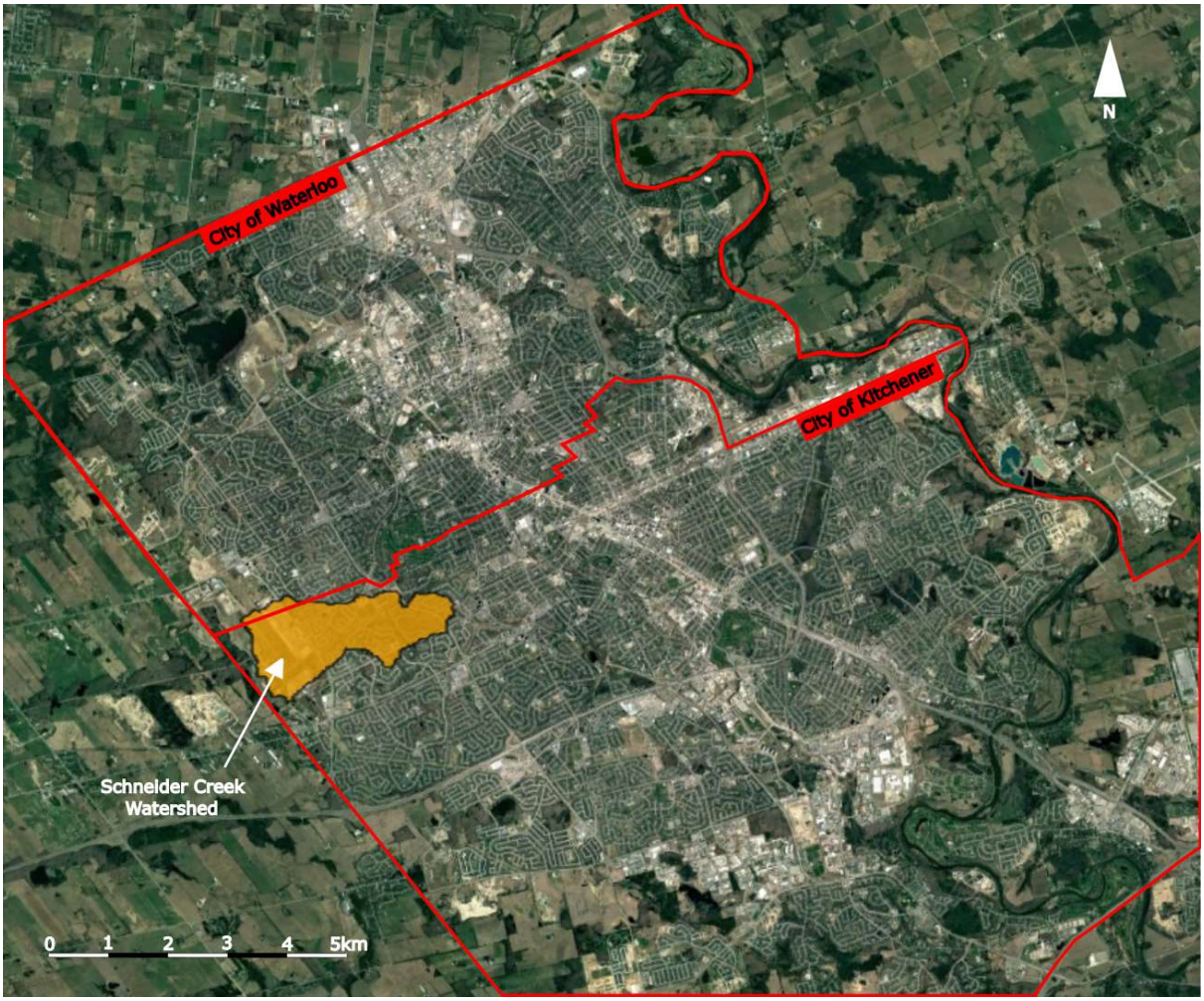

Figure 51: Location of Schneider Creek study area including municipal boundaries

Sections of Schneider Creek were initially straightened between 1945 and 1955. Anthropogenic impacts on the stream continued when sections of the straightened channel were replaced with a concrete-lined channel in 1982 (Stantec, 2014). These sections remained as a concrete-lined channel until 2014 when Stantec Ltd. re-naturalized several reaches of the channel. The restored sections saw all concrete removed, replaced with a meandering river with access to a wide flood plain. Photos of the river before and after the restoration can be seen in Figure 52.

Figure 52: (A) Schneider Creek concrete channel (Krick, 2014) (B) Channel on June 19, 2015 after Fall 2014 construction (MacVicar, 2015) (C) Restored meandering channel (Muirhead, 2016)

In an Environmental Assessment of Victoria Park Lake performed by Stantec Ltd. in 2008, Schneider Creek was identified as a significant source of sediment, resulting in sediment build-up in the lake and constant dredging (Stantec, 2008). This report led to the restoration efforts of 2014. The goal of the restoration included improving water quality parameters such as dissolved oxygen, increasing aquatic habitat in the reach and minimizing the impact of suspended sediment entering Victoria Park Lake

The study reach was chosen to allow comparison between the restored reach and natural sections of the river. Locations of the study sites are in Figure 53. As can be seen, the study reach begins in Monarch Woods, a natural section of Schneider Creek which was not previously straightened or lined with concrete. The study reach also spans the uppermost part of the restoration. The restoration continues downstream, past the extent of Figure 53.

Figure 53: Restored and natural study site locations

5.1.2 – Channel Geomorphology

The upstream natural reach consists of a meandering channel with a large flood plain, surrounded by large valley walls. The main channel meanders through Monarch Woods and follows a riffle-pool morphology. There is significant access to the flood plain which is covered by both live organic matter and fallen wooded debris. The live organic matter consists of a mixture of low-lying plants such as ferns, and large, mature trees with a wide diversity of species. The trees are mostly healthy, however, there is significant wooded debris which enters the channel during rain events or due to human activity. While large pieces of fallen wooden debris are removed from the channel or floodplain on occasion, the timing of removal is irregular. Fallen trees will sometimes be cut into smaller pieces before either being forgotten about or left behind to be transported into the main stream channel. The inconsistent removal of wooded debris leads to frequent log jams forming in the channel. These logjams are often left in place once formed.

The amount of incision in the main channel is low resulting in low banks and easy access to the floodplain. As a consequence of the floodplain accessibility, cut-off channels have begun to form and with one cut-off channel now forming the path of the main channel. One other cut-off

channel has been eroding over the course of this study and will soon represent the main channel. Photos of a developing cut-off channel and an abandoned channel are shown in Figure 54 and Figure 55.

Figure 54: Developing cut-off channel. Cut-off channel is on the left and the main channel is on the right.

Figure 55: Developed cut-off channel with new main channel. New main channel is on the left. Previous main channel is on the right.

To design the restored reach, the natural reach was used as a reference. The morphology of the restored reach described in the following section is based on the Stantec report "Filsinger Park Stream Naturalization" from 2016. Based on the restoration goals, the channel was designed as a threshold channel. A threshold channel is defined as a channel which has minimal bedload movement during the design flow, in this case, the bankfull flow (Stantec, 2014). The definition of a bankfull event varies greatly depending on the author, ranging between the elevation at which the width/depth ratio for the cross-section is at a minimum to the elevation of the upper limit of sand-sized particles in the boundary sediment (Williams, 1978). For this design, the bankfull cross-sectional area of other Southern Ontario streams were assessed based on a variety of bankfull markers to create a rating curve. Using the rating curve, the approximate bankfull cross-sectional area required to convey the appropriate design flow was determined (Stantec, 2014). Significant flood plain access was critical in the design to allow for deposition of suspended sediment during high flow events.

The channel was classified as a B4c using Rosgen terminology (Rosgen, 1994). This classification means the restoration design required most of the channel to be designed as a class B4 channel with steep valley sides, gravel substrate with intermittent cobble and boulders. Small sections of the stream were also designed as a "C" type channel with higher sinuosity. The study reach in question for this thesis was designed as a class B4 channel. The restored channel also incorporated a riffle-pool design with coarse-bed riffles designed to be stationary, acting as grade control, followed by pools along the meander bend. The design created a cobble-bed channel meandering through a valley with easy access to a wide floodplain. The main channel incorporated river cobble as well as specifically placed large pieces of riprap for grade-control. Root wads and tree trunks were integrated into the banks to create a more natural bank and reduce the energy conveyance downstream.

The floodplain was stabilized with coconut matting, providing stability until vegetation rooted. In addition to coconut matting, seed mix was spread and a variety of larger plants were placed throughout the floodplain. These plants were specifically chosen to provide stability to the banks and increase roughness of the floodplain. Larger plants include willows, dogwood and oak and maple trees. Overall, this design resulted in a shallow, meandering channel with an accessible flood plain and stable riffle sections.

5.2 – Data Collection

5.2.1 – Geomorphological Surveys

A variety of surveys were performed to collect data on the geomorphology and physical characteristics of the stream. The thalweg of the main channel was surveyed in 2016 for both the restored and natural reaches to determine the slopes (Figure 56). The average slope of the upstream reach is 0.63% while the downstream slope averages 0.82%. Due to the recent construction, it can be seen the restored section has sharp changes in slope, associated with steep drop-offs into pool. The upstream section, while still having variability, has more gradual transitions.

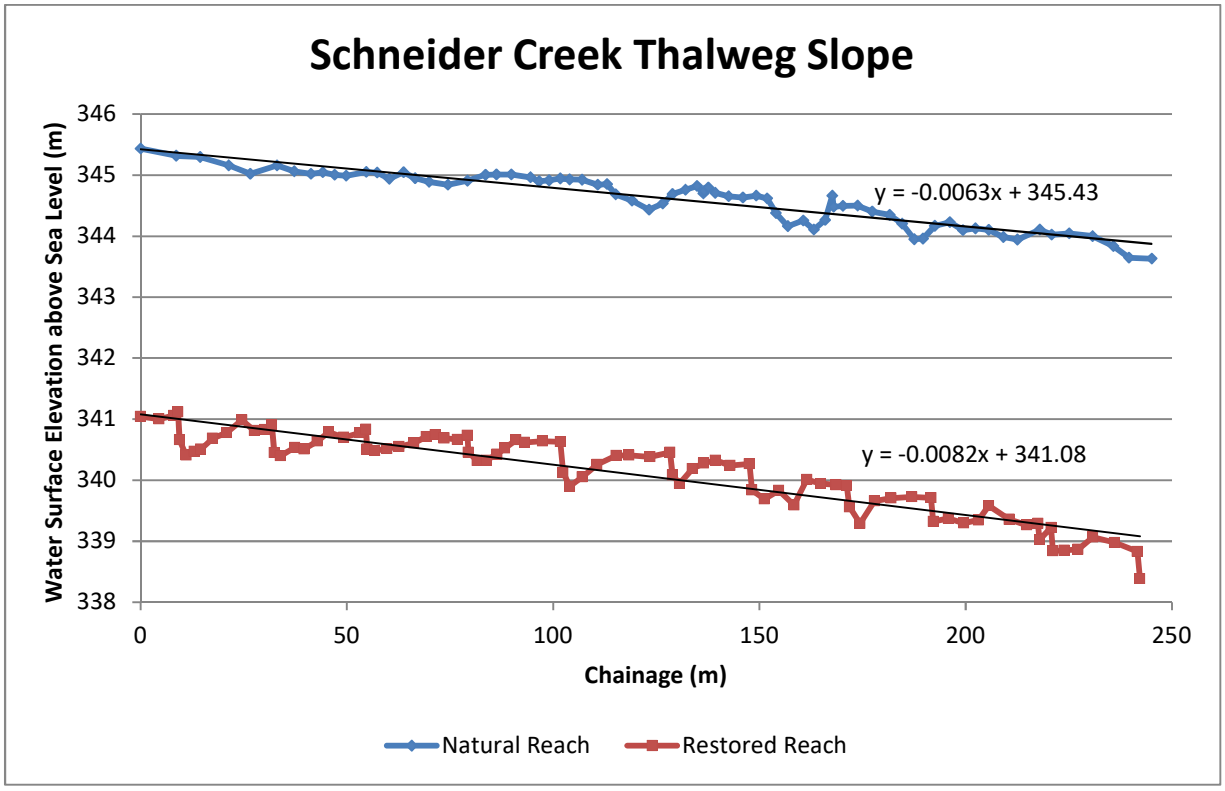

Figure 56: Schneider Creek Thalweg Slope

Pebble counts were performed in 2015 in both the restored and natural reaches using the Wolman methodology (Wolman, 1954). The resulting grain size distributions can be seen in Figure 57. Pebble counts were performed in both pools and riffles to ensure an unbiased sample. It can be seen the natural reach had similar grain size distribution between the riffle and pool while the restored section distributions varied greatly. The riffle sections consisted of significantly coarser material (D50 = 80 mm) compared to the pool section (D50 = 24 mm). The restored pool D50 was similar to the overall restored section D50 of 23 mm.

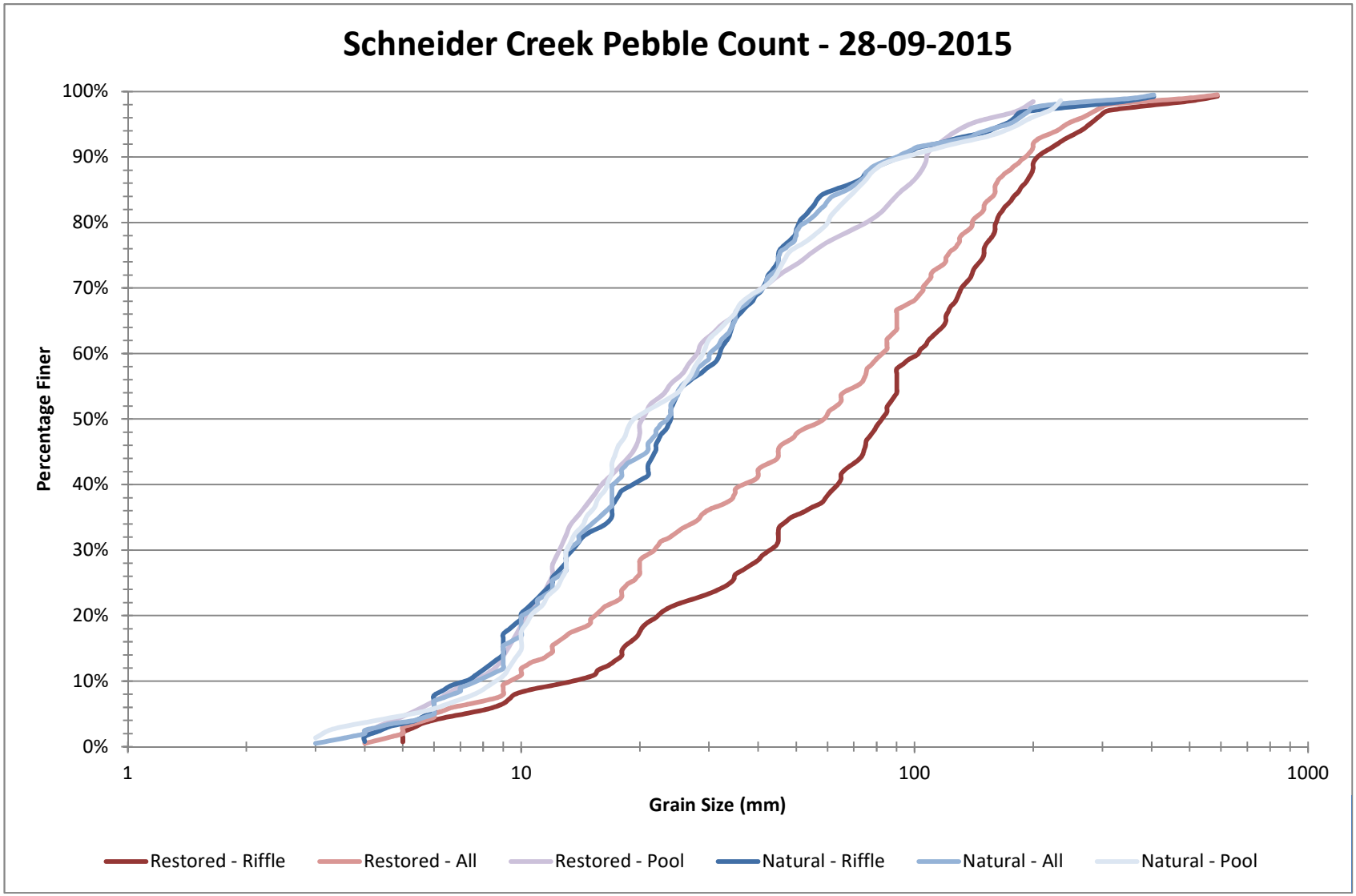

Figure 57: Grain size distribution - Restored and Natural

5.2.2 – Automated Station Installation

Once the study site was determined, the location of the automated bedload tracking system was decided upon. Up to 4 antennae can be attached to the MAR and must be placed in close proximity to communicate properly. The limit for distance from the antenna to the MAR is 20m. If the MAR is placed greater than 20m from the antenna there is potential for noise generated during signal transmission to reduce the detection range of the antenna. For the current study, the goal was to get a better understanding of the mechanics behind bedload transport in a riffle-pool sequence. For this reason, the antennae were to be placed through one riffle-pool sequence. Placement of the antenna was to be at the beginning of a riffle, end of a riffle, middle of the pool and the start of the following riffle. Water level gauges were also placed at each of these locations to ensure the hydraulic conditions during bedload transport are known. Additionally, since the automated station will record the time of movement of each particle, the rising and falling limbs of the hydrograph can be compared to the mobility data separately to investigate the hysteresis effect of bedload transport. Figure 58 is a conceptual figure depicting the locations of the antennae, tuner and MAR with respect to the main channel and the floodplain. The MAR was placed outside the floodplain to prevent water damage. In order to test the system in the field, a single antenna was installed into the bed of the stream. The installed antenna was the second most upstream antenna, immediately adjacent to SCrk30 water level gauge.

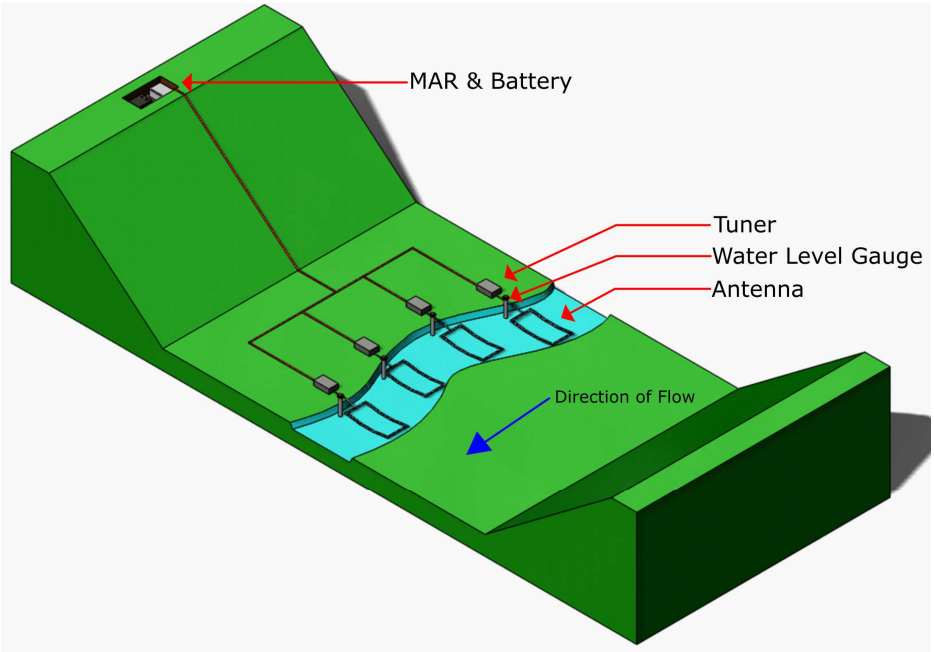

Figure 58: Antenna, tuner and MAR locations with respect to the main channel and flood plain. Not to scale.

The construction methodology of an antenna is as follows. As discussed in Section 4.5, the antenna casing consisted of a sheet of PVC with 3 grooves machined in place for the wires. The bed of the river was surveyed to ensure that the antenna would conform to the bed of the river. Once at the proper angles the pieces were zip-tied in place (Figure 49). Once the casing was properly angled and secured, the wiring was placed into the grooves to create the loop. It is important to form the angles of the antenna first otherwise the wiring will pop out of the grooves at the angles joints as they are adjusted. Once the wiring was put into place, E6000 adhesive glue was used to secure the wiring, preventing any future movement. The glue was then left to set in place for 24 hours. A photo of the antenna while the glue is drying can be seen in Figure 59. The excess zip-tie ends were also cut prior to field installation.

Figure 59: Antenna construction in the lab

To place the antenna in the stream bed, a groove the width of each PVC piece of the casing was dug into the bed of the stream. It was difficult to achieve the precise width of each PVC piece due to the substrate material consisting of large cobble, however, enough of a trench was dug to ensure the antenna didn't stick up from the bed of the stream. Once in place, the antenna was secured to the bed of the stream by hammering rebar into the bed of the stream and zip-tying the

rebar to the antenna. The rebar was then cut as to not block movement of particles and debris downstream. The cobble removed from the stream bed during installation of the antenna was then placed within and around the antenna, including on top in certain sections, to ensure the antenna was as integrated into the bed of the stream as possible. Photos of the final installation of the antenna from November 2016 and the current state of the antenna from July 2018 are shown in Figure 60. The antenna wires were placed facing the bed of the stream to ensure no damage to the wires as stones moved over top. Due to small shifts in the wire orientation as well as different surroundings, the antenna was retuned upon being placed into the field.

Figure 60: (A) Antenna upon initial installation in November 2016 (B) Antenna in July 2018

A trench was dug into the bank for placement of the wires. This trench connected wires from the antenna to the tuner and the tuner to the MAR. As shown in Figure 58, the tuner was

placed at the top of the bank. This placement of the tuner was done to reduce the noise and increase the detection range of the antenna. The closer the tuner is to the loop the better the detection range. A hole was dug 20cm into the ground for placement and burial of the tuner. By burying the tuner, the possibility of damage or disturbance by natural or anthropogenic sources was reduced. The standard tuner sold by Oregon RFID was used as it can provide a waterproof seal around the wires. The waterproof nature of the tuner is vitally important since, due to the proximity to the stream bed, the tuner has high potential to be submerged under water during a rain event. The trench for wires continued after the tuner, through the floodplain and up the valley wall.

The MAR, which is not waterproof, needed to be placed well outside the floodplain in a relatively dry area. In order to facilitate the placement of the MAR, a large hole was dug immediately on top of the flood plain, underneath dense tree cover. The hole was approximately 1m long, 0.5m wide and 0.5m deep and due to the elevation of the box, the only water which could potentially reach the MAR is rainfall or overland runoff. In the hole, a large, plastic container was placed for storage of the MAR and battery (Figure 61). The lid could be clamped shut, resulting in a container which would prevent any rainwater or overland flow from reaching the MAR. Small holes were drilled near the top of the box to allow the wires to enter the box, however, these were sealed with electrical tape once the wires were fed into the box. Small amounts of snow fell into the plastic box during installation and can be seen in Figure 61. The snow was removed and the box was dried prior to turning the system on. No water or snow entered the MAR. The plastic box was placed under dense tree cover in order to remain undisturbed by humans in the area. In addition, the box was both labeled and covered with a variety of wooded debris to ensure camouflage from any parties not involved in the study. Overall, 14m of wire was required to connect the tuner to the MAR, within the 20m limit stipulated by OregonRFID.

Figure 61: MAR and battery installed into the plastic container

The float switch was installed in the well pipe used for water level logger SCrk30. A hole was drilled into the well pipe cap to feed the wires from the float switch to the MAR. Since the float switch used was plastic and would float in the stream naturally, the switch was weighted down by gluing metal washers to the top of the gauge. Additionally, to suspend the float switch at the appropriate elevation, a metal wire was attached around the float switch with a hook at the top of the wire to attach to the same screw eye in the cap which the water level gauge is attached to. The length of the metal wire could be adjusted to match the float switch elevation desired to begin tracking. For this field test, the wire was made to have the float switch positioned approximately 10cm above the baseflow water level. While this elevation is lower than when the stones would begin to move, this elevation was chosen to test if the system would turn on and off properly.

5.2.3 – Preliminary Field Test

As described in the previous section, an initial prototype of the automated tracking system was installed into Schneider Creek. Upon installation, 23 tracer stones were placed in the stream immediately upstream of the antenna on December 12th, 2016 to test the system. Upon returning to site on December 14th, 2016, the tuner was found to have leaked with water freezing inside the tuner. This tuner was replaced the following day and the field test continued. The electrical components of the system (MAR, battery) were then removed on December 19th, 2016. Analysis of the MAR upon removal showed no detections of RFID tags during the time in the field, however, text files were created and saved to the USB drive, indicating the MAR was turned on

and off by the float switch multiple times during this week. The stones were unable to be retrieved from the stream bed until May 2017 due to ice in the river. Upon removal, several stones were downstream of the antenna, however, it is unknown if this movement occurred while the antenna was recording or in the several months after the system had been shut down for the winter.

While the MAR did not record any detections while in the field the presence of text files indicating the system was turned on and off was a promising development. Unfortunately, upon further analysis of the MAR in the lab, it was determined the MAR and the Raspberry Pi were not communicating properly and any detections received by the box would not be received by the Raspberry Pi. The issues associated with communication of detections were outlined in Section 4.3.

5.2.4 – Tracer Particle Seeding

For this study, a total of 450 stones were to be placed into the river, 210 in the natural reach and 240 in the restored reach. These tracers were separated into 5 size classes matching the D50, D75, D90, D93 and D97 of the natural reach. The size classes remained the same for the restored reach, however, due to the different grain size distribution, the percentile classes were different. The classes matched the D15, D25, D50, D75 and D90 of the restored reach. To properly normalize the data, the D50 must be included in the grain seeding distribution. Table 3 depicts the size class ranges and the stones seeded in each class both upstream and downstream.

Table 3: Tracer distribution

Natural Reach			**Restored Reach**		
Size Class	Corresponding Grain Size	Number of Tracers	**Size Class**	Corresponding Grain Size	Number of Tracers
16 – 23mm	D50	60	**16 – 23mm**	D15	60
32 – 45mm	D75	60	**32 – 45mm**	D25	60
64 – 91mm	D90	60	**64 – 91mm**	D50	60
128 – 181mm	D93	20	**128 – 181mm**	D75	40
181 – 256mm	D97	10	**181 – 256mm**	D90	20

Stones from the smallest size class (16-23mm) were too small to drill into for tag insertion. Instead, synthetic stones were created using the resin mixture described in Section 3.4 with a 12mm tag placed inside. The Wobblestone design discussed in Chapter 4 was not included in this field study as it was not complete at the time of seeding. All other stones were taken directly from Schneider Creek. A hole was drilled large enough to insert a 23mm tag before being filled with resin to seal the hole. The volume, weight, A, B and C-axes and density were calculated for each stone. Figure 62 and Figure 63 depict the grain size distribution of the natural and restored sections of the study area including the tracer distribution. Included in the figure is the riffle grain size distribution stipulated by Stantec in the 2016 design report. The riffle grain size stipulated by Stantec was significantly larger than what was observed in the field, likely due to mixing with native material. Only the riffle grain size distribution was stipulated in the design as the riffle must be properly sized to remain stable. The pool material is not thought to be a controlling factor for the stability of the design and therefore was not tracked.

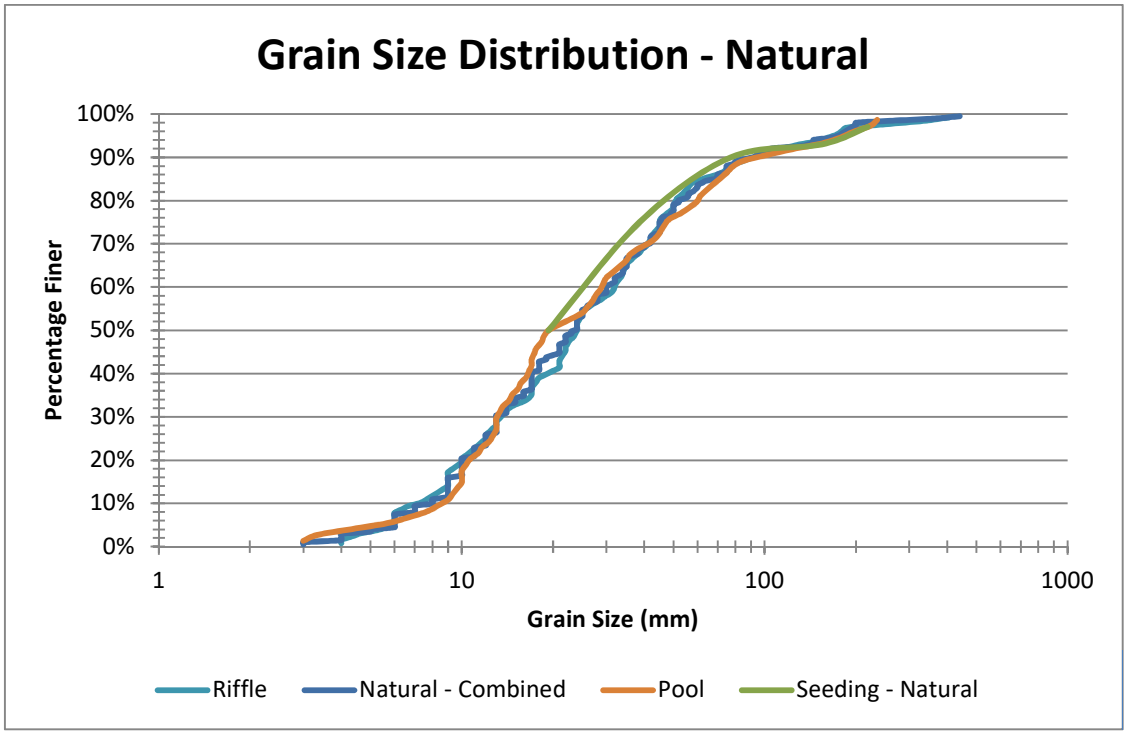

Figure 62: Natural section pebble count with seeding distribution

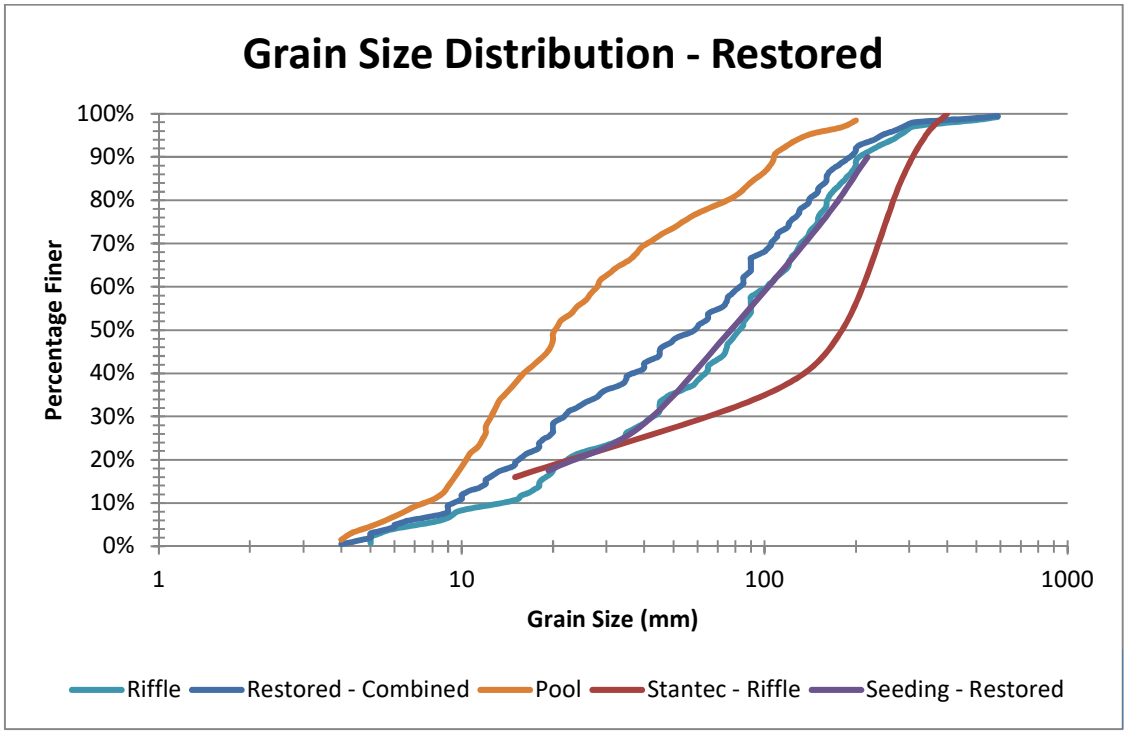

Figure 63: Restored section pebble count with seeding distribution

As shown in Figure 62 and Figure 63, the grain size distribution in riffles and pools of the natural section have minimal variation whereas the restored section has significant differences between the riffles and pools. The riffles are far coarser than the pools, however, the grain size distribution of the riffles in September 2015 is much finer than the grain size distribution stipulated in the design report by Stantec in 2014. The finer grain size distribution could be due to the material put in place during construction, however, it could also indicate the coarse riffles of the restored section are collecting fine sediment since construction completion. As the restored section stabilizes over time the grain size distribution in the riffle may adjust closer to the natural reach grain size distribution. The tracer grain size distribution for the restored reach was based upon the riffle grain size distribution. The tracer grain size distribution for the natural reach was able to match both the riffle and pool grain size distribution since the distributions were so similar.

Stones were placed into the stream on September 22nd, 2017. In order to achieve proper spacing to prevent tag collision when detecting stones, the tracers were seeded across 2 riffles in each the restored and natural reaches, 4 riffles total. Each riffle was divided into 5 sections, the size of which depended on the length of the riffle. The seeding distribution per section is shown in Table 4:

Table 4: Tracers placed per section

Natural Reach		Restored Reach	
16 – 32mm	6	**16 – 32mm**	6
32 – 45mm	6	**32 – 45mm**	6
64 – 91mm	6	**64 – 91mm**	6
128 – 181mm	2	**128 – 181mm**	4
181 – 256mm	1	**181 – 256mm**	2
Total	21	**Total**	24

Placement was random within each section, however, extra care was taken to ensure tracers were not placed within 50cm of each other to prevent signal collision. To place the stones, an existing stone of similar size was located within the seeding section and replaced with a tracer stone. This method sought to replicate local hydraulic conditions and particle-to-particle interaction of natural stones. In the restored section, tracers were seeded in the two consecutive riffles upstream of the stationary antenna array to collect transport data as the tracers moved through the array. Locations of the tracers placed during seeding can be seen in Figure 64 and Figure 65. The stones are clustered into two riffles per study area as described in the seeding procedure.

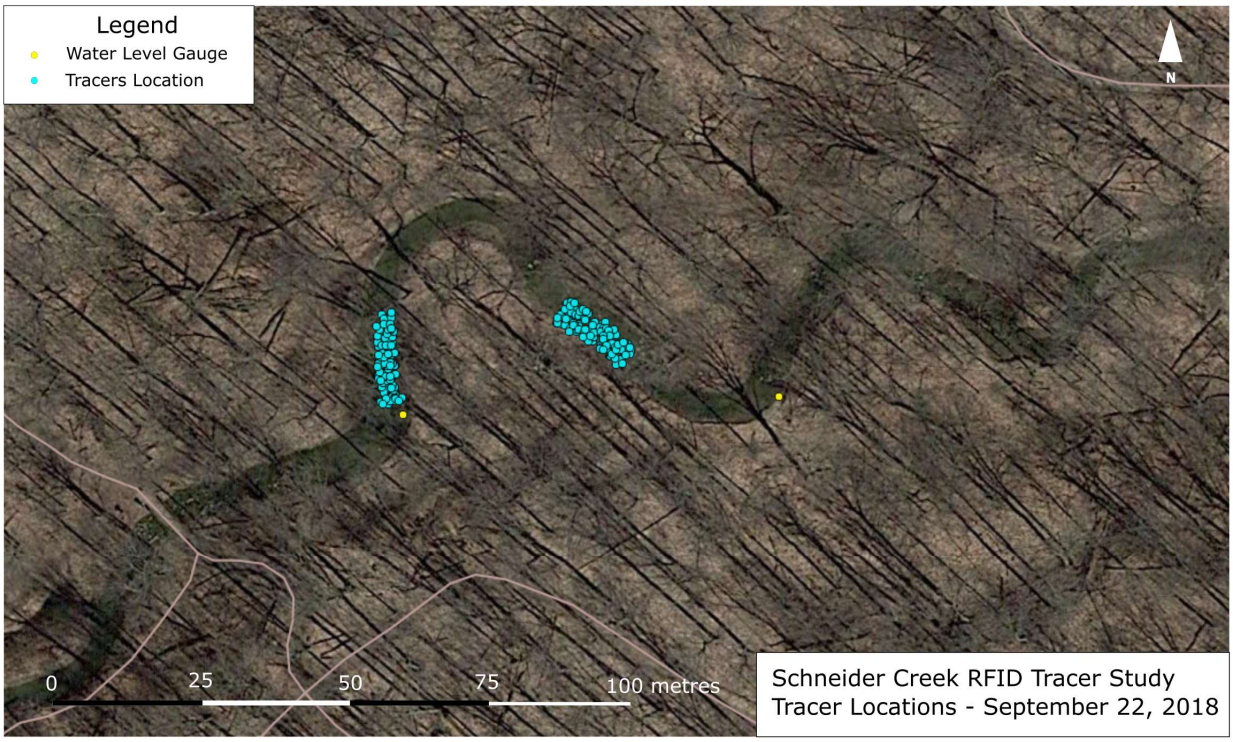

Figure 64: Natural reach tracer location - September 22, 2017 - seeding

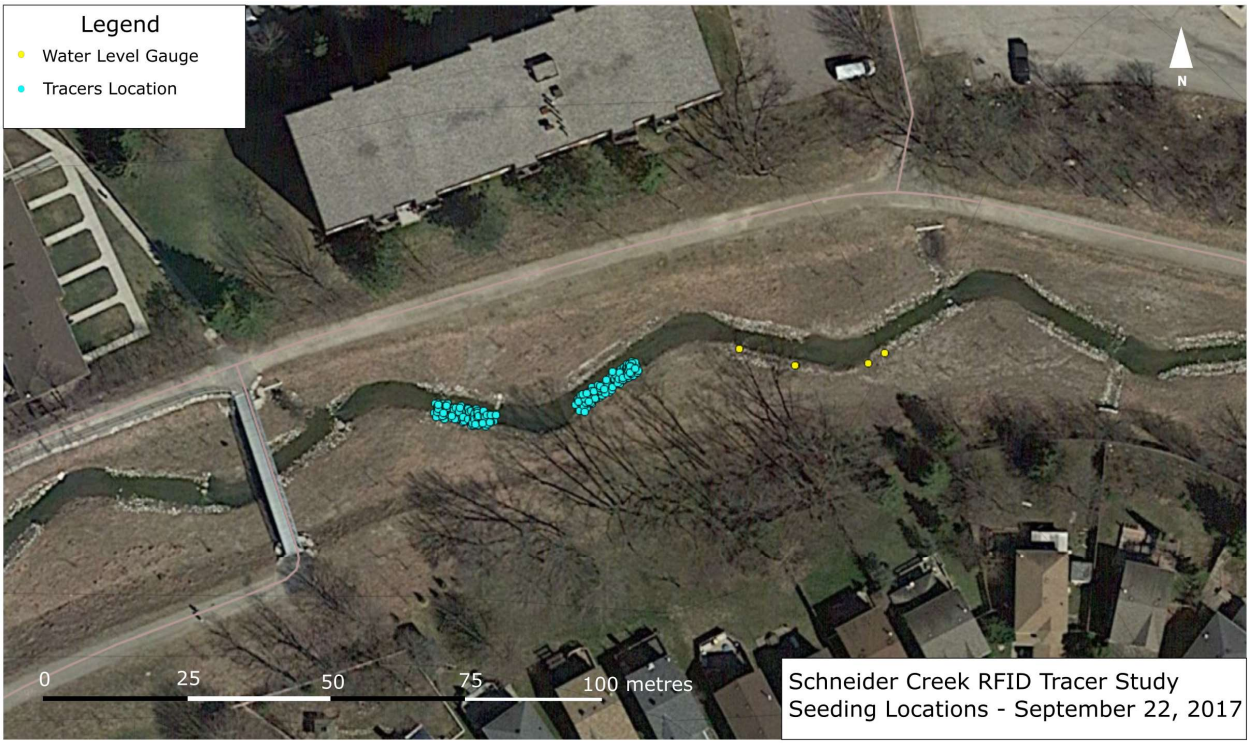

Figure 65: Restored reach tracer locations - September 22, 2017 – seeding

5.2.5 – Water Level Gauge Placement

Water level was recorded at multiple locations within the channel to characterize floods. Each gauge was comprised of a drive well point that was hammered into the stream bed and a HOBO Water Level Data Logger (UL20L-004) produced by ONSET. The logger was hung by a wire attached to the cap placed over the well so that is suspended below the stream bed and could easily be removed to download the data. These water level loggers record pressure and temperature at a specified interval. An atmospheric gauge was installed as well to correct the pressures recorded by the water level loggers. Cross-sections were surveyed at each gauge location and in combination with the atmospheric pressure, the depth of water at each gauge can be determined relative to the bed of the river. Two water level gauges were installed in the upstream natural reach and four gauges were installed in the downstream restored reach as shown in Figure 66. The natural reach gauges were placed at the top of the study reach for reference when comparing flows in the natural and restored sections.

Figure 66: Water level and atmospheric gauge locations

The restored reach gauges were placed in close proximity to one another, 4 gauges within 25 metres, through one riffle-pool section. The approximate locations of the downstream gauges are shown in Figure 67 relative to a riffle-pool sequence. Figure 67 is not to scale.

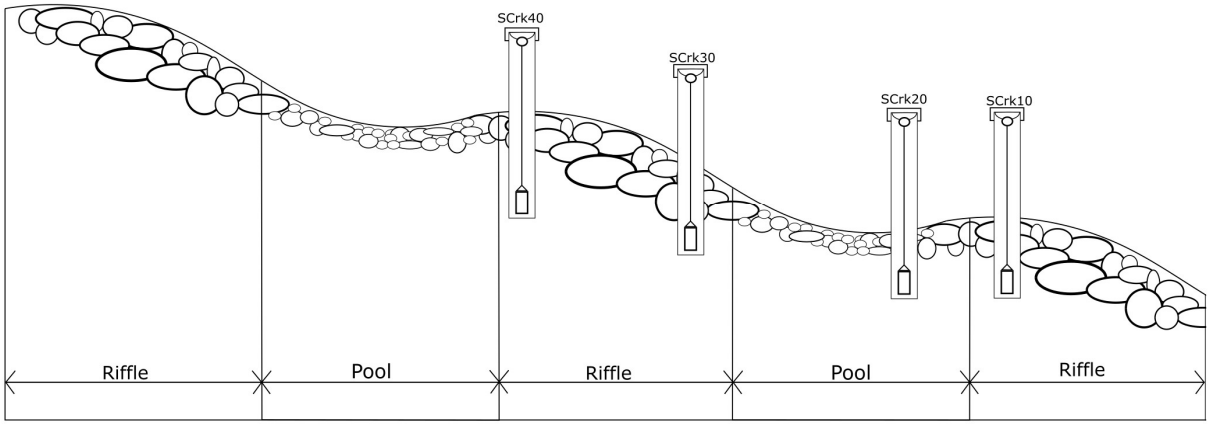

Figure 67: Restored section water level gauge locations

While riffle-pool morphology is a common restoration technique, there is limited field data available surrounding the effect of pool-riffle morphology on the water surface profile during a flood event. The high-resolution data provided by the water level gauges at Schneider Creek offers the opportunity to gain insight into the true effect of a riffle-pool sequence on the water surface profile. By placing 1 gauge at the beginning of a riffle, end of a riffle, in the pool and at the following riffle crest, the water surface slope profile at baseflow and during flood events through a riffle-pool morphology can be recorded. Preliminary data and analysis of water surface profiles during flood events can be found in Appendix A. Continued research is required expand on the preliminary data collected during this study. These gauges were in operation between December 2015 and August 2018. The most upstream gauge (SCrk60) was destroyed during the winter of 2017-2018 and was not replaced.

5.3 – Inter-flood Tracking Results

Tracer movement was tracked using handheld RFID antennae. Handheld RFID antennae include a large loop antenna and a smaller stick antenna purchased from Oregon RFID. The loop antenna has a detection range of 1.0m and is generally used to find tracers which have moved out of the riffle and have greater than 1.0m of separation from other stones (Chapuis et al., 2014). The stick antenna has a detection range of 0.2m and is generally used to pin-point the locations of any

tracers found with the loop antenna as well as locate any tracers which have not moved and remain in the riffle.

In April 2018, tracer movement was tracked using the loop and stick antenna. From September 2017 to April 2018 there was 79% recovery rate of tracer particles. This low recovery rate is at least partially due to the use of 12mm tags in the synthetic tracer particles. As discussed previously, 12mm tags have a smaller detection range than 23mm tags, particularly when they are horizontal. Overall, the recovery rate of 23mm tags was 89%, which is typical of other tracking studies in similar sized rivers (e.g. MacVicar et al., 2015) while the recovery rate of 12mm tags was relatively low at 52%.

Figure 68: Natural reach tracer locations - April 23, 2018

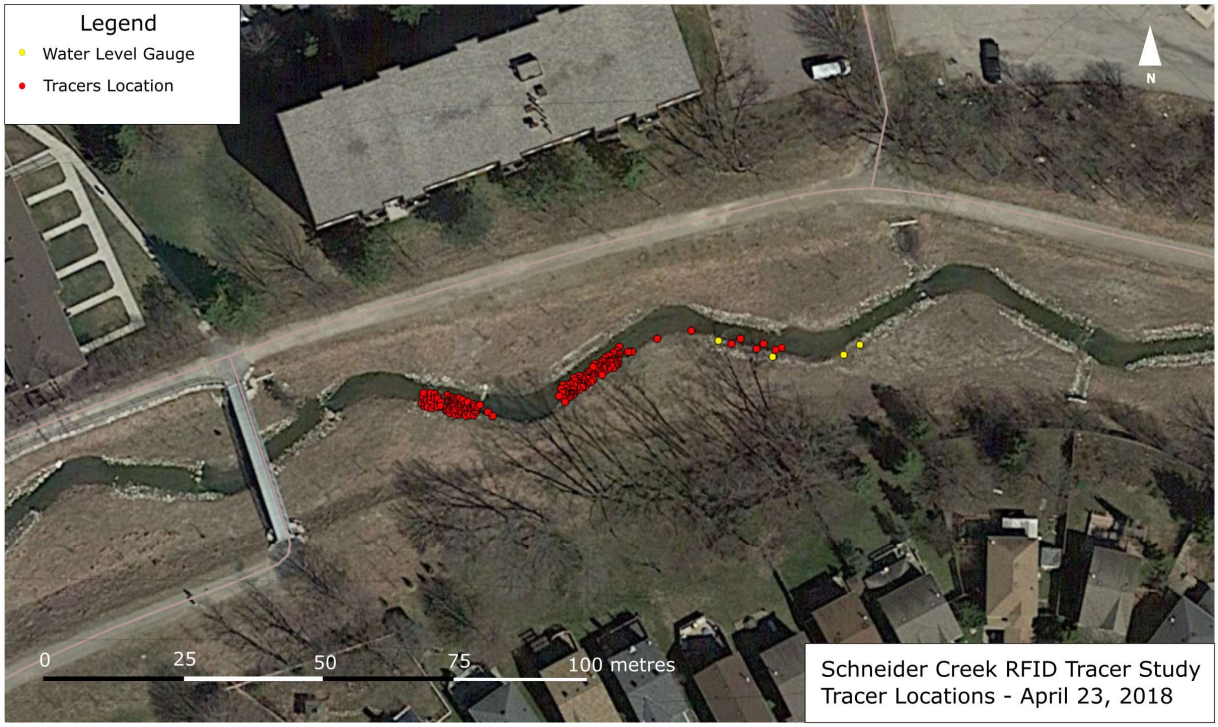

Figure 69: Restored reach tracer locations - April 23rd, 2018

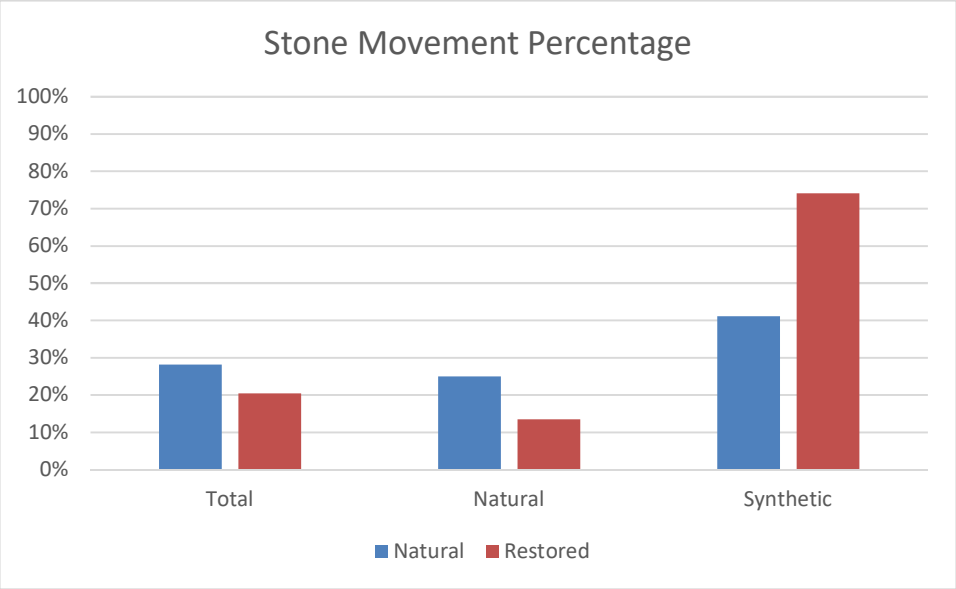

Figure 70: Stone movement from September 2017 - April 2018

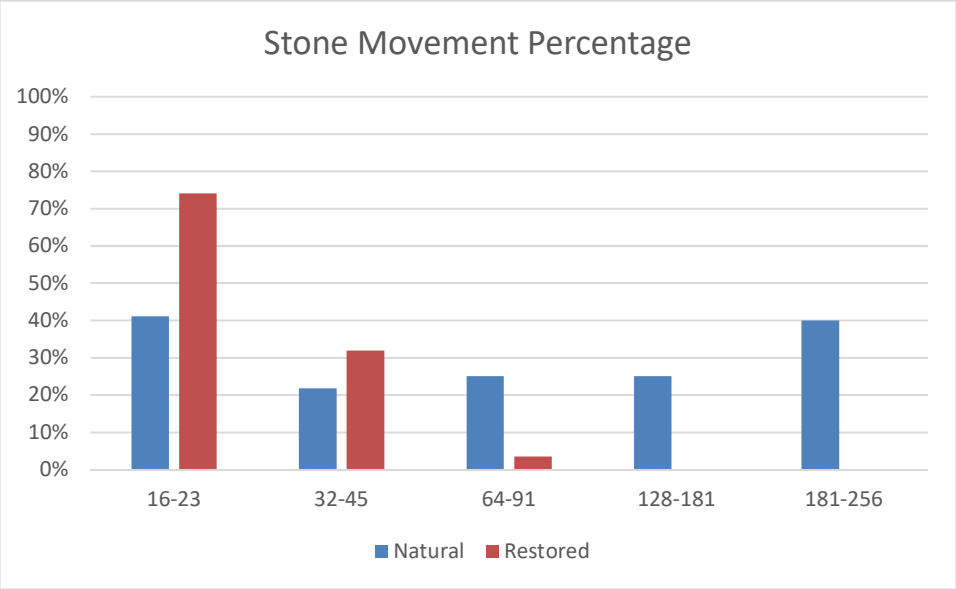

Figure 71: Stone movement based on clast size from September 2017 - April 2018

Figure 70 and Figure 71 compare the mobility of particles in the natural reach and the restored reach. A stone was considered mobile if it moved greater than 40cm or double the 20cm stick antenna detection range to account for inaccuracy during tracking. Overall mobility was higher in the natural reach while consisting of evenly distributed movement across all clast sizes. However, the restored reach saw significant movement in the 16-23mm clast size group with minimal movement in the 64-91mm clast size group and no movement in the top two categories. Additionally, the mobility of synthetic tracers was higher than natural tracer particles increasing by 64% in the natural reach and 89% in the restored reach. This result is skewed since synthetic tracers were only seeded as the smallest size class while natural stones comprised the 4 largest size classes. This result does not indicate synthetic stones are more likely to move than natural stones. It does indicate the smaller stones are more likely to move in the restored reach than the natural reach. The increased mobility of smaller stones in the restored reach could be largely due to the difference in bed slope as shown in Figure 56 and the difference in grain size distribution. The smallest size class is equivalent to the D50 in the natural reach compared to the D15 in the restored reach. Figure 72 demonstrates percent mobility when comparing the natural to restored reach based on equivalent percentile of the grain size distribution. Comparing the mobility of the D50, D75 and D90 demonstrates there is greater mobility in the natural reach than the restored reach based on percentile within the grain size distribution.

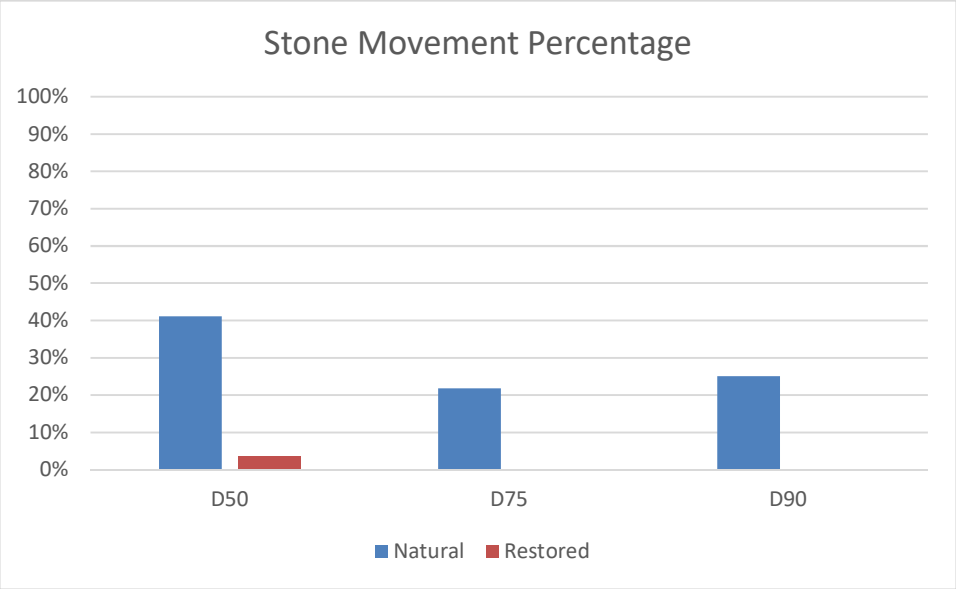

Figure 72: Stone mobility based on equivalent size class comparison

Travel distance was quantified based on a straight line from the initial tracer position to the final tracer position, not following the thalweg of the channel. The average travel distance of each size class is presented in Figure 73. It can be seen the smallest class of tracers traveled the furthest in the restored reach while the largest size class (181-256mm) produced the largest travel distance in the natural reach.

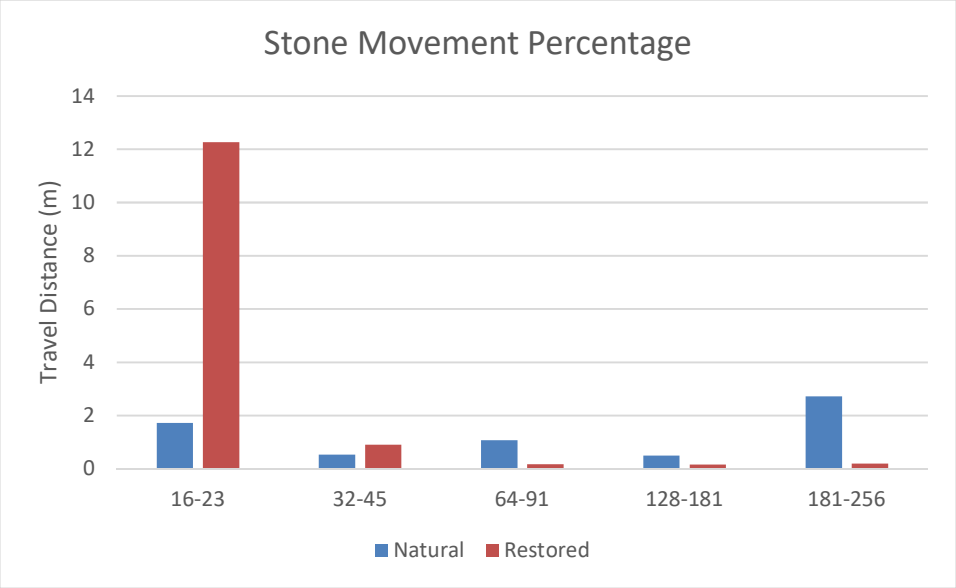

Figure 73: Average travel distance of each size class

5.4 – Discussion

The automated station was partially installed during this case study. While the electrical components were unable to be tested, the antenna casing designed was tested for durability for greater than 1.5 yrs. The antenna remained intact and secured to the bed of the stream for 2 winter seasons and 1 summer season, sufficiently proving this casing as a viable design for installing antennae into the bed of the stream. This casing provided significant protection from any debris passing overtop of the antenna and camouflage from potential anthropogenic impact.

Stone movement from September 2017 to April 2018 demonstrated several trends. The first trend was the significant movement of particles in the D25 range in the restored reach with minimal to no movement of particles greater than D50. The movement of these small particles indicates the riffles constructed in the restoration were stable through this time period, with only smaller particles moving. This trend contrasts with the mobility profile of the natural reach. In the natural reach there was an even distribution of mobility across the seeding distribution. The largest size class of 181-256mm had 40% movement while the smallest size class of 16-23mm had 41% movement. These numbers could be skewed due to the low number of tracers seeded in the larger size classes and the low recovery rates of smaller stones. However, there was still significantly more movement of larger particles in the natural reach than the restored reach.

Average travel distance in the natural reach was greatest for the largest size class at 2.7m and the smallest in size class of 128-181mm at 0.49m. The restored reach presented a more uniform average travel distance except for the smallest size class presenting an average travel distance of 12.3m. The large travel distance of the largest size class in the natural reach is surprising. All 4 stones which moved in this size class moved greater than 1 metre with 2 stones moving greater than 4 metres. While the high mobility of the largest size class is a surprising result, these numbers have the potential to be skewed due to the minimal stones seeded in the class as well as only 1 tracking event.

The final trend to note was the lack of tracer particle detection in pools. While several stones moved from one riffle to the next, there were very few stones found in the pool sections of the study reach. Overall, in the natural reach there were 4 stones detected in pool sections while only 2 stones were detection in pool sections in the restored section. Each of these stones were detected either at the very start of the pool or along the point bar established on the inner edge of

the pool. With low recovery rates it is difficult to determine whether tracers were moving through pool unimpeded or if the tracers have become buried in the pools. Additional tracking at Schneider Creek is necessary to determine the answer to this question.

Chapter 6.0 – Conclusions

RFID tags are a versatile, durable method of tracking and identifying tracers. Used to track bedload movement in stream channels, they allow the identification of individual tracer particles, leading to a greater understanding of the movement of these particles during flood events. While a significant step forward from previous bedload tracking technologies, the ability of RFID tracer particles to accurately quantify bedload transport has been limited in two key aspects; inter-flood tracking and; inconsistent detection range. These two limitations were addressed in this thesis through the development of the "Wobblestone" and a customized stationary antenna array.

The Wobblestone design presents an innovative method of maintaining the RFID tag detection range. By creating a uniform detection range, researchers will be able to determine the location of the RFID tag with far greater accuracy including the burial depth of the tag. The precise locating of the tracer particle can be done through triangulation of the detection location or using the voltage return from the detection signal. This thesis presents the development of the Wobblestone design. Additional research must be performed to create a methodology for determining the exact tag location using the two methods previously mentioned.

The customized stationary antenna array can track individual particles as they move during a flood event, providing in-flood data on individual particle movement. This system collects and synthesizes the data for up to 4 antennae spread through the river. In order to reduce the manual labour required to track bedload movement, the system is capable of remaining online for up to 30 days, depending on the number of storm events which occur. The data collected during each storm event can be collected onto either an easily accessible USB drive or sent via the 3G network to an online Dropbox account for real-time data analysis. The design presented in this thesis represents a near-functioning prototype. Issues remain surrounding the communication of data from the Raspberry Pi used to control the reader and the USB/3G drive. However, this is a proof-of-concept which needs minor alterations before installation for a field test.

The Schneider Creek case study has provided valuable insight into the movement of bedload in a natural stream compared to a restored stream. Preliminary results showed the natural reach had greater mobility than the restored reach including a more uniform mobility profile. This conclusion supports the restoration goals which were for minimal movement of bedload to occur. Further tracking including the installation of the stationary antenna array is necessary to fully quantity the similarities and differences between the two study sites.

Future work to build on the research presented in this thesis includes; the completion and installation of the customized stationary antenna array for field testing; seeding of Wobblestone tracer particles in a field study and; in-depth analysis of the bedload transport rates in the natural and restored reaches of Schneider Creek.

References

12mm HDX+ PIT Tag. (2018, June 3). Retrieved from Oregon RFID: https://www.oregonrfid.com/products/hdx-pit-tags/12mm-hdx-pit-tag/

Allen, J., Hart, R., & Tranquili, J. V. (2006). The use of Passive Integrated Transponder (PIT) Tags to trace cobble transport in a mixed sand-and-gravel beach on the high-energy Oregon Coast, USA. *Marine Geology*, 63-86.

Amazon. (2018, 06 15). *DTECH 10 ft USB to RS232 DB9 Female Serial Port Adapter Cable with FTDI Chipset Supports Windows 10, 8, 7 Mac, Linux*. Retrieved from https://www.amazon.ca/dp/B06WVC9KC8/ref=pe_3034960_236394800_TE_dp_1

Armstrong, J. D., Braithewaite, V. A., & Rycroft, P. (1996). A flat-bed passive integrated transponder antenna array for monitoring behaviour of Atlantic Salmon parr and other fish . *Journal of Fish Biology*, 539-541.

Arnaud, F., Piegay, H., Vaudor, L., Bultingaire, L., & Fantino, G. (2015). Traching specifications of low-frequency radio identification bedload tracking from field experiments: Differences in antennas, tags and operators. *Geomorphology*, 37-46.

Belleudy, P., Valette, A., & Graff, B. (2014). Monitoring of bedload in river beds with a hydrophone: first trials of signal analysis. *Hydraulic Engineering Repository*, 1731-1740.

Bernhardt, E. S., Palmer, M. A., Allan, J. D., Alexander, G., Barnas, K., Brookes, S., . . . Sudduth, E. (2005, April 29). Synthesizing U.S. River Restoration Efforts. *Science*, pp. 636-637.

Bogen, J., & Moen, K. (2003). Bed load measurements with a new passive ultrasonic sensor. *Norwegian Water Resources and Energy Directorate*.

Bradley, N., & Tucker, G. (2012). Measuring gravel transport and dispersion in a mountain river using passive radio tracers. *Earth Surface Processes and Landforms*, 1034-1045.

Bright, C. (2014). *Development of an RFID approach to monitoring bedload sediment transport and a field case study.* Waterloo: University of Waterloo.

Buffin-Belenger, T., Bergeron, N., & Dube, J. (2013). *River ice formation.*

Burtin, A., Cattin, R., Bollinger, L., Vergne, J., Steer, P., Robert, A., . . . Tiberi, C. (2011). Toward the hydraulic and bedload monitoring from high-frequency seismic noise in a braided river: the "torrent de St. Pierre", French Alps. *Journal of Hydrology*, 43-53.

Camenen, B., Le Coz, J., Paquier, A., & Lagouy, M. (2010). An estimation of mobility over an apline river gravel bare (Arc en Maurienne, France) using PIT-tag tracers. *5th International Conference on Fluvial Mechanics*.

Carre, D., Biron, P., & Gaskin, S. (2007). Flow dynamics and bedload sediment transport around paired deflectors for fish habitat enhancement; a field study in the Nicolet River. *Canadian Journal of Civil Engineering*, 761-769.

Cassel, M., Depret, T., & Piegay, H. (2017). Assessment of a new solution for tracking pebbles in rivers based on active RFID. *Earth Surface Processes and Landforms*, 1938-1951.

Cassel, M., Piegay, H., & Lave, J. (2016). Effects of transport and insertion of Radio Frequency Identification (RFID) on resistance and shape of natural and synthetic pebbles: applications for riverine and coastal bedload tracking. *Earth Surface Processes and Landforms*.

Chapuis, M., Bright, C., Hufnagel, J., & MacVicar, B. (2014). Detection ranges and uncertainty of passive Radio Frequency Identification (RFID) transponders for sediment tracking in gravel rivers and coastal environments. *Earth Surface Processes and Landforms*, 2109-2120.

Chapuis, M., Dufour, S., Provansal, M., Couvert, B., & de Linares, M. (2015). Coupling channel evolution monitoring and RFID tracking in a large, wandering, gravel-bed river; Insights into sediment routing on geomorphic continuity through a riffle-pool sequence. *Geomorphology*, 258-269.

Cohen, H., & Laronne, J. (2005). High rates of sediment transport by flash floods in the Southern Judean Desert, Israel. *Hydrological Processes*, 1687-1702.

Curtiss, G., Osborne, P., & Horner-Devine, A. (2009). Seasonal patterns of coarse sediment transport on a mixed sand and gravel beach due to vessel wakes, wind waves and tidal currents. *Marine Geology*, 73-85.

Einstein, H. A. (1937). *Bedload transport as a probability problem.*

Einstein, H. A. (1950). *The Bed Load Function for Sediment Transport in Open Channel Flows.* Washington: United States Department of Agriculture.

ELA Innovations. (2012). *Waterproof Active RFID Tag.* ELA Innovations.

Ergenzinger, P., & Conrady, J. (1982). A new tracer technique for measuring bedload in natural channels. 77-80.

Garcia, C., Laronne, J., & Sala, M. (2000). Continuous monitoring of bedload flux in a mountain gravel-bed river. *Geomorphology*, 23-31.

Gibbons, J. W., & Andrews, K. (2004). PIT Tagging: Simple Technology at it's best. *BioScience*, 447-454.

Gilbert, G. K., & Murphy, E. C. (1914). *The transportation of debris by running water.* Washington: United States Geologic Survey.

Gintz, D., Hassan, M., & Schmidt, K.-H. (1996). Frequency and Magnitude of Bedload Transport in a Mountain River. *Earth Surface Processes and Landforms*, 433-445.

Habersack, H., Kreisler, A., Rindler, R., Aigner, J., Seitz, H., Leidermann, M., & Laronne, J. (2016). Integrated automatic and continuous bedload monitoring in gravel bed rivers. *Geomorphology*.

Harris, T., & Richards, K. S. (1995). Design and Calibration of a Recording Bedload Trap. *Earth Surface Processes and Landforms*, 711-720.

Hassan, M., Voepol, H., Schumer, R., Parker, G., & Fraccarollo, L. (2013). Displacement characteristics of coarse fluvial bed sediment. *Journal of Geophysical Research*, 155-165.

Helley, E. J., & Smith, W. (1971). Development and Calibration of a pressure difference bedload sampler. *United States Geologic Survey*.

Hilldale, R., Carpenter, W., Goodwiller, B., Chambers, J., & Randle, T. (2015). Installation of impact place to continuously measure bed load: Elwha River, Washington, USA. *Journal of Hydraulic Engineering*.

Hobbs, R. J., & Harris, J. A. (2001). Restoration Ecology: Repairing the Earth's Ecosystems in the New Millenium. *Restoration Ecology*, 239-246.

Houbrechts, G., Levecq, Y., Vanderhayden, V., & Petit, F. (2011). Long-term bed mobility in gravel-bed rivers using iron slag as a tracers. *Geomorphology*, 233-244.

Hubbell, D. W. (1964). Apparatus and Techniques for measuring bedload. *Geologic Survey Water Supply*.

Hufnagel, J. (2016). *Flume Construction and RFID Tracking Techniques for Fluvial Sediment Transport Studies.* Waterloo: University of Waterloo.

Hufnagel, J., & MacVicar, B. (2018). Design and performance of a Radio Frequency Identification scanning system for sediment tracking in a purpose-build experimental channel. *Journal of Hydraulic Engineering*.

Ion Products. (2018). *Sensor Geophones.* Ion Products.

Johnston, P., Berube, F., & Bergeron, N. E. (2009). Development of passive flat-bed integrated transponder antenna grid for continuous monitoring of fishes in natural streams. *Journal of Fish Biology*, 1651-1661.

Julien, P. (1995). *Erosion and Sedimentation.* Cambridge: Cambridge University Press.

Julien, P. (2002). *River Mechanics.* Cambridge: Cambridge University Press.

Lamarre, H., & Roy, A. (2008). A field experiment on the development of sedimentary structures in a gravel-bed river. *Earth Surface Processes and Landforms*, 1064-1081.

Lamarre, H., & Roy, A. (2008). The role of morphology on the displacement of particles in a step-pool river system. *Geomorphology*, 270-279.

Lamarre, H., MacVicar, B., & Roy, A. (2005). Using Passive Integrated Transponder (PIT) Tags to investigate sediment transport in gravel-bed rivers. *Journal of Sedimentary Research*, 736-741.

Laronne, J., & Reid, I. (1992). Recording bedload discharge in a semiarid channel, Nahal Yatir, Israel. *Erosion and Sediment Transport Monitoring in River Basins*, 79-86.

Lauth, T. J., & Papanicolaou, A. N. (2008). Experimental/Feasibility Study of Radio Frequency Tracers for Monitoring Sediment Transport and Scour around Bridges. *World Environment and Water Resources Congress*.

Lauth, T. J., & Papanicolaou, A. N. (2009). Application of Radio Frequency Tracers to Individual and Group Particle Displacement within a Laboratory. *World Environment and Water Resources Congress*.

Leibault, F., Bellot, H., Chapuis, M., Klotz, S., & Deschatres, M. (2012). Bedload tracing in high-sediment-load mountain stream. *Earth Surface Processes and Landforms*, 385-399.

Leidermann, M., Tritthart, M., & Habersack, H. (2013). Particle path characteristics at the large gravel-bed river Danube: results from a tracer study and numerical modelling. *Earth Surface Processes and Landforms*, 512-522.

Leopold, L. B., Wohlman, M., & Miller, J. (1964). *Fluvial Processes in Geomorphology.* San Francisco: W. H. Freeman.

Leopold, L., & Emmett, W. (1976). Bedload Measurements, East Fork River, Wyoming. *Proc. Nat. Acada. Sci.*, 1000-1004.

Leopold, L., & Emmett, W. (1977). Bedload and River Hydraulics - Inferences from East Fork River, Wyoming. *U.S. Geological Survey*.

Leopold, L., Emmett, W., & Myrick, R. (1966). *Channel and Hillslope Processes in a Semiarid area New Mexico.* Washington: US Geological Survey.

Lewis, J. (1991). An improved bedload sampler. 1-8.

Lucia, A., Recking, A., Martin-Duque, J., Storz-Peretz, Y., & Laronne, J. (2013). Continuous monitoring of bedload discharge in small, steep sandy channel. *Journal of Hydrology*, 37-50.

MacVicar, B., & Roy, A. (2011). Sediment mobility in a forced riffle-pool. *Geomorphology*, 445-456.

MacVicar, B., Chapuis, M., Buckrell, E., & Roy, A. (2015). Assessing the performance of in-stream restoration projects using Radio Frequency Identification (RFID) transponders. *Water*, 5566-5591.

Mao, L., Dell'Agnese, A., & Comiti, F. (2017). Sediment motion and velocity in a glacier-fed stream. *Geomorphology*, 69-79.

McGee, W. J. (1908). Outlines of Hydrology. *Bulletin of the Geological Society of America*, 193-220.

Meyer-Peter, E., & Muller, R. (1948). Formulas for bedload transport. *Proceedings of the 2nd Congress* (pp. 36-64). Stockholm: International Association of Hydraulic Structures Research.

Milan, D. (2013). Virtual velocity of tracers in a gravel-bed river using size-based competance duration. *Geomorphology*, 107-114.

Milan, D. J., Heritage, G. L., & Large, A. R. (2002). Tracer pebble entrainment and deposition loci: influence of flow characteristics and implications for pool-riffle maintenance. *Geologic Society*, 133-148.

Millar, I., Warrick, J., & Morgan, C. (2011). Observations of coarse sediment movement on the mixed beach of the Elwha Delta, Washington. *Marine Geology*, 201-214.

Miller, I., & Warrick, J. (2012). Measuring sediment transport and bed distrubance with tracers on a mixed beach. *Marine Geology*, 299-302.

Ministry of Natural Resources and Forestry. (2018, July 23). *Ontario Flow Assessment Tool*. Retrieved from http://www.gisapplication.lrc.gov.on.ca/OFAT/Index.html?site=OFAT&viewer=OFAT&locale=en-US

Mizuyama, T., Laronne, J., & Satofuka, Y. (2010). Calibration of a passive acoustic bedload monitoring system in Japanese mountain rivers. *U.S. Geological Survey*.

Mizuyama, T., Oda, A., Laronne, J., Nonaka, M., & Mastsuoka, M. (2010). Laboratory tests of a Japanese Pipe Geophone for continuous acoustic monitoring of bedload. *U.S. Geological Survey*.

Moustakidis, I. (2012). Detection of Erosion/Deposition Depth using a Low Frequency Passive Radio Frequency Identification (RFID) Technology. *University of Iowa*.

Nichols, M. H. (2004). A radio requency identification system for monitoring coarse sediment particle displacement. *Applied Engineering in Agriculture*, 783-787.

Olinde, L., & Johnson, J. (2015). Using RFID and accelerometer-embedded tracers to measure probabilities of bed load transport, step lengths and rest times in a mountain stream. *Water Resources Research*, 7572-7589.

Omega. (2018). *Compact Liquid-Level Switches.*

Oregon RFID. (2018, July 18). *HDX & FDX*. Retrieved from https://www.oregonrfid.com/resources/hdx-fdx/

Oregon RFID. (2018). *Low Frequency Installation Guide.* Oregon RFID.

Papangelakis, E., & Hassan, M. (2016). The role of channel morphology on the mobility and dispersion of bed sediment in a small gravel-bed stream. *Earth Surface Processes and Landforms*, 2191-2206.

Papangelakis, E., Muirhead, C., Schneider, A., & MacVicar, B. (In Review). A new synthetic Radio Frequency Identification tracer stone with a weighted inner ball for improved bedload tracking precision. *Earth Surface Processes and Landforms*.

Papanicolaou, T., & Elhakeem, M. (2010). Autonomous measurements of bridge pier and abutment scour using motion-sensing radio transmitters. *Iowa Department of Transport*.

Parker, G. (2009). M.S. Yalin's contributions to bedload transport in rivers: 46 years of hindsight. *Canadian Journal of Civil Engineering*, 1579-1586.

Paul, M. J., & Meyer, J. L. (2001). Streams in the Urban Landscape. *Annual Review of Ecology and Systematics*, 333-365.

Phillips, C., Martin, R., & Jerolmack, D. (2013). Impulse framework for unsteady flows reveals superdiffusive bedload transport. *Geophysical research letters*, 1328-1333.

Prentice, E., & Park, D. (1984). A study to determine the biological feasibility of a new fish tagging system. *Coastal zone and estuarian studies*.

Reid, I., & Frostick, L. (1986). Dynamics of bedload transport in Turkey Brook, a coarse-grained alluvial channel. *Earth Surface Processes and Landforms*, 143-155.

Rennie, C., Millar, R., & Church, M. (2002). Measurement of bedload velocity using an acoustic doppler current profiler. *Journal of Hydraulic Engineering*, 473-483.

Richardson, K., Benson, I., & Carling, P. (2003). An instrument to record sediment movement in bedrock channels. *Erosion and sediment transport measurement in rivers; Technological and methedological advances*, 228-235.

Rickenmann, D., & McArdell, B. (2008). Calibration of piezoelectric bedload impact sensors in the Pitzbach mountain stream. *Geodinamica Acta*, 35-52.

Rickenmann, D., Turowski, J., Fritschi, B., Klaiber, A., & Ludwig, A. (2012). Bedload transport measurements at the Erlenbach stream with geophones and automated basket samplers. *Earth Surface Processes and Landforms*, 1000-1011.

Rosgen, D. (1994). A classification of natural rivers. *Catena*, 169-199.

Schmandt, B., Aster, R., Scherler, D., Tsai, V., & Karlstrom, K. (2013). Multiple fluvial processes detected by riverside seismic and infrasound monitoring of a controlled flood in the Grand Canyon. *Geophysical Research Letters*, 4858-4863.

Schmidt, K.-H., & Ergenzinger, P. (1992). Bedload entrainment, travel lengths, step lengths, rest periods - studied with passive (iron, magnetic) and active (radio) tracer techniques. *Earth Surface Processes and Landforms*, 147-165.

Schneider, J., Hegglin, R., Meier, S., Turowski, J., Nitshe, M., & Rickenmann, D. (2010). Studying sediment transport in mountain rivers by mobile and stationary RFID antennas. *River Flow*.

Schumm, S., Harvey, M., & Wateson, C. (1984). *Incised channels; morphology, dynamics and control.*

Shields, I. (1939). Application of similarity principles and turbulence research to bedload movement. *Hydrodynamics Laboratory - California Institute of Technology*.

Slaven, S. (2013). *Monitoring tracer stones through the potholes of Fall Creek Gorge near Williamsport, Indiana.* Urbana: University of Illinois.

Slaven, S., Slaven, I., & Anders, A. (2014). New Gripping and Binding Device greatly improves preparation of natural clasts for RFID tracking. *Journal of Hydraulic Engineering*.

SLIP Plate. (2018, June 18). *SLIP Plate #4*. Retrieved from https://www.slipplate.com/product/slip-plate-no-4

Stantec. (2008). *Victoria Park Lake Improvements Class Environmental Assessment.* Waterloo.

Stantec. (2014). *Filsinger Park Stream Naturalization, Kitchener, Ontario.* Waterloo.

Steffensen, M., Theim, J., Stamplecoskie, K., Binder, T., Hatry, C., Langlois-Anderson, N., & Cooke, S. (2013). Biological effectiveness of an inexpensive nature-like fishway for passage of warm water fish in a small Ontario stream. *Ecology of Freshwater Fish*, 374-383.

Tritthart, M., Gmeiner, P., Leidermann, M., & Habersack, H. (2018). A meso-scale gravel tracer model for large gravel-bed rivers. *Journal of Applied Water Engineering and Research*.

Tsakiris, A., Papanicolaou, T., Moustakidis, D., & Abban, B. (2015). Identification of the Burial Depth of Radio Frequency Identification Transponders in Riverine Applications. *Journal of Hydraulic Engineering*.

Tucker, D. N., & Tucker, G. E. (2012). Measuring gravel transport and dispersion in a mountain river using passive radio tracers. *Earth Surface Processes and Landforms*, 1034-1045.

Vanoniv, A. (1975). Sedimentation Engineering. *American Society of Civil Engineers*, 22-36.

Violino, B. (2005). The History of RFID Technology. *RFID Journal*.

Viollet, P.-L. (2014). A short history of ancient canals fo agriculture and industry. *Congress on Industrial and agricultural canals.*

Williams, G. (1978). Bank-full discharge of rivers. *Water Resources Research*, 1141-1154.

Wolman, M. G. (1954). A method of sampling coarse river-bed material. . *Transactions of the American Geophysical Union*, 951-956.

Yu, A. (2016). *Design of a telemetry system for RFID sediment tracking in streams.* Waterloo: University of Waterloo.

Appendix A: Water Surface Profile Investigation

Preliminary research was preformed at Schneider Creek surrounding the water surface profile through a riffle-pool sequence. The research performed demonstrated some unique results when compared to traditional theories. The following section outlines a brief description of conventional theory of water surface profiles in riffle-pool morphology followed by analysis of 4 flood events. Further research to be performed includes additional analysis of future storm events, comparison with laboratory data and potential adjustment of water level gauge location.

A-1: Conventional Water Surface Profile Theory

The water surface profile during a flood event can provide valuable information as to the physical mechanisms which govern the formation of riffle-pool sequence. The most widely recognized theory surrounding the water surface in a riffle-pool sequence is that, at base flow, the water surface slope is greater in the riffle, flat across the pool and steep once again through the following riffle. However, as the water level rises, the effect of the geometry of the riffle-pool sequence decreases and the slope profile of the water surface becomes more uniform. This theory is demonstrated in Figure 74:

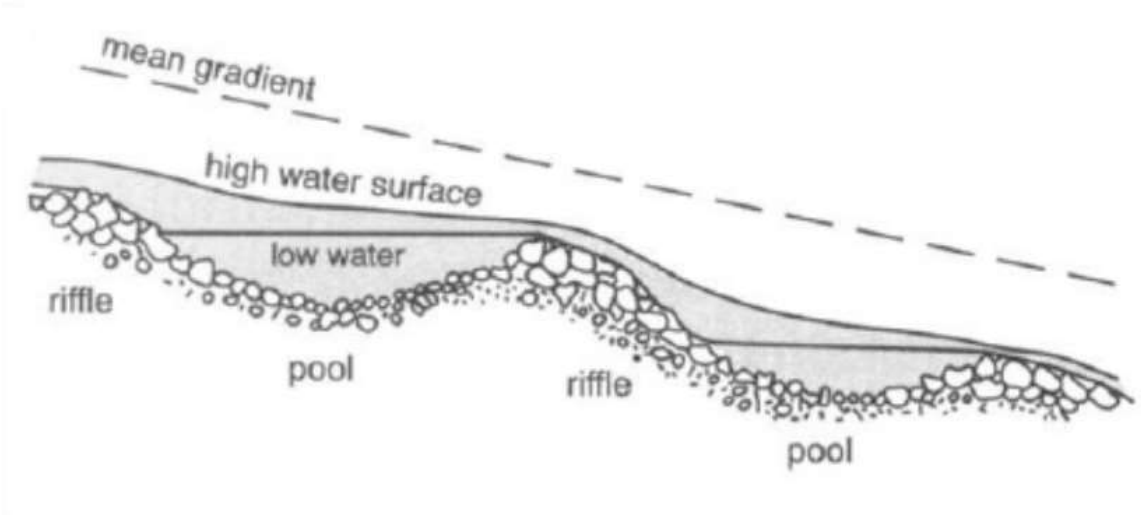

Figure 74: Idealized riffle-pool water surface elevation at high and low flow (Buffin-Belanger et al., 2013)

While the theory of a more uniform slope during a flood event is widely accepted, there is minimal data to prove this hypothesis. High resolution recordings of the water level at each point in the riffle pool sequence during a storm event is required in order to determine the resulting water

surface profile and as such, the physical mechanisms behind the development of riffle-pool morphology.

A-2: Study Methodology and Data Collection

The analysis of the water surface profile through a riffle-pool sequence was accomplished through the placement of 4 water level gauges through a single sequence with an atmospheric gauge placed for correction as discussed in Section 5.2.3. These water level gauges were set to record the pressure at the gauge every two minutes from March to December and every 7 minutes in January and February. The pressures recorded by the water level gauge were then compared to the atmospheric gauge data to determine the water level at each individual gauge.

This study will focus on events with a water level rise of greater than 30 cm at their peak. At a water surface elevation of 30 cm greater than baseflow the river begins to enter the floodplain, signifying a noteworthy event. The water level rise was assessed using the gauge furthest upstream (SCrk40). Events which occurred during the winter months (December-March) were discounted due to the presence of ice in the river. Ice build up around the pressure transducer can produce higher than expected pressures resulting in artificially high-water levels. Four storm events were identified which fit the criteria listed above between December 2015 and June 2018. These events were analyzed by examining the hydrographs and water surface slope profiles. Rainfall data will be taken from either the Kitchener/Waterloo climate gauge, located at 43°27'39.000" N, 80°22'43.000 W (Climate ID: 6144239), or the Roseville climate gauge, located at 43°21'13.026" N, 80°28'25.056" W (Climate ID: 6147188). Climate Gauge 6144239 is located 12.4 km directly east of the study site while Climate Gauge 6147188 is located 10.5 km south of the study site.

From August 11th to August 13th, 2016, Waterloo region experienced 25.5 mm of rainfall according to Climate Gauge 6144239, with 17.2 mm of rain falling on the peak day of August 13th. Climate Gauge 6147188 recorded 42 mm of rainfall for the same time period with 19.6mm falling on August 13th specifically. The rainfall resulted in a high-water event in Schneider Creek, raising the water level 0.33m above the seasonal baseflow elevation (Figure 75). The high-water event lasted a total of 10 hrs, beginning at 4:20 PM on August 13th, 2016 before receding to baseflow by 2:20 AM on August 14th, 2016. The hydrograph shows two spikes in the hydrograph. The initial spike takes 14 minutes to reach a peak water depth while the second spike begins 6 minutes later and takes 10 minutes to reach a peak water depth. The occurrence of two peaks could be due to

the presence of stormwater outlets upstream of the study site. Additionally, as different from the other hydrographs analyzed, the water level remained close to peak flow for approximately 1hr before the water level began to drop.

Climate Gauge 6144239 reports 3.6 mm of rainfall fell on August 20th, 2016. The rainfall data for August 19th, 2016 is missing, however, Climate Gauge 6147188 shows a total of 7.8 mm of rainfall for August 19th and 20th, 2016. Despite this minimal amount of rain, the water level in Schneider Creek rose 0.57 m above seasonal baseflow elevation. It is possible a localized storm passed through the Schneider Creek watershed, leaving the rainfall gauges unaffected. The high-water event lasted 24 hours, beginning at 10:11 PM on August 20th, 2016 before receding to baseflow by 10:09 PM on August 21st, 2016. The hydrograph, seen in Figure 76, shows two spikes. The initial spike takes 16 minutes to reach a peak water depth while the second spike begins 50 minutes later and takes 26 minutes to reach a peak water depth. The occurrence of two peaks once again suggests two sections of the high-water event, an initial, smaller flow followed by a larger, more intense flow. The two peaks could be due to the presence of stormwater outlets upstream as mentioned previously, or inconsistent rainfall intensity. Inconsistent rainfall intensity is possible as the amount of rainfall recorded in the area is inconsistent and does not explain the significant rise in water level which occurred.

On August 24th and 25th, 2016, Climate Gauge 6147188 reports 81 mm of total rainfall while Climate Gauge 6144239 reports 40.7 mm of rainfall. Peak rainfall of 66 mm and 31.9 mm were recorded respectively on August 25th, 2016. The rainfall event resulted in a 0.55 m rise in water level above seasonal baseflow elevation. The hydrograph, seen in Figure 77, shows a single peak, as different from the previous two storm events. The high-water event lasts a total of 11 hrs from 1:17 PM on August 25th, 2016 to 12:25 AM on August 26th, 2016. The water level rose from baseflow to peak in 28 minutes.

On August 2nd, 2017, Climate Gauge 6147188 reports 30.1mm of rainfall. The rainfall event resulted in a 0.55m rise in water level above seasonal baseflow measurements. The hydrograph, seen in Figure 78, shows a single peak. The high-water event lasts a total of 33 hrs from 5:11 PM on August 2nd, 2017 to 1:21 AM on August 4th, 2017. The water level rose from baseflow to peak in 28 minutes.

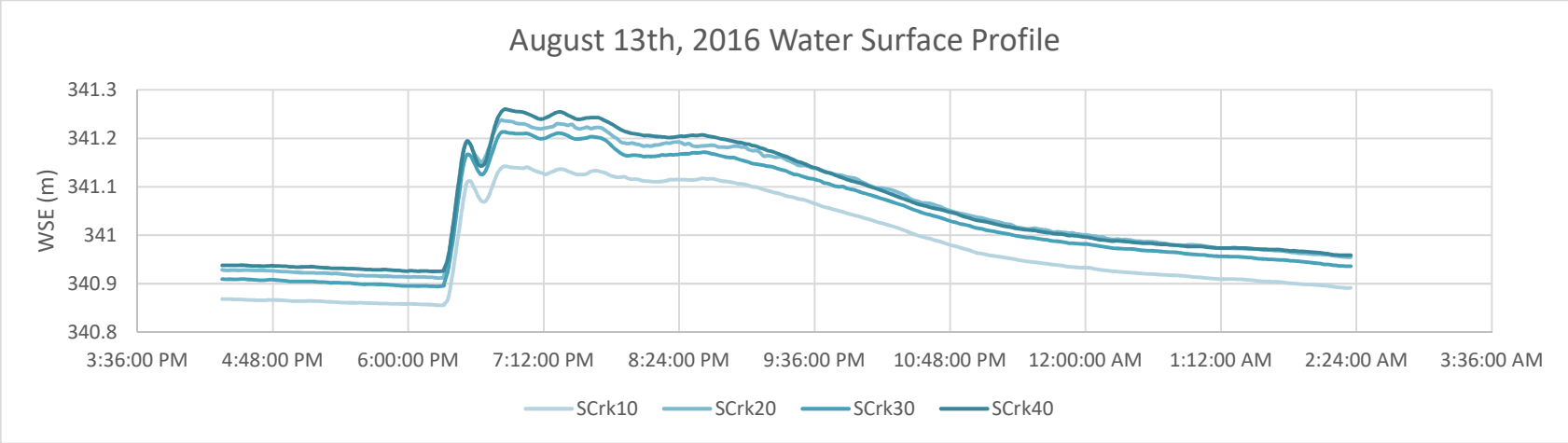

Figure 75: Hydrograph for high-water event beginning on August 13th, 2016

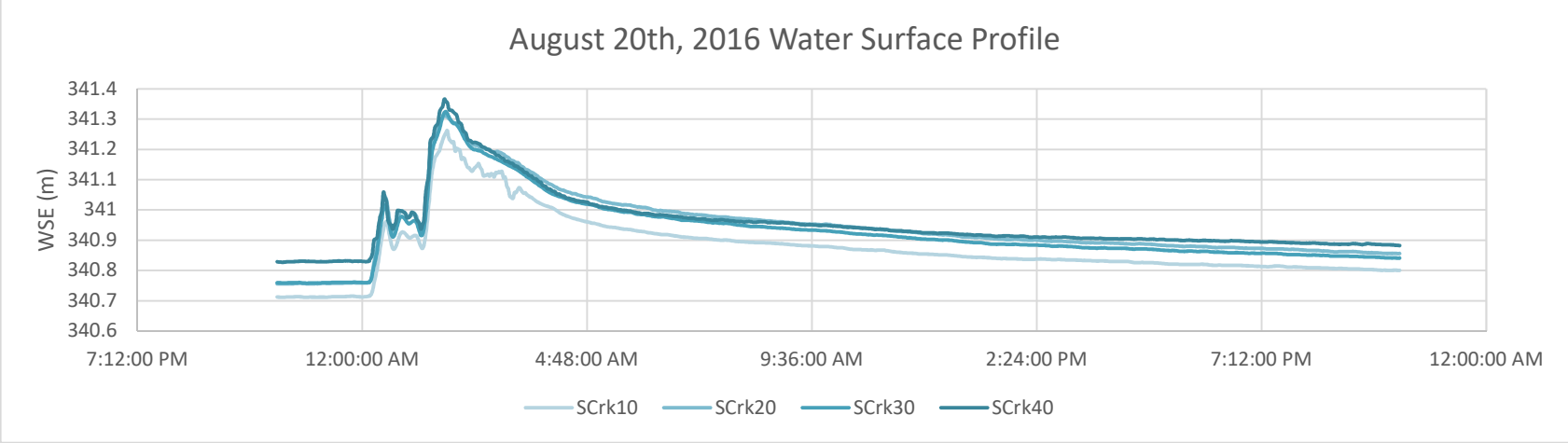

Figure 76: Hydrograph for high-water event beginning on August 20th, 2016

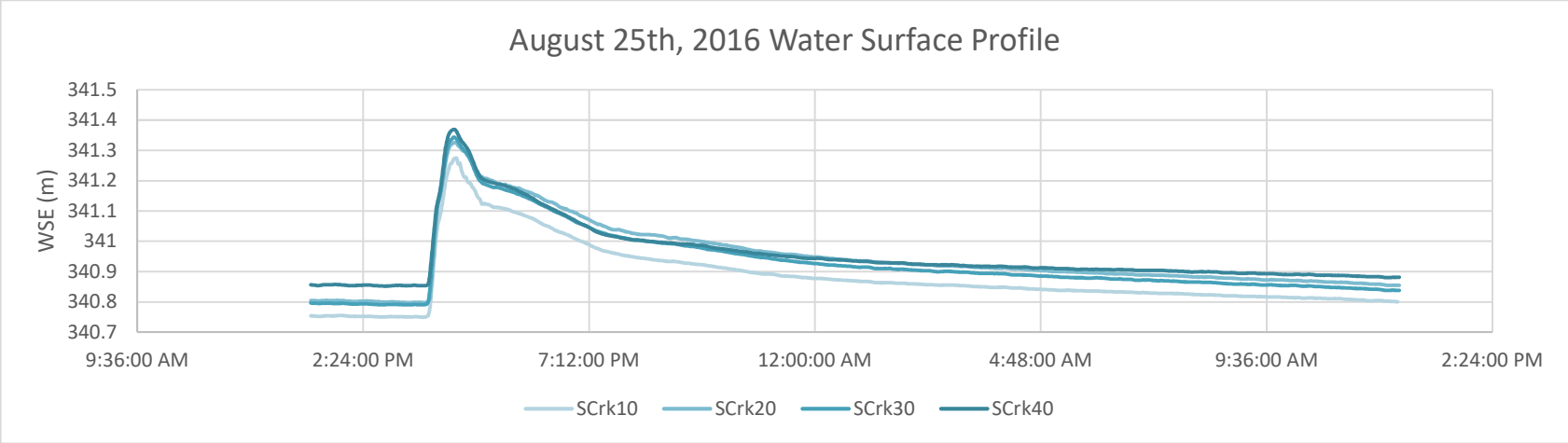

Figure 77: Hydrograph for high-water event beginning on August 25th, 2016

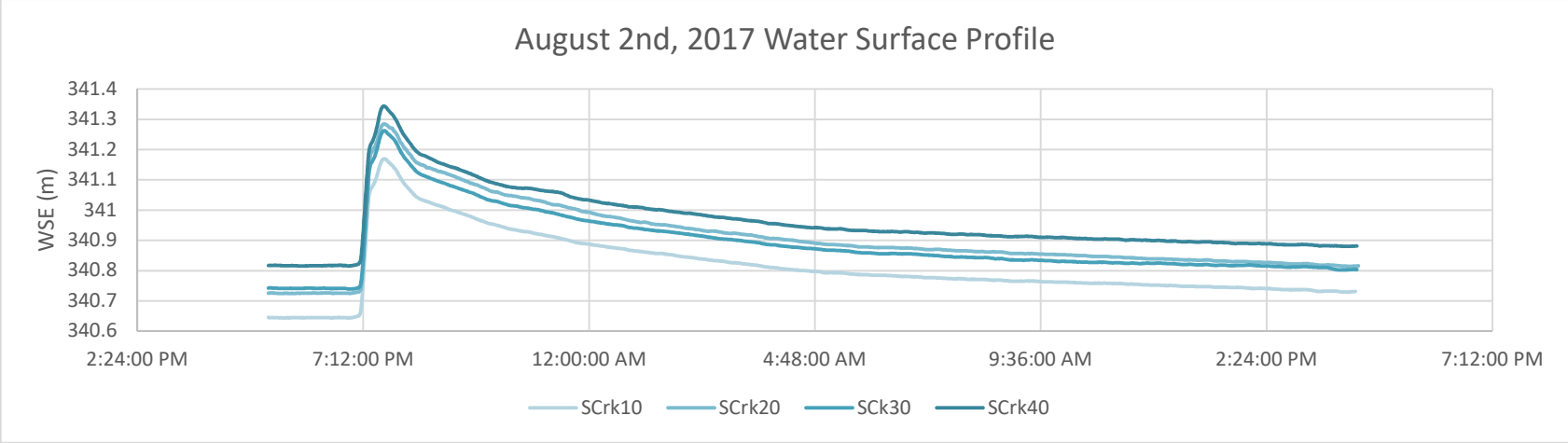

Figure 78: Hydrograph for high-water event beginning on August 2nd, 2017

A-3: Results

The water surface elevations determined in the previous hydrographs have been analyzed to determine the slope from gauge to gauge at each point in the hydrograph. The produces a slope profile of the water surface for the duration of the high-water event. It should be noted a negative slope presented on the graph depicts an adverse slope. Section 40-30 is through a riffle section while 30-20 depicts the slope profile in the pool. Section 20-10 is the exit of the pool, entering the next riffle section. BF, RL and FL labels on the graphs represent the slope during baseflow, the rising limb of the hydrograph and the falling limb of the hydrograph respectively. Baseflow in all 4 slope profiles presented as positive slopes in the riffle sections with a slope close to flat in the pool sections as expected

Figure 79 depict the water surface slope profile for the event occurring on August 13, 2016. This event was the smallest of the 4 events, raising water level by 0.33 m, or approximately 0.20 m less than the other three events. The slope profile shows a large increase in slope during the rising limb of the hydrograph in section 20-10 followed by several hours of significant fluctuation at a slope greater than the baseflow slope. While the slope experienced minor fluctuations in section 40-30 and 30-20 during the rising and initial falling limbs of the hydrograph, there were no significant changes to the slope during this event in these sections.

Figure 80 depict the water surface profile and slope profile for the high-water event occurring on August 20th, 2016. With a water level rise of 0.57 m, this event had the largest rise in water level despite minimal precipitation being recorded. During the rising limb of the hydrograph, the slope in sections 40-30 and 30-20 drop slightly producing an adverse slope in the pool section (30-20). Section 20-10 experiences significant increase in slope with severe fluctuation in slope for several hours after the peak of the high-water event. Fluctuations cause the slope in section 20-10 to be measured as low as 0.00373 m/m and as high as 0.0437 m/m.

Figure 81 depict the water surface profile and slope profile for the high-water event occurring on August 25th, 2016. This event produced a water level rise of 0.55 m, close to the maximum water level rise of 0.57 m. During the rising limb of the hydrograph, sections 40-30 and 20-10 experience a sharp drop in water surface slope with the slope in section 20-10 becoming adverse. Section 30-20 increased significantly during this time as well, going from a near flat slope to a slope of 0.011 m/m, greater than the bed slope of 0.0082 m/m. These fluctuations produce a

moment in the river when a near flat water surface occurs at the first riffle followed by a steep slope through the pool and an adverse slope as the pool transitions to the following riffle. After the initial spike/drop, the slopes sharply return closer to their baseflow values with section 40-30 maintaining a lower slope than at baseflow while sections 30-20 and 20-10 maintain a larger slope than at baseflow. The water surface slope profile following the initial spike/drop demonstrates a more uniform slope through the riffle and pool section before a steep water surface slope occurs exiting the pool. As the falling limb continues and the high-water event recedes, each section slowly returns to the baseflow slope values.

Figure 82 depict the water surface profile and slope profile for the high-water event occurring on August 2nd, 2017. This event produced a water level rise of 0.55 m, slightly below the maximum water level rise of 0.57 m and very similar to the event occurring on August 26, 2017. The rising limb of the hydrograph produces a minor increase in slope through the initial riffle section (40-30). This increase is followed by a minor decrease in slope in section 30-20 creating an adverse slope through the pool section. A sharp decrease in the slope through section 20-10 follows. These changes to the water surface slope during the rising limb of the hydrograph depict a situation where the slopes in the riffles become steeper while the slope in the pool becomes slightly adverse during the rising limb of the hydrograph. This initial reaction to the rising limb of the hydrograph is followed by slopes which are lower than baseflow in sections 40-30 and 30-20 (adverse in section 30-20) while section 20-10 experiences significantly higher slopes than at baseflow.

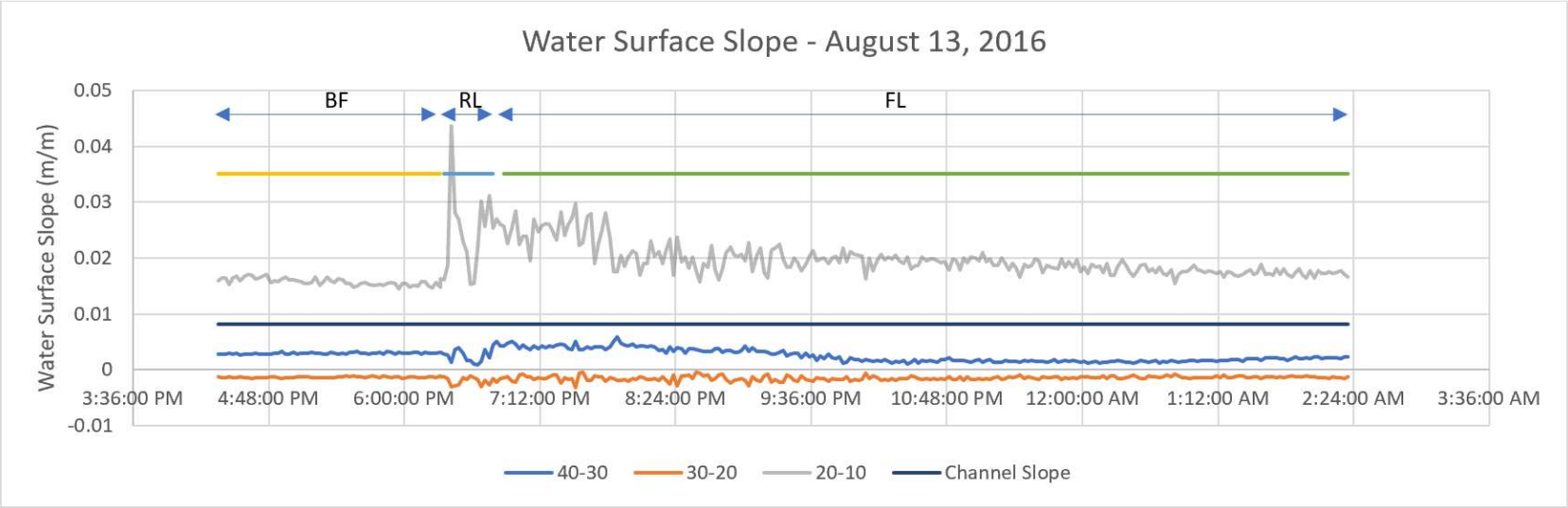

Figure 79: Water surface slope profile for high water event August 13th, 2016

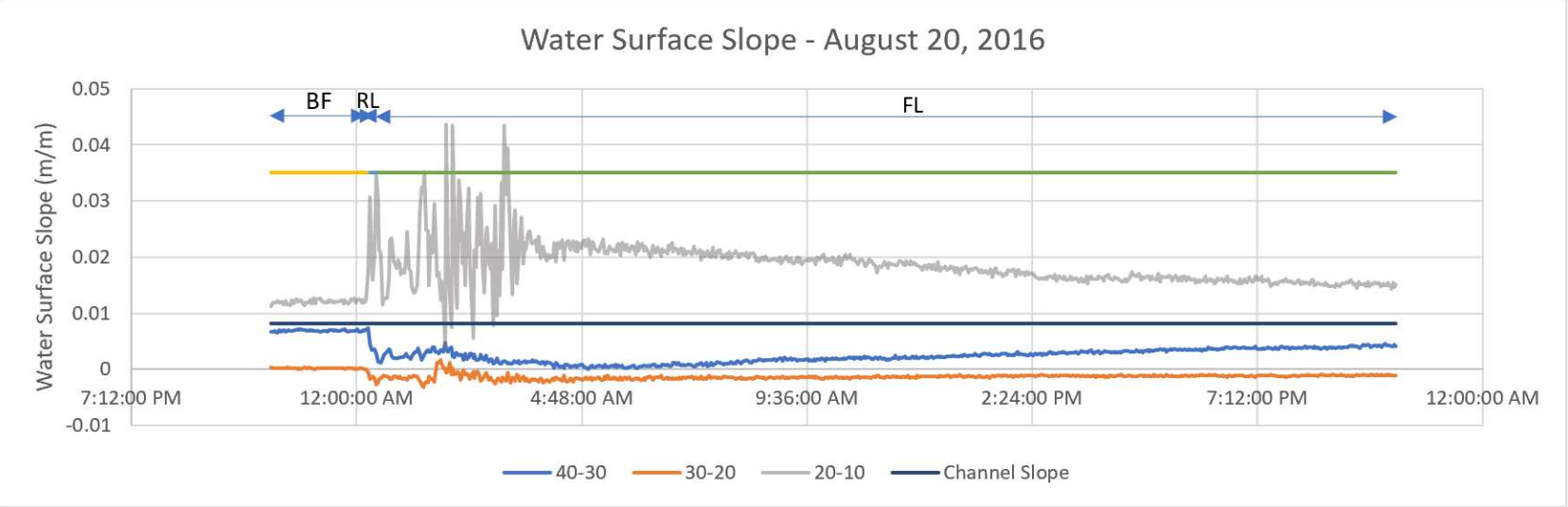

Figure 80: Water surface slope profile for high water event August 20th, 2016

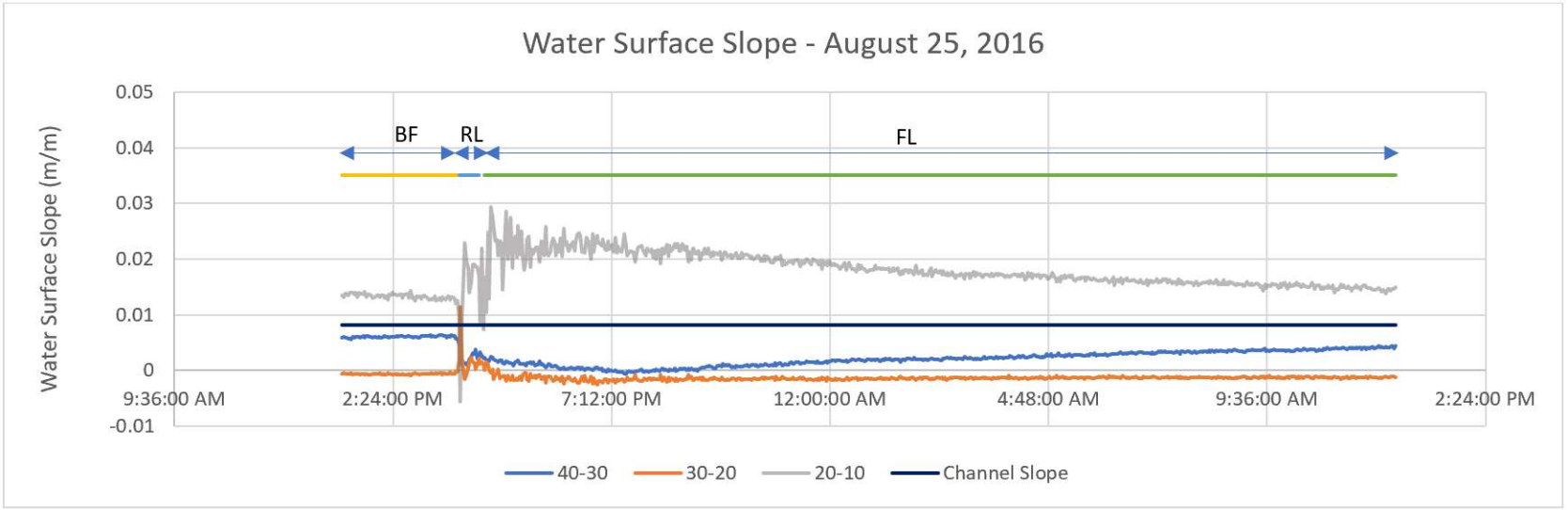

Figure 81: Water surface slope profile for high water event August 25th, 2016

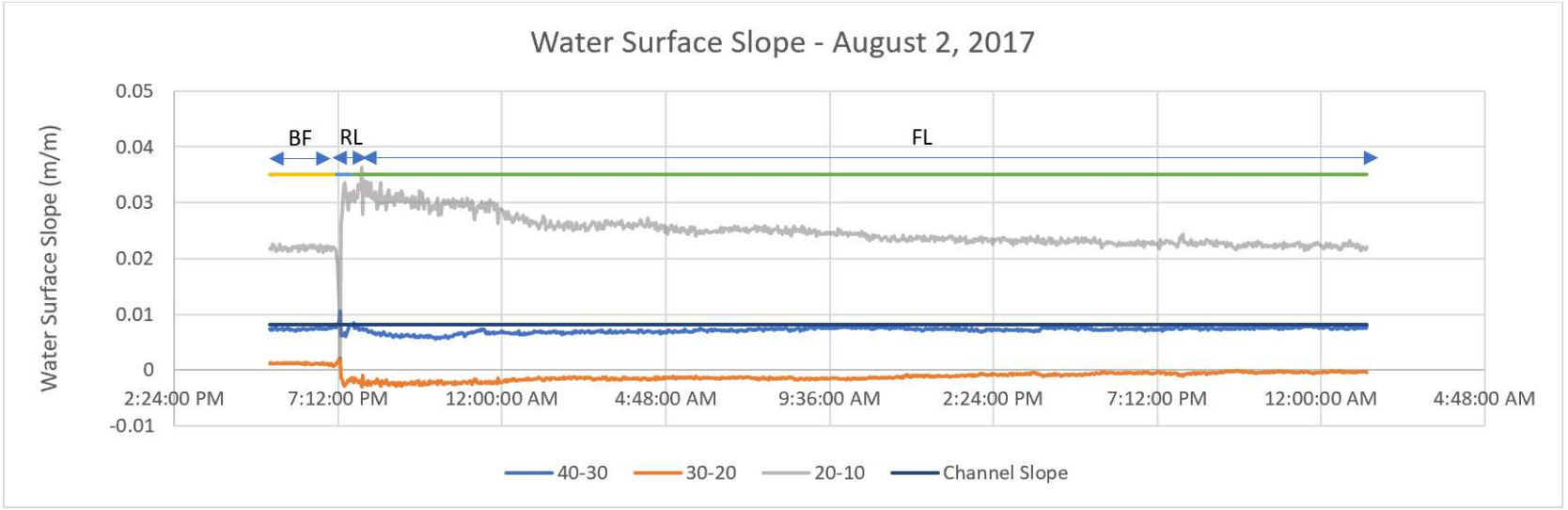

Figure 82: Water surface slope profile for high water event August 2nd, 2017

A-4: Discussion

Each event produced a unique slope profile and while there are some similarities between the profiles, there are few overarching trends which have occurred. Each profile presented a baseflow profile similar to the conventional theory shown in Figure 74, however, the slope profiles during the high-water event varied greatly.

When comparing the shape of the hydrograph, the 4 slope profiles can be split into 2 groups; the events with 2 peaks (August 13th and 20th, 2016) and the events with one peak (August 25th, 2016 and August 2nd, 2017). The events with 2 peaks produced significantly more fluctuation in section 20-10 with minimal effect on sections 40-30 and 30-20. In comparison, the events with 1 peak produced an initial spike/drop in the water surface slope in each section followed by minor fluctuations as the slope returned to baseflow values. A double-peak hydrograph likely results in a slower rise in water level, preventing significant spikes/drops during the rising limb of the hydrograph. In addition, the double-peak hydrographs experience slightly greater fluctuation in water level after the peak while single peak hydrographs will smoothly transition back to baseflow. The significant fluctuation of the water surface slope exiting the pool could be explained by the unsteady flows caused by a double peak and continued water level fluctuation during the falling limb of the hydrograph.

When looking at the overall change in water level which occurred at the peak, there were 3 events which produced a greater than 0.5m increase in water depth. In each of these events the slope through the riffle section dropped as expected. However, the slope profile through the pool section (30-20) became adverse during the flood event which was unexpected. Finally, these high flow events also produce an increased slope at the tail of the pool. An adverse slope followed by a steep slope entering the next riffle indicates increased shear stress and acceleration of flow. These results demonstrate, if the water level becomes high enough, pool-riffle morphology has the potential to form adverse water surface slopes in pool sections with increased shear stress and velocity entering the following riffle section. This conclusion contrasts with the conventional view of the water surface profile in a riffle-pool morphology during a high-water event depicted in Figure 74. The occurrence of an adverse slope would significantly affect the hydraulic conditions occurring in a pool while increased shear stress at the start of a riffle could increase bedload transport rates. If the occurrence of an adverse slope or additional shear stresses were not anticipated when designing a riffle-pool morphology then the design could experience velocity

and force profiles different from those expected, resulting in unpredictable effects on the restoration.

While these results present some interesting correlations, there needs to be significantly more data points to draw a conclusion. Due to the short time duration of the rising limbs of the hydrograph (<30 minutes) there were limited data points to analyze the slope profile during the rising water level. The sharp rise and fall which occurs during the rising limb is only comprised of a couple of measurements making it difficult to discern the true nature of what is occurring. Additionally, in the 2.5 years of water level monitoring, only 4 events were captured when the water level rose by 0.3m for a sustained period of time resulting in limited events to analyze. A greater length of study with more high-water events is required to firmly conclude the effects of a rising water level on the slope profile through a riffle-pool sequence.

The water surface profile data collected using 4 water level gauges through a riffle-pool section of the restored reach present an interesting hypothesis of the slope profiles. The development of an adverse slope through the pool of a riffle-pool section, even if it is temporary, is contrary to conventionally understanding of the slope profile during a flood event. Further research should focus on continued analysis of the water level data from Schneider Creek as well as potential lab experiments to determine the physical forces creating this phenomenon.